

# **PROCESSING AND ANALYSIS OF ULTRASOUND IMAGES FOR DISEASE DIAGNOSIS**

A Thesis

Submitted in partial fulfillment of the requirements for the

award of the degree of

**DOCTOR OF PHILOSOPHY**

in

**(PHYSICS)**

By

**Vishal Sharma**

**(Reg. No. 41400745)**

**Supervised By:**

**Dr. Kailash Chandra Juglan**

**Professor, Department of Physics**



**LOVELY PROFESSIONAL UNIVERSITY  
PUNJAB  
2020**



## **CERTIFICATE**

This is to certify that Mr. Vishal Sharma has completed Ph.D. Thesis titled “**Processing and Analysis of Ultrasound Images for Disease Diagnosis**” under my Guidance and supervision. To the best of my knowledge, the present work is the result of his original investigation and study. No part of the project has ever been submitted for any other Degree or Diploma at any University.

The Project is fit for the submission and the partial fulfillment of the conditions for the award of Doctor of Philosophy in Physics.

**Date:**

**Signature of Supervisor**

Dr. Kailash Chandra Juglan  
Professor  
Department of Physics  
Lovely Professional University  
Phagwara, Punjab

## **DECLARATION**

I hereby declare that thesis “**Processing and Analysis of Ultrasound Images for Disease Diagnosis**” submitted by me for the degree of **Doctor of Philosophy in Physics** to the Lovely Professional University Phagwara is the result of my original and independent work under the guidance of **Dr. Kailash Chandra Juglan**. This work has not previously formed the basis for the award of any degree, fellowship, diploma or other similar titles in this or any other University.

**Date:**

**Vishal Sharma**

**Registration No. 41400745**

## **Acknowledgment**

I devote this space to acknowledge all those, who have made this degree a reality. I was never alone during this task. Completing the Ph.D. and writing this thesis was an amazing journey that would not have been possible without the support and encouragement of many outstanding people.

First of all, I would like to express my deepest appreciation and sincere gratitude to the mentor who shaped my dreams into reality, my supervisor Dr. Kailash Chandra Juglan, Professor, Department of Physics, Lovely Professional University. His faith in me has always made me more confident to do better work. With the help of my thesis supervisor, I was able to acquire the necessary motivation and knowledge to achieve my goals. His incessant guidance and encouragement helped me in making valuable contributions. He has always been present to support and encourage me in my professional life when times were tough

I am especially grateful to Dr. Lovi Raj Gupta, Executive Dean, Lovely Faculty of Technology and Sciences and Dr. Ramesh Chand Thakur, Head of School, School of Chemical Engineering and Physical Sciences for sharing their vital time, experience and vast knowledge in several discussions. Thank you very much for guiding me through this important period of my life. Thanks to both of you for your enduring support.

I offer special thanks to Hon'ble Chancellor for providing all the necessary facilities in the university to carry out the research work. I wish to express thankfulness to all the faculty and staff of the University for their kind help and support.

I am very grateful to the members of Research Degree Committee for the academic support and their inputs are greatly appreciated.

I gratefully acknowledge Dr. Jatin and Dr. Rupali (Radiologists from Delta Diagnostic Centre, Patiala), and the Radiologists from PGIMER Chandigarh for their valuable support. I would like to thank Dr. Mandeep Singh, Associate Professor, Thapar Institute of Engineering & Technology, Patiala for providing the database for carrying out the proposed work and for his critical comments, innovative ideas and suggestions during the various phases of thesis work. My thanks are also extended to

my friends Dr. Manish Dhawan, Dr. Alok Jain, Mr. Gurmail Singh, Ms. Shreya and Ms. Preeti Khurana for their valuable, useful and light discussions. My gratitude also extends towards Mr. Navdeep Singh Dhaliwal, Dr. Amit Dutt and Dr. Nitin Tandon for their immense help, pertinent advices and encouragement especially in the most difficult moments of this journey.

Lastly, I would like to thank my family and parents for all their love and encouragement. My parents raised me with a love of science and supported me in all my pursuits. I owe them much more than I would ever be able to express, so I keep it plain and simple: Thank you so much for your love and care! I am indebted to my brother Dr. Vipul Sharma who has been my backbone during this period. The smiling faces of kids Geetansh, Hitul and Krisha has always made me refreshing.

My final words go to the almighty, who has been the prime mover in all my efforts. I owe my deepest sincere gratitude to “RAM NAAM” who has given me the strength, the spirit, the will, the courage to work in the right direction to achieve all the goals of my life.

**VISHAL SHARMA**

## **ABSTRACT**

In medical domain, a large number of images are produced by different imaging modalities such as Digitized X-rays Films, Digital Mammogram, Computed Tomography (CT), Cardiac Catheterization, Magnetic Resonance Imaging (MRI), Positron Emission Tomography (PET), Digital Electronic Microscopy (DEM), Digital Subtraction Angiography (DSA), Nuclear Medicine, Doppler Ultrasound etc., however Ultrasound imaging is still widely used because it is non-invasive, economical and portable. Some of the familiar applications of ultrasound imaging are growth monitoring of fetus, to identify problems in abdomen and to analyse the variety of diseases in tissues like liver and kidney.

Fatty liver is a disease that occurs when the fat content of 'hepatocytes' increases, resulting in a difference in the texture of the liver surface. Analysis of quantitative texture may also provide essential information that is otherwise difficult to obtain through visual analysis of ultrasound image. Study on Computer-Aided Diagnosis (CAD) has grown at a higher rate in the area of medical imaging and diagnostic radiology in the last few years. It introduces the pattern recognition software that analyses suspicious features on the image and helps the radiologists to solve the problem of fatty liver disease. There are many issues to be considered in the design of a CAD System that includes Region of Interest (ROI) extraction, feature extraction, selection of optimal features from the extracted features and classifier. The most important issue in the design process is the use of appropriate visual features and the methodologies to extract them from raw images, as these affect the subsequent processes of the CAD system.

In India and Western countries, fatty liver disease (steatosis) is a highly prevalent condition of all liver diseases. Radiologists measure the fatty tissue mainly by a highly subjective visual interpretation of the ultrasound image of the liver. Automatic methods of image classification seek to emulate such a visual decision and classify images based on the underlying characteristics of the textures. With widespread acceptance of ultrasound imaging as a tool, it is important to efficiently process images using computer vision techniques.

A review of related work in processing and analysis of ultrasound images has been done. From the literature survey it has been found that in recent years many approaches have been proposed for the analysis of ultrasound images and major work has been done in the area of Computer Aided Diagnosis of fatty liver (*Steatosis*). A major current focus is on use of machine learning techniques to classify the liver ultrasound images and feature selection to find an optimal set of features that can not only capture the texture of images but also enhances the semantic interpretability.

For the classification of fatty and normal images the present research work has focused on liver ultrasound images. Radiologists are more interested in the image subpart (Region of Interest) rather than the image as a whole. ROI is a sub-part of the picture containing very valuable diagnostic information. In the past, several researchers used ROI to analyse texture. Since a ROI is used as the 'representative' of the image and all other computations and diagnoses depend on the ROI, the selection of a suitable image area as ROI is therefore very crucial. In this thesis work, from the ultrasound liver image ROI of size 30×30 pixels size has been extracted from the full ultrasound image. This size of ROI also decreases the computational cost of extracting the texture features from the small sized ROI. For carrying out this work, 90 ultrasound liver images are collected from Delta Diagnostic Centre Patiala, India. Experienced radiologists are requested to acquire the images and to label them as per the standard procedure. For speckle reduction a modified fourth order partial differential equation-based filter has been used. In order to enhance the edges and fine details in the ultrasound image 'edge-map' technique has been used. To further increase the efficacy, after feature extraction from the region of interest all the features have been normalized.

Texture analysis is an important and useful area of study in many computer imaging and machine vision applications. The fatty liver image visually differs from normal liver image in terms of tonal variations (intensity-based like contrast, brightness etc.). Over the last few years, the researchers have suggested several models for texture analysis. We can categorize these models into structural, statistical, model-based and transform-based models. Each model visualizes texture in a different way and it is always a challenging task to determine the optimal texture model for liver tissue classification. Different texture models such as "Haralick's Spatial Gray Level Co-



occurrence Matrix (SGLCM), Gray Level Difference Statistics (GLDS), First-order Statistics (FoS), Statistical Feature Matrix (SFM), Law's Texture Energy Measures (TEM), Fractal and Fourier Power Spectrum (FPS)" were used in the proposed work to extract the features from ROI. In this thesis, four different methods have been proposed for the classification of liver ultrasound images into two categories.

The first proposed method is based on the use of Decision Tree Classifier with Principal Component Analysis (PCA). Decision Tree is a Supervised Machine Learning algorithm where the data is continuously split according to a certain parameter. Further, the use of PCA has been widely studied in the literature for the dimensionality reduction process. Therefore, extracted features are first fed to the Decision Tree Classifier. The experimental results showed that an accuracy of 88.9% has been obtained with Decision Tree Classifier. Further in the next experiment PCA has been used for projecting original data into a new coordinate space. From the experimental results it has been found that when PCA is used for reducing the dimensionality and the transformed features are passed to Decision Tree Classifier an accuracy of 93.3% has been achieved. The experimental results show that Decision Tree with PCA approach can not only simplify the decision tree model but can also increase the Decision Tree prediction accuracy. It has been found from the experimental results that Decision Tree with PCA outperforms in comparison to Decision Tree.

In the second proposed method, the extracted forty-five features are passed to K-Nearest Neighbour (K-NN) classifier and ten different distance metrics available in literature are explored for the classification purpose. Additional experiments were also conducted to find the best value of K which reduces the number of errors we encounter while retaining the ability of the algorithm to make predictions accurately when given data that it has not seen before. It was found from the experimental results that the proposed method using K-NN classifier yielded best results with City Block distance metric and a value of k as 7. The overall accuracy obtained with these parameter settings is 96.7%.

The third proposed method is based on the use of Neural Network (NN) for the classification of liver ultrasound images. A NN classification system mimics the human

reasoning. The neural network created for classification purpose is a two-layer feedforward neural network in which sigmoid function has been used in the hidden layer and SoftMax transfer function has been used in the output layer of the neural network. After the extensive experiments it has been found that an overall accuracy of 98.9% has been achieved with this approach.

Finally, in the last proposed work the performance of 4 classifiers i.e. Sequential Minimal Optimization (SMO), IBk, AdaBoostM1 and BF-Tree is evaluated for 5 different experiments based on different number of selected best features. Mutual Information (MI) feature selection method has been used for selecting the best features, which gives output on the basis of their weight. From the experimental results, it was found that with the 20 best features selected by the MI feature selection technique, the proposed CAD system can provide 95.55% accuracy and sensitivity of 97.77%. The experimental results indicate that the proposed method can be used with greater precision to distinguish fatty and normal ultrasound images. The experimental results also proved that feature selection has significant impact on the classification accuracy.

The current research work is expected to make a major impact in the field of ultrasound imaging. Finally, a few suggestions based on the experimental results and observations have been provided for future work.

# CONTENTS

	Page No.
Certificate	i
Declaration	ii
Acknowledgement	iii
Abstract	v
Contents	ix
List of Figures	xiii
List of Tables	xvi
List of Abbreviations	xix
<b>CHAPTER 1: INTRODUCTION</b>	<b>1-10</b>
1.1 Motivation	1
1.2 Medical Imaging Modalities	2
1.3 Ultrasound Imaging	3
1.4 Fatty Liver and Diagnosis of Fatty Liver Disease	5
1.5 Computer Aided Diagnosis System	7
1.6 Liver Ultrasound Database	10
1.7 Significance of the Proposed Research Work	11
1.8 Organization of Thesis	11
<b>CHAPTER 2: REVIEW OF LITERATURE</b>	<b>11-40</b>
2.1 Introduction	11
2.2 Ultrasound Image Enhancement	12
2.2.1 Speckle Reduction Filters	12
2.2.2 Relevant Literature on Speckle Reduction	14
2.3 Texture Analysis and Liver Tissue Characterization	20
2.3.1 Structural Texture Model	20

2.3.2	Statistical Texture Model	20
2.3.3	Model Based Textures	20
2.3.4	Transform Based Texture Model	21
2.4	Computer Aided Diagnosis of Liver Ultrasound Images	22
2.4.1	Previous Work in Processing and Analysis of Liver Ultrasound Images	28
2.5	Performance Evaluation Metrics	36
2.6	Research Gaps	38
2.7	Objectives of the Proposed Work	39
2.8	Conclusion	40
<b>CHAPTER 3: MATERIAL AND METHODS</b>		<b>41-79</b>
3.1	Introduction	41
3.2	Proposed Method I (Based on Decision Tree Classifier with Principal Component Analysis)	41
3.2.1	Image Dataset Used	41
3.2.2	Speckle Reduction	42
3.2.3	Region of Interest (ROI) Extraction	43
3.2.4	Feature Extraction	43
(i)	Haralick's Gray Level Cooccurrence Matrix based Features	47
(ii)	Gray Level Difference Statistics (GLDS) Features	53
(iii)	First-order Statistics (FoS) Features	55
(iv)	Law's Texture Energy Measure (TEM) Features	57
(v)	Fourier Power Spectrum (FPS) Features	58
(vi)	Statistical Feature Matrix (SFM) Features	61
(vii)	Fractal Features	62

3.2.5	Principal Component Analysis	66
3.2.6	Classification with Decision Tree Classifier	67
3.3	Proposed Method II	69
	(Based on K-Nearest Neighbour Algorithm)	
3.3.1	Extraction of Region of Interest and Features	69
3.3.2	Classification with K-Nearest Neighbour Classifier	71
3.4	Proposed Method III	73
	(Based on a Two-Layer Feedforward Neural Network)	
3.4.1	Region of Interest Extraction and Feature Extraction	73
3.4.2	Creation of Two Layer Feedforward Neural Network	74
	(i) Division of Dataset	74
	(ii) Training of Designed Network	74
3.5	Proposed Method IV	75
	(Based on a Sequential Minimal Optimization and Mutual Information Feature Selection)	
3.5.1	Region of Interest Extraction	77
3.5.2	Texture Feature Extraction	77
3.5.3	Feature Selection using Mutual Information (MI)	77
3.5.4	Classification with Sequential Minimal Optimization	78
3.6	Conclusion	79
	<b>CHAPTER 4: RESULTS AND DISCUSSION</b>	<b>80-114</b>
4.1	Introduction	80
4.2	Performance Evaluation of Proposed Method I	80
	(Based on Decision Tree Classifier with Principal Component Analysis)	
4.3	Performance Evaluation of Proposed Method II	88
	(Based on K-Nearest Neighbour Algorithm)	

4.4	Performance Evaluation of Proposed Method III (Based on a Two-layer Feedforward Neural Network)	97
4.5	Performance Evaluation of Proposed Method IV (Based on Sequential Minimal Optimization and Mutual Information Feature Selection)	104
4.5.1	Experiment 1 - Performance Evaluation of 5 Best Features Selected by MI Feature Selection Method	104
4.5.2	Experiment 2 - Performance Evaluation of 10 Best Features Selected by MI Feature Selection Method	108
4.5.3	Experiment 3 - Performance Evaluation of 15 Best Features Selected by MI Feature Selection Method	108
4.5.4	Experiment 3 - Performance Evaluation of 20 Best Features Selected by MI Feature Selection Method	109
4.5.5	Experiment 5 - Classification Performance of All Features	110
4.5.6	Comparative Analysis of Different Kernel Functions of SMO Classifier	111
4.5.7	Comparison with previous work	112
4.6	Discussion	113
	<b>CHAPTER 5: SUMMARY AND CONCLUSIONS</b>	<b>115-119</b>
5.1	Summary	115
5.2	Conclusions	116
5.3	Scope for Future Work	119
	<b>REFERENCES</b>	<b>120-135</b>
	<b>LIST OF PUBLICATIONS</b>	<b>136</b>

## LIST OF FIGURES

<b>Figure No.</b>	<b>Caption</b>	<b>Page No.</b>
Figure 1.1	Block Diagram of Ultrasound Imaging Process	5
Figure 1.2	Normal and Fatty ultrasound liver images of the human body	6
Figure 1.3	Causes of Fatty Liver Diseases and diagnosis of FLD	7
Figure 3.1	Steps carried out in Proposed Method I	42
Figure 3.2	Region of Interest Extraction from full image	44
Figure 3.3	Different texture models used in the proposed work	46
Figure 3.4	Directions of Maximum Variance	66
Figure 3.5	Steps performed in Principal Component Analysis	68
Figure 3.6	Flowchart of proposed methodology used in Proposed Method II	69
Figure 3.7	Steps carried out in Proposed Method III	73
Figure 3.8	Training of Designed Neural Network	75
Figure 3.9	Flowchart depicting the working of Proposed Method IV	76
Figure 4.1	Plot of number of observations with Decision Tree classifier	81
Figure 4.2	Positive Predictive Value and False Discovery Rate when Decision Tree classifier used	81
Figure 4.3	True Positive Rate and False Negative Rate when Decision Tree classifier used	82

Figure 4.4	ROC curve when Decision Tree classifier used	82
Figure 4.5	Plot of number of observations when Decision Tree classifier with PCA used	84
Figure 4.6	Positive Predictive Value and False Discovery Rate when Decision Tree classifier with PCA used	85
Figure 4.7	True Positive Rate and False Negative Rate when Decision Tree classifier with PCA used	85
Figure 4.8	ROC curve when Decision Tree classifier with PCA used	86
Figure 4.9	Parallel Coordinate Plot	86
Figure 4.10	Plot of number of observations with k-NN Classifier	90
Figure 4.11	True Positive Rate and False Negative Rate when k-NN classifier used	90
Figure 4.12	Positive Predictive Value and False Discovery Rate when k-NN Classifier used	91
Figure 4.13	ROC curve when k-NN classifier used	91
Figure 4.14	True Positive Rate and False Negative Rate with Euclidean Distance Metric	93
Figure 4.15	True Positive Rate and False Negative Rate with Chebyshev Distance Metric	93
Figure 4.16	True Positive Rate and False Negative Rate with Minkowski Distance Metric	94
Figure 4.17	True Positive Rate and False Negative Rate with Mahalanobis distance Metric	94



Figure 4.18	True Positive Rate and False Negative Rate with Cosine Distance Metric	95
Figure 4.19	True Positive Rate and False Negative Rate with Correlation Distance Metric	95
Figure 4.20	True Positive Rate and False Negative Rate with Spearman Distance Metric	96
Figure 4.21	True Positive Rate and False Negative Rate with Hamming Distance Metric	96
Figure 4.22	True Positive Rate and False Negative Rate with Jaccard Distance Metric	97
Figure 4.23	Neural Network parametes used and progress of network	98
Figure 4.24	Train Network results Cross Entropy CE and Percent Error % E	99
Figure 4.25	Plot validation performance of network	100
Figure 4.26	Plot of training state values	101
Figure 4.27	Plot of error histogram	101
Figure 4.28	Plot of Confusion Matrix	102
Figure 4.29	Plot of Receiver Operating Characteristic	103
Figure 4.30	Box plot of highly discriminant features extracted from models SGLCM	106
Figure 4.31	Box plot of highly discriminant features extracted from models FoS and FPS.	107

## LIST OF TABLES

Table No.	Caption	Page No.
Table 1.1	Types and size of some commonly used digital medical images	4
Table 2.1	Literature Review of Speckle Suppression Techniques	15
Table 2.2	Literature Review of Computer Aided Diagnosis of Liver Ultrasound Images	24
Table 2.3	Evaluation of Classification Accuracy	37
Table 3.1	Various models used for feature extraction	44
Table 3.2	Description of Features	50
Table 3.3	Feature values of Region of Interest obtained by Haralick's GLCM Model for Fatty Liver Ultrasound Images	52
Table 3.4	Feature values of Region of Interest obtained by Haralick's GLCM Model for Normal Liver Ultrasound Images	52
Table 3.5	Feature values of Region of Interest obtained by GLDS Model for Fatty Liver Ultrasound Images	54
Table 3.6	Feature values of Region of Interest obtained by GLDS Model for Normal Liver Ultrasound Images	54
Table 3.7	Feature values of Region of Interest obtained by FoS Model for Fatty Liver Ultrasound Images	56
Table 3.8	Feature values of Region of Interest obtained by FoS Model for Normal Liver Ultrasound Images	56

Table 3.9	Feature values of Region of Interest obtained by Law's TEM Model for Fatty Liver Ultrasound Images	59
Table 3.10	Feature values of Region of Interest obtained by Law's TEM Model for Normal Liver Ultrasound Images	59
Table 3.11	Feature values of Region of Interest obtained by FPS Model for Fatty Liver Ultrasound Images	60
Table 3.12	Feature values of Region of Interest obtained by FPS Model for Normal Liver Ultrasound Images	60
Table 3.13	Feature values of Region of Interest obtained by SFM Model for Fatty Liver Ultrasound Images	64
Table 3.14	Feature values of Region of Interest obtained by SFM Model for Normal Liver Ultrasound Images	64
Table 3.15	Feature values of Region of Interest obtained by Fractal Model for Fatty Liver Ultrasound Images	65
Table 3.16	Feature values of Region of Interest obtained by Fractal Model for Normal Liver Ultrasound Images	65
Table 3.17	Distance Metrics used in the Proposed Method II	72
Table 4.1	Parameter Settings for Decision Tree Classifier	80
Table 4.2	Parameter Settings for Decision Tree with PCA	84
Table 4.3	Comparison of Accuracy and Area Under ROC for Decision Tree Classifier and Decision Tree with PCA	87
Table 4.4	Parameter setting of K-NN Classifier	88
Table 4.5	Comparison of overall accuracy for different values of k	89

Table 4.6	Comparison of Overall Accuracy with different Distance Metrics	92
Table 4.7	Division of dataset into Training, Validation and Testing	98
Table 4.8	Performance Evaluation of Five Best Features	105
Table 4.9	Performance Evaluation of 10 Best Features	108
Table 4.10	Performance Evaluation of 15 Best Features	109
Table 4.11	Performance Evaluation of 20 Best Features	109
Table 4.12	Performance Evaluation of All Features	110
Table 4.13	Performance analysis of SMO classifier by using different kernel functions	111
Table 4.14	Comparison of Present Work with the Previous Related Researches	112

## **LIST OF ABBREVIATIONS**

ACR	American College of Radiology
AFBF	Adaptive Fast Bilateral Filter
ANN	Artificial Neural Network
AUC	Area Under Curve
AWMF	Adaptive Weighted Median Filter
BPN	Back Propagation Network
CAD	Computer Aided Diagnosis
CNN	Cellular Neural Network
CT	Computed Tomography
DCM	Digital Color Microscopy
DEM	Digital Electronic Microscopy
DFT	Discrete Fourier Transform
DSA	Digital Subtraction Angiography
DSIFT	Dense Scale Invariant Feature Transform
EPI	Edge Preserving Index
FDR	Fisher's Discriminant Ratio
FEC	Frequency Equalization Compounding
FLD	Fatty Liver Disease
FLDA	Fisher Linear Discriminant Analysis

FN	False Negative
FoS	First-order Statistics
FP	False Positive
FPDE	Fourth-Order Partial Differential Equation
FPS	Fourier Power Spectrum
GA	Genetic Algorithm
GLDS	Gray Level Difference Statistics
GLRLM	Grey Level Run Length Matrix
K-NN	K-Nearest Neighbor
LDA	Linear Discriminative Analysis
MADM	Multiple Attributes Decision Making
MRI	Magnetic Resonance Imaging
NM	Nuclear Medicine
PBR	Pathology Bearing Regions
PCC	Pearson's Correlation Coefficient
PDE	Partial Differential Equation
PSNR	Peak Signal to Noise Ratio
QTCT	Quantitative Tissue Characterization Technique
ROC	Receiver Operating Characteristic
ROI	Region of Interest

SC	Similarity Coefficient
SFM	Statistical Feature Matrix
SGLCM	Spatial Gray Level Co-occurrence Matrix
SGLD	Spatial Gray Level Dependency
SIFT	Scale Invariant Feature Transform
SMO	Sequential Minimal Optimization
SSIM	Structural Similarity Index Measure
SVD	Singular Value Decomposition
SVM	Support Vector Machine
TEM	Texture Energy Measures
TGC	Time Gain Compensation
TN	True Negative
TNF	True Negative Fraction
TP	True Positive
TPF	True Positive Fraction
US	Ultrasound
WEKA	Waikato Environment for Knowledge Analysis





# Chapter-1

## Introduction

### 1.1 Motivation

In medical domain, images are produced in ever increasing quantities by various imaging modalities like Cardiac Catheterization, Computed Tomography (CT), Digital Mammogram, Doppler Ultrasound, Digitized X-rays Films, Magnetic Resonance Imaging (MRI), Nuclear Medicine, Positron Emission Tomography (PET), Digital Subtraction Angiography (DSA), Digital Electronic Microscopy (DEM) etc., but still ultrasound imaging is extensively adopted, since it is non-invasive, economical and portable [1-3]. Some of the popular ultrasound imaging applications are monitoring fetal development, diagnosing problems in the abdomen and evaluating diseases in tissues such as the kidney and the liver [4-5]. Ultrasound imaging is commonly used to diagnose fatty liver (Steatosis) in liver complications. In India, the prevalence of fatty liver among adults is over 30% [6-8]. The term "Steatosis" refers to a condition that results due to the increase in fat content over 5 per cent of the hepatocyte weight. This metabolism results in a variation in liver surface texture. The visual inspection of such a variance in the texture of the liver surface is usually subjective since it relies on the radiologist's ability to analyse the difference in the grey level and the textural features of the liver tissue in an image. Quantitative texture analysis of liver images can however supply important information that is hard to acquire otherwise through visual examination of ultrasound images. Also, the diagnostic accuracy by visual perception in marginal cases is approximately 72% due to speckle noise [9]. One of the drawbacks associated with the Ultrasound imaging technique is speckle noise. Speckle not only deteriorates the visual quality of ultrasonic images but also masks several precise details of the tissues under inspection. Speckle is a locally clustered multiplicative noise with granular pattern, and this makes the ultrasound image visual quality low. The presence of speckle effects the automated image processing and analysis of an ultrasound image. Therefore, Speckle elimination is essential step prior to the implementation of any of such automated image processing technique.

Although a lot of work has been done in the area of speckle suppression and liver tissue characterization in ultrasound images, but still it is the subject of great significance due to increasing prevalence of fatty liver across the globe [10]. Therefore, a quantitative method with better accuracy is still need of the hour in biomedical imaging to assist the radiologists for better diagnosis.

The major objective of the proposed research work is processing and analysis of ultrasound images for disease diagnosis. This chapter presents an introduction about the various medical imaging modalities. This is followed by a concise literature review of the fatty liver and ultrasound imaging for disease diagnosis. At the end, the database used in the current research work and some contributions made in the proposed research work are presented, followed by the brief organization of the thesis.

## **1.2 Medical Imaging Modalities**

Medical imaging is a tool or procedure to generate images of interior of the body for various surgical actions and clinical studies, including visual depiction of the activities of the organs. Medical imaging comprises different imaging modalities and processes required for diagnostic and treatment purposes. Medical imaging helps to expose internal structures that are masked by the skin and bones, as well as to effectively treat disease. In medical domain, many images are produced by different imaging modalities such as “Digital Radiography, Mammography, Computed Tomography (CT), Cardiac Catheterization, Magnetic Resonance Imaging (MRI), Positron Emission Tomography (PET), Digital Electronic Microscopy (DEM), Digital Subtraction Angiography (DSA), Nuclear Medicine, Doppler Ultrasound” etc.

The field of medical imaging has its origins in Röntgen's accidental discovery in 1895 of a new form of electromagnetic radiation, X-rays. In the decades that followed, doctors have commonly used X-Ray radiography for finding the structural and physiological state of internal organs of the body that includes intestines, stomach, brain and lungs. Hospitals have also incorporated computers and digital imaging into radiology and medical imaging services. Computers are now used regularly for different activities, ranging from data collection and image creation to image display and analysis [11].

The need for computers and computing in image generation, processing, display, visualisation, and analysis continued to expand with the development of new imaging modalities. Computers are now part of almost every medical imaging system, including mammography, x-ray, ultrasonography, CT, Nuclear Medicine (NM), and MRI. Most departments of radiology have transformed into "totally digital" and "filmless" departments even using computers for image archiving and communication through the development of Picture Archiving and Communication System (PACS). The X-ray film which started the field of radiological imaging has almost disappeared [12].

Possibly the image is one of the most useful tools in medicine as it offers a mechanism for diagnosis, tracking drug treatment reactions and patient care with the benefit of being a very quick non-invasive procedure with very few side effects and an excellent cost-effective relationship. Hard-copy image formats, i.e. analog video films, were the initial medical image support but they became uncommon. The need for greater upkeep, storage space and the amount of material needed to view images in this format resulted in its disuse. Digital images address the aforementioned problems nowadays while providing the possibility of text annotations in metadata format. Since the large number of images are produced in medical domains, the image recovery systems are required to provide effective and reliable access of image database on the basis of their visual content (colour, shape and/or texture) [13].

Table 1.1 gives an overview of existing imaging modalities, image dimensions and number of images per exam in medical imageology.

### **1.3 Ultrasound Imaging**

Medical ultrasound is commonly used for many clinical applications such as abdominal imaging, fetal examination, hepatic diagnosis, echocardiography, etc. As ultrasound is a real-time imaging tool that uses no ionizing radiation, it is usually favoured over other imaging modalities. In addition, the equipment used for ultrasound imaging is compact and inexpensive in comparison with other modalities such as CT and MRI, and is thus commonly used in small clinics and rural areas. Even the World Health Organization's (WHO) flagship initiative, Door to Door Healthcare (D2DH), in

underdeveloped countries, uses ultrasound imaging as a primarily diagnostic method due to its portability and other aforementioned benefits [15].

**Table 1.1: Types and size of some commonly used digital medical images [14]**

S. No.	Modality	Image Dimensions	Gray Level (Bits)	Average Size/Per Examination
1	Cardiac Catheterization	512×512 or 1024×1024	8	500-1000 MB
2	Computed Radiography	2048×2048	12	8-32 MB
3	Computed Tomography (CT)	512×512	12	20 MB
4	Digital Color Microscopy (DCM)	512×512	24	Varies
5	Digital Electronic Microscopy (DEM)	512×512	8	Varies
6	Digital Subtraction Angiography (DSA)	512×512	8	4-10 MB
7	Digital Mammography	4096×4096	12	64 MB (a pair)
8	Digitized X-Ray films	2048×2048	12	8 MB
9	Doppler Ultrasound	512×512	24	15-24 MB
10	Magnetic Resonance Imaging (MRI)	256×256	12	8-20 MB up
11	Nuclear Medicine (NM)	128×128	8 or 16	2 MB
12	Spiral or helical CT	512×512	12	40-150 MB
13	Ultrasound (US)	512×512	8	5-8 MB

Ultrasounds are high frequency sound waves from 20 kHz to 10 GHz, which act as pressure waves in a medium. Ultrasound ranges from 1MHz to 30MHz as used in medical applications. Ultrasound echoes from pressure waves are used for medical examination to collect knowledge about tissue within the body. An ultrasonic image is obtained by positioning the ultrasound probe (piezoelectric transducer) on a patient's skin near the area of interest. The piezoelectric transducer converts the electrical signal into a pulse or wave of ultrasound which penetrates the body.

As the pulse propagates through the tissue, tissue structures generate reflections which travel back to the transducer. The intensity of a reflected signal contains the reflective structure information, and the delay between sending a signal and receiving an echo indicates the distance between the structure and the transducer. The transducer transforms those mechanical echoes back to electrical signals. Then, in an ultrasonic imaging system, these electrical signals are amplified, demodulated and ultimately transformed into real images. As the ultrasound wave frequency increases, it undergoes greater attenuation in the body and hence reduces the wave penetration. Frequencies between 3MHz and 5 MHz are thus used to view large body parts, such as liver and kidneys, from the skin at a depth of 15 to 20 cm [17-18].

The general schematic organization of an ultrasound imaging system is shown in Figure 1.1.

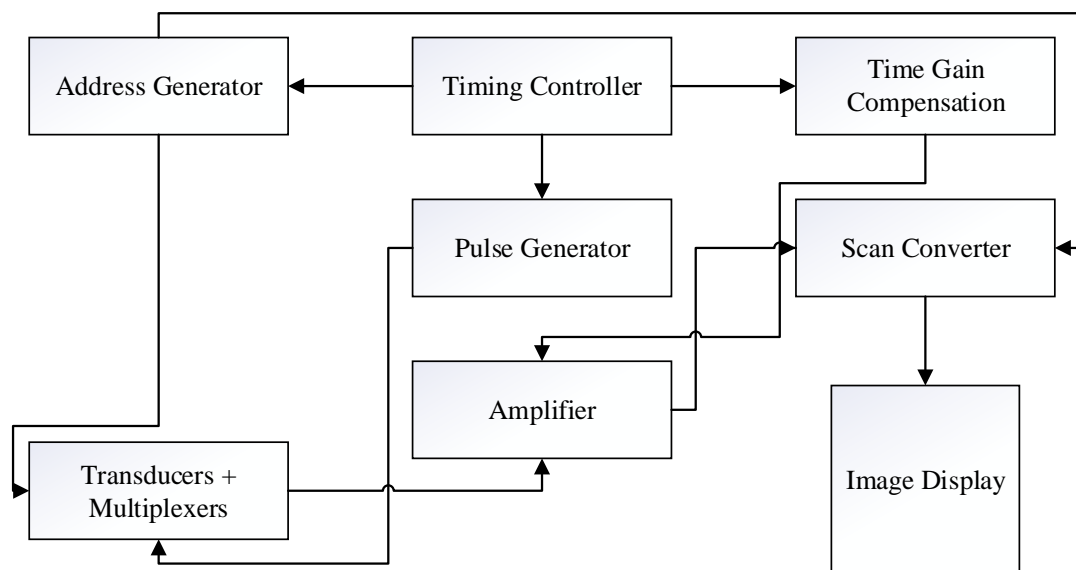
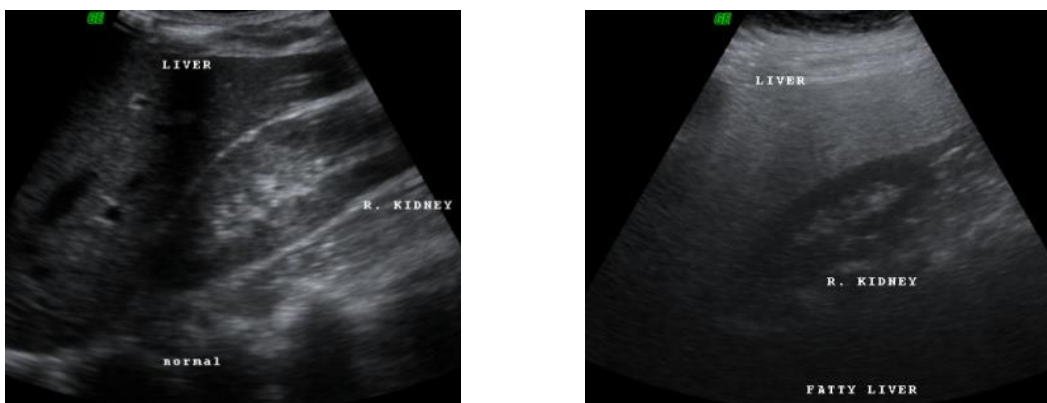


**Figure 1.1: Block Diagram of Ultrasound Imaging Process [16]**

## 1.4 Fatty Liver and Diagnosis of Fatty Liver Disease

Liver disease is a common term used for several damage that reduces the functioning of the liver. Liver disease may occur due to presence of toxin, infection, drugs, alcohol, injury, insulin resistance etc. All the reasons which cause liver disease may leads to inflammation, clotting abnormalities, scarring and liver failure [19]. Fatty Liver Disease (FLD) is one of the most widespread liver diseases [20]. Fatty Liver

(Steatosis) or FLD are the major problem which cannot be recognized with that much accuracy basically fatty liver diseases are caused due to more gathering of fat content of hepatocytes in liver cells [21]. There are two types of fatty liver diseases one is called as Alcoholic Steatosis and the other one is called as Non-Alcoholic Fatty Liver Disease (NAFLD). The Non-Alcoholic Fatty Liver Disease (NAFLD) first named in 1980 by Ludwig et al. [22]. The inflammation, condition known as alcoholic (ASH) or Non-Alcoholic Steatohepatitis (NASH) may lead due to the accumulation of triglycerides in the liver [23-24]. The usual causes of FLD includes overuse of alcohol, insulin resistance, obesity, hyperlipidaemia, metabolic syndrome [25]. It is roughly calculated that it affects 15- 24% of the world's population [26-27]. Out of which 90% of individuals consumes more than 60 gm of alcohol a day to increase cause of FLD and rest of the reason for FLD incorporate insulin resistance and all types of the metabolic disorder, for example, obesity, Type 2 diabetes, and hyperlipidaemia [28]. If FLD is not detected early it may lead to cirrhosis, liver cancer, steatohepatitis or damage to the liver and acute liver failure [29]. So, the early treatment and detection is important for control of the fatty liver diseases. The normal and fatty ultrasound liver images of the human body is shown in Figure 1.2.



(a) Normal liver of the human body identified by the clean inferior pattern.

(b) Fatty liver of the human body appear brighter and smoother.

**Figure 1.2: Normal and Fatty ultrasound liver images of the human body**

In medical imaging, the early diagnosis of FLD is consider as very essential task, because with the help of proper treatment, disease incurred damage can frequently be

reduced. Presently, a variety of methods is used to analyse of FLD and these methods are classified into two types FLD invasive techniques and non-invasive techniques [23, 30]. However, one of the invasive techniques to diagnose a fatty liver is Liver biopsy [31-32]. Since Liver biopsy detects FLD more accurately but patients have also suffered from pain and discomfort due to this invasive technique [33]. Many other non-invasive diagnostic techniques for FLD are being used like Computed Tomography, Functional Magnetic Resonance Imaging but among all Ultrasound is most popular image modality for fatty liver disease diagnosis because it allows to conceptualize the human tissues without damaging them and it is inexpensive and also has high sensitivity [34]. These diagnosis methods are briefly explained in the following paragraphs with summary of their advantages and limitations. Different types of causes and diagnosis techniques are shown in Figure 1.3.

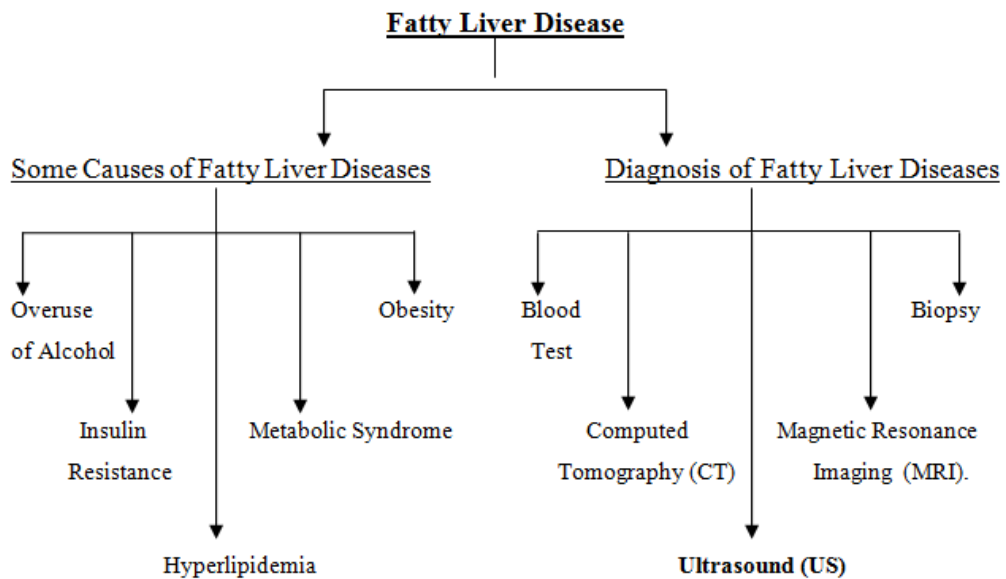


**Figure 1.3: Causes of Fatty Liver Diseases and diagnosis of FLD**

## 1.5 Computer Aided Diagnosis System

In therapeutic imaging and diagnostic radiology, Computer-Aided Diagnosis (CAD) has ended up a standout amongst the most important research topic [35]. It introduces the pattern recognition software that analyse suspicious features on the image and help the radiologists to solve the problem FLD. CAD system helps to increase the detection rate of identification of disease by reducing the false negative

rate and can be applied to digital images for the purpose of inscribing a variety of diagnostic problems. CAD technique reduces the pain and discomfort of the patient and also reduces the cost which is required at the time of treatments for liver diseases [36-37]. To develop the CAD system for Ultrasound images Texture analysis is required to extract various textural features [38].

“Texture is basically a property that signifies the area and structure of an image or it may also be described as a normal repetition of a component or example on a surface. Surfaces of an image are compound visual patterns that are made out of elements or areas with sub-patterns with the qualities of color, brightness, shape, size, etc.” A continuing texture in an image indicates a set of its features that are consistent, steadily changing or roughly regular [39]. Likewise, it might be viewed as a similar gathering in an image [40]. Texture analysis is one of the most important techniques in a range of applications, from medical imaging to remote detection. In texture analysis, the most important task is to extract texture characteristics that most thoroughly represent knowledge in the unique picture about the spatial distribution of gray-level changes. Various features have been investigated for diagnosis of FLD. These include “Spatial Gray-Level Co-occurrence Matrices (SGLCM) given by Haralick et al [41], Fourier Power Spectrum (FPS) given by Lendaris and Stanley [42]. Gray Level Difference Statistics (GLDS) are introduced by Weszka and Dyer [43]”. These all models are used to extract various features to analyse texture of the liver disease, then feature selection techniques is used to extract the best features among them all. In the last few years, various classification methods are used to characterize liver diseases. Classifier like Bayesian classifier, classification of liver ultrasound images using texture analysis with the help of Fuzzy logic [44-46], Neural-Network Based Classifier [47-49], Support Vector Machine (SVM) classifier [50-52]. In this thesis various feature extraction models and classifiers are used to propose a CAD system, which are briefly explained in chapter 3.

## **1.6 Liver Ultrasound Database**

In this research work, 90 ultrasound liver images are collected from Delta Diagnostic Centre Patiala, India. Out of 90 images, half of the images are of fatty liver. To create this medical image dataset, 90 patients (within the age group of 25 – 60 years)



has been examined by experienced radiologists. The ultrasound images are captured by ultrasound machine named as Voluscan730 PRO (General Electric Medicare). The machine works with the curved array probe of 68 mm at the frequency of 3.6 MHz. The Time Gain Compensation (TGC) setting is preserved in such a way that the degree of background grey is approximately the same across the depth. Patients are advised to prevent the effects of shifting liver glycogen and water storage on ultrasound imaging for the eight hours before ultrasound scanning. Experienced radiologists are requested to acquire the images and to label them as per the standard procedure.

## **1.7 Significance of the Proposed Research Work**

With the ultimate goal of processing and analysis of Ultrasound images this thesis makes some contributions that are closely related to the classification of liver ultrasound images for disease diagnosis. The *first contribution* is extensive literature survey done in the area of ultrasound imaging in which various existing approaches and methods have been studied and analysed in detail. The *second contribution* is related to speckle reduction and extraction of texture features from the region of interest using wide variety of texture models available in the literature as texture-based analysis is very useful in ultrasound tissue characterization. The *third contribution* has focussed on feature selection i.e. identifying and extracting the better features to capture the texture of images and improve correlation to the human visual similarity. The *fourth contribution* is based on use of different classifiers available in literature for the classification task with extensive parameter setting which is a unique kind of study in itself. For carrying out the proposed work, 90 ultrasound liver images have been collected from Delta Diagnostic Centre Patiala, India. The performance is evaluated using commonly used medical statistics: Sensitivity, Specificity, Accuracy and Area under ROC Curve.

## **1.8 Organization of Thesis**

The thesis is organized in five chapters. The **Chapter 1** gives the introduction of the research work and discusses the motivation behind the present research work. A brief literature review of the Medical Imaging and Fatty Liver Diagnosis has been

presented. A description of Image Database used in the proposed work and significance of proposed research work has also been discussed in this chapter.

**Chapter 2** gives a review of literature i.e. overview of Image Enhancement and various Computer Aided Diagnosis Systems for fatty liver. The significance and background of the various texture models are also discussed in this chapter. Performance indices used for evaluation are presented in this chapter. At the last of this chapter, research gaps and objectives of the research work are presented.

**Chapter 3** presents material and methods. In this chapter, the proposed methods for the classification of Liver Ultrasound images have been discussed. For the classification of liver ultrasound images, this thesis presents four different methods.

**Chapter 4** presents results and discussion. In this chapter various results of the proposed approaches have been discussed in detail. A wide variety of parameters have been used for evaluating the performance of the proposed methods.

**Chapter 5** concludes the research contributions and highlights the important findings based on the experimental analysis and observations. Scope for the future work and possible extensions to this work are also discussed in this chapter for the new researchers in this area.

## **Chapter-2**

### **Review of Literature**

#### **2.1 Introduction**

In medical field, liver plays a vital role in human body, as it maintains quality of blood as well as performs very important functions like storage of carbohydrates, excretion, fats and fatty acids etc. Liver also helps in filtering the harmful substances which may cause damage to human health and leads to liver diseases. However, liver diseases can occur due to alcohol consumption, taking drugs, by injury or by infection and as a result leads to liver failure, obesity, diabetes, blockage or damage [7]. According to the scenario, the most common example of liver disease which has been noticed worldwide is Fatty Liver Disease (FLD) or also known as Fatty Liver Steatosis, which cannot be recognized with very high accuracy [4, 6]. Fatty Liver Diseases are caused due to more gathering of fat content of hepatocytes in liver cells. The overuse of alcohol, insulin resistance, obesity, hyperlipidemia, metabolic syndrome are the main causes of FLD [2]. It is roughly calculated that it affects 15 to 24 percent of the world's population [4]. If FLD is not detected early, it may lead to cirrhosis, liver cancer, steatohepatitis or damage to the liver and acute liver failure. So, the early treatment and detection is important for the control of the FLD. For the identification of fatty liver diseases invasive and non-invasive techniques are available. The invasive involves liver biopsy whereas non-invasive diagnostic techniques involves functional Magnetic Resonance Imaging (fMRI), Computed Tomography (CT), Ultrasound etc. Invasive techniques detect FLD accurately but these techniques cause more pain and discomfort to the patients as compared to non-invasive techniques. Therefore, non-invasive is more preferable by the radiologists. Furthermore, Ultrasound is the most popular imaging modality for FLD diagnosis because it allows to conceptualize the human tissues without damaging them and at the same time it is inexpensive and has high sensitivity rate [7, 19].

As per author's knowledge, the ultrasound images show sensitivity of around 60% to 100% and specificity of around 75% to 100%. But this imaging modality is an

operational dependable which leads to failure. To reduce operational dependability and to get the consistent output, many CAD systems have been developed by scientists [8]. These systems reduce the pain and discomfort of the patient and also reduces the cost which is required at the time of treatments for liver diseases. To develop the CAD system for diagnosis of FLD, shape and texture analysis are used. However, in this thesis the major focus is put on the texture analysis of ultrasound images.

## **2.2 Ultrasound Image Enhancement**

Medical ultrasonic imaging uses pulsed acoustic waves which a handheld transducer transmits and receives. Ultrasound imaging is found to be established technology that has been used worldwide. Ultrasound imaging has lot of benefits that includes scalable, no ionizing radiation and cost effective that makes this technology affordable. But when the ultrasound signals propagate through tissues, the quality of image reduces.

### **2.2.1 Speckle Reduction Filters**

Speckle is a locally correlated multiplicative noise that has granular pattern, and this makes the visual quality of ultrasound image poor. Speckle also hinders the automatic image analysis task very difficult. Therefore, it is important to suppress the speckle noise in the preprocessing stages. The random variation in the power of the back scattered waves causes speckle noise. Speckle may contain some important information related to the diagnosis, but still it is treated as outlier because it considerably reduces the quality of image which leads to problems in discriminating fine details inside the images [53-54]. Work on the removal of speckle from ultrasonic images is narrowly divided into 4 categories:

- Homogeneity of pixels intensity
- Local statistics in a window
- Wavelet based filters
- Partial differential equation/an-isotropic diffusion-based filters

The research on speckle reduction from ultrasound images is broadly classified into four categories. The first one is based on local statistics in a window, second category

is based on homogeneity of pixels intensity, third is partial differential equation or anisotropic diffusion-based filters, and the fourth is wavelet based or other multi-resolution based filters. The early methods of speckle suppression from ultrasound images involved averaging the pictures of the same tissue that are uncorrelated and developed under diverse spatial points [55-56]. Even though these methods suppress speckle considerably, but multiple images of the same object are needed for the same [57]. A Partial Differential Equation (PDE) based *anisotropic diffusion* filter is used to remove noise from ultrasound images [58-59]. Yu and Acton have introduced Speckle Reduction Anisotropic Diffusion (SRAD) technique in which diffusion constant is replaced with “*instantaneous coefficient of variation*” as a function of local gradient magnitude and Laplacian of image [60]. However, for reference a uniform portion has to be manually selected which is dependent on the user. You et al. proposed Fourth-Order Partial Differential Equations (FPDE) for speckle removal [60]. With this method, speckle can be suppressed easily but the edges and some fine details are not maintained. Recently, a modified version of SRAD is also proposed by Mittal *et al.* which further enhances the visual quality of ultrasound images [62]. Many researchers have carried out a significant image enhancement work using wavelet transform to refine the ultrasound images [63-64]. Gupta *et al.* proposed a new speckle reduction filter called *Homo-Gentresh*, which is adaptive and versatile [65-66]. The method utilizes *Homomorphic* wavelet thresholding technique by modeling speckle as Generalized Nakagami distribution rather than Gaussian one. A collection of wide-band 2D directive filters based on modified Gabor function have been proposed by Dantas and Costa, in which, each filter works in a specific direction to refine the image with reduced speckle while preserving the resolution [67]. Gungor et al. speckle noise reduction method improved the performance of edge-sensitive filter [68]. The authors generated a homogeneity map based upon the local statistics of the window for every pixel in the image. Yang et al. proposed a hybrid technique in which considered a non-Local Mean filter and the local statistics of speckle for reduction [69]. Zhang et al. proposed a new method that applied the concept of wavelet and guided filter to liver ultrasound images for speckle reduction [70]. For performance evaluation, the authors have used clinical images, and further result analysis declared that the proposed method

has strong ability in removing the speckle noise by maintaining the fine details of the image that includes edges of the disease bearing region.

The de-noised findings of clinical medical ultrasound images indicate that the approach proposed not only has a good capacity to de-speckle, but also retains the specifics of the image, such as the edge of a lesion.

Most of the above said filters perform well in homogenous areas but they lack near the edges either by leaving the speckle near the edges or they blur the edges while filtering.

### **2.2.2 Relevant Literature on Speckle Reduction**

In the last few years, many investigators have proposed numerous approaches for speckle reduction. This section describes the latest work done in the area of speckle reduction.

In order to preserve the edges after image processing Gungor et. al. proposed the homogeneity map method [68]. The authors have applied edge and smoothing filters on the speckled image. The results obtained show that the proposed method ensures the effective performance.

A two low-rank approximation-based method has been proposed by Sagheer et al. for the despeckling of ultrasound images [71]. For performance evaluation the authors have used simulated and clinical ultrasound images. The performance has been evaluated by Peak Signal to Noise Ratio (PSNR), Structural Similarity Index Measure (SSIM), Edge Preserving Index (EPI) and Naturalness Image Quality Parameter (NIQE) parameters. The authors have compared the performance of proposed method with state of art methods.

Khvostikov et. al. have analysed the benefits of anisotropic diffusion speckle filtering method over the total variation method [72]. The introduced method results in speckle filtration without any additional parameters.

A new way, based on TV regularisation and updated bay shrinkage, was proposed by Elyasi et al. [73]. For performance evaluation, the authors used synthetic and real ultrasonic images. The results are compared with common filtering techniques

and a Wavelet domain technique as well as parameters such as PSNR, SNR, RMSE, SSIM, NSD, MSD and an average time to evaluate the quality of the image.

All the initial techniques for extracting speckles from ultrasonic images included averaging the images that are uncorrelated and collected in various spatial areas [74] Although these methods significantly suppress speckle, yet multiple images of the same object are required for processing [57]. An anisotropic diffusion filter based on Partial Differential Equation (PDE) is often used to eliminate speckle from ultrasonic images [58-59]. The Table 2.1 summarizes the literature review in terms of Speckle suppression technique used with their corresponding results.

**Table 2.1: Literature Review of Speckle Suppression Techniques**

<b>Ref. No</b>	<b>Year</b>	<b>Authors</b>	<b>Speckle Suppression Techniques used</b>	<b>Results</b>
[61]	2000	Kaveh et al.	Fourth-Order Partial Differential Equations (FPDE)	Speckle can be suppressed easily but the edges and some fine details cannot be maintained
[63]	2001	Achim et al.	Wavelet transform	The proposed approach is found to be expensive in terms of estimation of the distribution parameters at different scale on interest.
[60]	2002	Yu and Acton	Speckle Reduction Anisotropic Diffusion (SRAD)	In comparison to previous speckle reduction techniques, the proposed SRAD method is found to be good.
[64]	2003	Michailovich et al.	Wavelet transform	The output of the proposed algorithm is tested. It is shown that this algorithm,

				built on the basis of the "Gussian" reflectivity function, remains applicable to wider distribution classes
[65]	2005	Gupta et al.	Homo-Genthresh	Homomorphic wavelet thresholding technique was used by modeling speckle as Generalized Nakagami distribution rather than Gaussian one.
[67]	2007	Dantas and Costa	2D directive filters with modified Gabor function	Each filter works in a specific direction to refine the image with reduced speckle while preserving the resolution.
[62]	2010	Mittal et al.	Modified version of SRAD	Visual analysis by SRAD method of processed images reveals that speckles are minimized at the expense of object textures appearance.
[68]	2015	Gungor et al.	Edge-sensitive filter	In order to generate the homogeneity map local statistics of the window for each of the pixel has been used.
[69]	2016	Yang et. al.	Local statistics and non-local mean filter	The experimental results indicate that the proposed filters exhibit the best quantitative measurements (SNR, MSE, SSIM, and SV)



[70]	2016	Zhang et al.	Wavelet and guided filter	The experimental results show the good skill of the proposed system.
[75]	2017	Zhu et al.	Low-rank minimization Approach	The proposed method provides results that are better quantitatively and qualitatively.
[76]	2018	Dass R.	Wiener Filter and Discrete Wavelet Transform in Homomorphic Region	The findings show that the technique proposed is statistically as well as visually efficient in comparison with other techniques.
[77]	2019	Jubaiahmed et al.	Contourlet transform based anisotropic nonlinear diffusion filtering	The results indicate that the proposed technique has better noise removal performance.

In addition to the above-mentioned models, the models for speckle reduction i.e. total variation proposed by Rudin et al. [78] and anisotropic smoothing model proposed by Yu et al. [79] are found to be better as compared to other existing models. The wavelet-based techniques also play a major role in the speckle filtration. These techniques can be categorized as: (a) homomorphic filtering comprises of the wavelet filtering in the image-logarithm ascent to an exponential operation, (b) non-homomorphic filtering [80-81] screens the wavelet coefficients of actual image.

Singh et. al. proposed a hybrid algorithm to suppress the speckle and for denoising of ultrasound images [82]. The proposed algorithm performed better than other SR filter because it completely eliminates speckle noise by collecting local and non-local data. The effects of tests on synthetic, simulated and actual ultrasound pictures are used to check the condition. Compared with other common noise reduction methods, the proposed hybrid algorithm is present. The results verify that the proposed

hybrid model with reference to MSE, SNR, and MSSIM values exhibits the best denoising efficiency. It is further observed that the proposed algorithm may retain the contrast level in denoted ultrasound images during de speckling.

Roy et al. al. suggested a novel technique to de-noise the speckle that affects the properties of fuzzy set theory [83]. The definition of degree of conformity not only effectively separated the speckle structures from the edges of the Ultrasound images from the blurry and blurred structures, but also retained the organ structural details in photographs. The performance in terms of less computational time of the proposed filter is observed as better than all other filters used in speckle denoising in Ultrasound images except the SRAD filter, with least computational time.

Deka et al. shows the potential for incomplete and over-complete representations to de-speck photographic and actual ultrasound images distorted by correlated speckle noise [84]. The approach proposed goes through two stages. The authors have used K-SVD based denoising approach, in which they have combined this approach with a simple noise estimation method in order to remove the noise from the ultrasound images. The results depict that the proposed method performs better in terms of visual and quantitative aspects as compared to the well-known available spatial domain filters.

Arnal et al. suggested parallel strategy where the de-speckling algorithm parallels multiprocessor shared memory with OpenMP and multicore cluster using a hybrid combination of MPI and OpenMP [85]. The experimental results show that the due to use of parallel implementations there is a significant speedup in the process that results in reduced computational time.

Frequency Equalization Compounding (FEC) technique proposed by Yoon et.al. successfully aims at enhancement of contrast in abdominal imaging [86]. As a result of weighting factors and frequency dependent attenuation for each sub-band, the proposed study focusses on the estimation of the center frequency downshift. These estimated results can be employed in dynamic quadrature demodulation and image compounding. The study results are verified by using in vitro phantom and the in vivo studies and it is observed that proposed method shows merits over the classical FC methods.

Zhu et.al suggests an optimization method with simultaneous preservation of features in ultrasonic images to eliminate speckle noise from the ultrasound pictures [87]. With the feature asymmetry metric, the proposed study applies various restrictions in features and speckle noise. The study is effective in separating the speckle noise and features by using the theory of phase congruency in US images. During comparison with the traditional gradient-based metric the proposed study is found to be more reliable to the huge differences in image contrast.

Gupta et.al in their study of despeckling techniques in ultrasound images observed that after using the combination of NSST threshold approach along with nonlinear modified anisotropic diffusion equation despeckled images are obtained with better output in terms of noise suppression and edge preservation [88]. In the proposed study, the noise components with larger amplitude are reduced with the help of diffusion process on low- frequency approximation coefficients and thresholding, thereby increasing denoising performance with improved preservation of edges.

Adaptive Fast Bilateral Filter (AFBF) created on local characteristics to reduce the speckles and enhance the accuracy of ultrasound images, was proposed by Shao et.al [89]. The filter was proposed keeping into account the fact that for better diagnosis suppression of noise and preservation of structure is very crucial in post processing techniques. The proposed filter has been derived from the conventional filter. In order to separate the speckle from the tissue structure a local characteristic matching method has been used by the authors. Analysis in phantom and in vivo imaging shows that the method can preserve the structure efficiently and reduce the noise in the images.

The results of the disease diagnosis from ultrasound images can be improved by reduction of speckle noise. The authors proposed an innovative approach for measuring the performance of the suggested approach by using 2D FIR filter with the ABC algorithm to reduce the speckle noise by calculating MSE, PSNR and SNR values [90]. The proposed system was tested with synthetic image, fetal ultrasound images and clinical noisy ultrasound images. The image denoising was accomplished profitably by using a population based computational scheme. The greatest improvement of the proposed system is that it is very easy to implement, and better results can be obtained.

## 2.3 Texture Analysis and Liver Tissue Characterization

Texture is a complex visual pattern which is composed of objects that are grouped together based upon attributes such as size, brightness, slope, colour, etc [91]. Russ et al. has defined the texture as variation in local brightness from pixel to pixel in a small region in an image [92]. Texture models are usually classified into four classes; *structural*, *statistical*, *model-based* and *transform methods*.

### 2.3.1 Structural Texture Model

In this model, the texture is composed of texture elements (primitives) such as similar pattern lines which are finely defined in an image [93-94]. For proper description of the texture, placement rules for the primitives needs to be well defined. The benefit of the structural model is that the representative details of the image can be simply understood [95]. However, structural texture techniques can only describe regular texture patterns, which limit their applicability [96].

### 2.3.2 Statistical Texture Model

*Statistical texture model* describes a set of useful techniques that portray the texture of a region by calculating the higher-order moments of the grayscale histograms from the image [97]. These techniques represent the non-deterministic characteristics that maintain associations between the grey levels of an image. In grey-level images, the textures differ largely in their second order moments. Spatial Gray Level co-occurrence Matrix (SGLCM) is the most accepted second order statistical feature for texture analysis [98]. Similarly, Grey Level Run Length Matrix (GLRLM) symbolizes rough textures that have many pixels in a constant gray level run and fine textures are characterized to have many few pixels in gray level run length [94]. The basic working of GLRLM lies on the calculation of higher order statistics of the gray level histogram.

### 2.3.3 Model based Textures

The *Model based* texture analysis makes the most of the inter-pixel relationship: a weighted average of the intensities of the pixels is calculated that lie in its neighbourhood. The parameters estimated from the image model are the descriptors of the textural feature. Few examples include the Fractals and Markov Random Fields (MRF). Stochastic and Fractal model attempt to characterize image texture by using a

generative image model and stochastic model respectively [99-101]. The fractal model is commonly used for natural texture Modeling.

#### 2.3.4 Transform based Texture Model

*Transform Texture* models include the Fourier model [91], Wavelet transforms and Gabor [102]. In these models an image is represented in a co-ordinate system that matches to the characteristics of a texture (such as frequency) [103-104]. In other words, a new image is created using spatial frequency properties of the variations in the pixel intensities. Features that are derived from a set of Gabor filters are widely used for image segmentation [105].

“The ultrasound quantitative tissue characterization is an image processing technique, which reveals the hidden patterns to extract more information about tissue function and pathology than it is being observed through visual analysis [106]. Initial research in the area of tissue characterization to detect cirrhosis in the liver, had been done by Wells and Mountford [107-108]. In a significant research by Chivers and Hill, a scientific technique is used to retrieve the quantitative data from the tissue using scattering [109]. Since then, this branch of medical ultrasound has undergone considerable development. A lot of methods for Ultrasound Tissue Characterization (UTC) have been proposed and they are broadly classified into three categories [110].” These characterization techniques are (i) Radio Frequency (RF) analysis using spectral analysis of RF signals, (ii) Elastography of the tissue and (iii) Texture analysis of ultrasound images. The first category is based on RF signals that are received from the beam former before they fetched to display system. The second category is tissue characterization through *elastography*. In this imaging process brightness of the image depends upon the stiffness of tissue. An ultrasound probe emits vibrations that cause a shear wave in the liver, which corresponds to liver stiffness [111]. In another study, Fukushima et al. measured liver elastography in patients with Non-Alcoholic Steato-Hepatitis (NASH) and demonstrated that liver elasticity is able to predict the fibrosis [112]. However, this method has a limited sensitivity and specificity, as shown by the Lewis. According to him, the modality was able to differentiate various stages of liver fibrosis with sensitivity of 86% and specificity of 85% [111]. Although RF signal-based liver tissue characterization is used by number of researchers [106, 113-114], but most

of the researchers have used the third type of tissue characterization technique for liver; the texture analysis [115-119]. The main reason for this choice is that, when steatosis occurs, the liver surface changes significantly. This variation in the surface of liver makes the texture analysis a suitable tool to analyse this organ. Moreover, the texture analysis is directly related to the visual features in the ultrasound image, and radiologists are comfortable to correlate the texture features with the visual information. The texture analysis is very useful to characterize the liver because of its size and the quasi-periodic scattering structures found throughout the healthy tissue [119]. It has been established that, texture analysis-based liver classification and liver tissue characterization methods outperform other techniques [116-118].

Many feature models are available for the classification of the liver tissue (normal and abnormal) from an ultrasound image [120]. The most common texture feature models include: The SGLCM by Haralick [98], the TEM proposed by Laws [121], and the FPS by Landeris [42]. These models have been effectively applied to many real-world texture identification problems. The Statistical Feature Matrix (SFM) is also a useful texture model used to identify surface textures [120]. Weszka and Dyer proposed a Grey Level Difference Statistics (GLDS) for classification of terrain mainly through texture analysis [43]. Mandelbrot proposed fractal-based features for the identification of roughness in natural surfaces. Wu et al. proposed Multiresolution fractal dimensions also called Fractal Features (FF) which utilizes previously mentioned texture models for liver tissue classification [122]. Thijssen et al. concluded high significance of SGLCM parameters for the characterization of the ultrasound images [106].

## **2.4 Computer Aided Diagnosis of Liver Ultrasound Images**

In the field of diagnostic radiology and imaging, Computer-Aided Diagnosis (CAD) research has evolved at greater pace in recent years. It introduces the pattern recognition software that analyses suspicious features on the image and helps the radiologists to solve the problem of fatty liver disease. The CAD systems aim to increase the detection rate of a disease by reducing the false negatives. CAD systems can be applied to digital images for the purpose of inscribing a variety of diagnostic problems. CAD technique reduces the pain and discomfort of the patient and also reduces the cost which is required at the time of treatments for liver diseases. To develop the CAD system

for Ultrasound images texture analysis is required to extract various textural features. Texture signifies the structure and surface characteristics of an image usually described as a regular repetition of a pattern on a surface. Textures of an image consist of complex patterns varying in brightness, color, shape, size, etc. A texture is said to be constant if its characteristics are constant otherwise, it is gradually changing. Foremost, texture features are extracted completely represent the distribution of spatial information of gray-level in the original image. Various features have been investigated for diagnosis of FLD. The brief summarization of related researches is as shown in Table 2.2.

**Table 2.2: Literature Review of Computer Aided Diagnosis of Liver Ultrasound Images**

Ref. No	Year	Source	Ultrasound images Used		Image Size in pixels	Feature Extraction	Feature Selection	Classifier	Accuracy Rate
			Normal	Fatty					
[126]	2007	Chittaranjan National Cancer Institute, Kolkata	76	24	NA	SGLDM	Student's t test	Neural Network	NA
[127]	2009	Not mentioned in the paper	42	42	256×256	GWT	NA	FFNN and BPNN	94%
[26]	2008	Municipal hospital	25	68	767 × 572	GLCM, NFLSD, NGTDM and NFFGR	Statistical	SVM	97%



[34]	2009	US Modality in a hospital	10	10	NA	RF and Speckle image.	NA	Naive Bayes	95%
[118]	2012	Multan Institute of Nuclear and Radiologists	39	30	560×450	WPT & DWT	NA	SVM, v-LSVC	95%
[116]	2012	By radiologist in a hospital	42	58	1024 × 1024	GLCM, GLRLM, HOS based features, and DWT.	NA	RBPNN, K-NN, Naive Bayes	93.30%
[128]	2012	DDC, Patiala & PGIMER Chandigarh	15	15	640×480	SFM, TEM, SGLCM, FPS	FDR	Bayesian classifier.	92%
[21]	2014	DDC, Patiala & PGIMER Chandigarh	90	90	640×480	GLDS, FOS, FPS, SGLCM, SFM, TEM	FDR AND PCC	Information fusion-based classifier	95%

[45]	2016	University of Malaya Medical Centre, Malaysia	50	50	1024 × 1024	GIST descriptor models	ROC, Student's t-test, Bhattacharyya distance, Wilcoxon signed-rank test	AdaBoost classifier, Decision tree, Discriminant classifier, Naive Bayes, Probabilistic Neural Network, Support Vector Machine, K-Nearest Neighbour	98%
[146]	2017	Taba Imaging Center, Iran	28	47	768 × 1024	GLCM and Wavelet Packet Transform (WPT)	NA	SVM	94.91%
[147]	2018	Asian Institute of Gastroenterology, Hyderabad, India	196	173 Grade I, 157 Grade II and 124 Grade III	NA	Curvelet transform and SVD	NA	Cubic kernel SVM and K-Nearest Neighbor	96.90%

[142]	2018	University of Malaya Medical Centre, Kuala Lumpur, Malaysia	78	62	256 × 256	bi-directional empirical mode decomposition and Radon transform	Particle Swarm Optimization	Probabilistic Neural Network	92.95%
[148]	2018	Delta Diagnostic centre, Patiala & PGIMER Chandigarh	45	45	NA	FPS, SFM, SGLCM, GLDS, FOS, TEM, FF.	Mutual Information	SMO, IBk, AdaboostM1 and BF Tree	95.55%
[37]	2019	Faculty of Medicine, Cairo University	25	32	768 × 1366	First-order gray level parameters, GLCM, Local binary patterns	Wilcoxon rank-sum test	kernel-based SVM, s kNN, linear SVM, and LDA	98.80%
<p><b>Note:</b> - NA stands for Not Applicable</p>									

### **2.4.1 Previous Work in Processing and Analysis of Liver Ultrasound Images**

Computer Aided Classification methods are being used since 1972 when Mountford and Wells classified normal and abnormal liver using A-mode ultrasounds [107-108]. Later on Yajima et al. in 1983 performed a research for liver classification using different classifiers on ultrasound images through texture features [123]. He revealed that liver classification using computer aided methods have more than 90% accurate. Since then many researchers have used B-mode ultrasound images for liver tissue classification.

Weszka et al. compared three standard approaches that are used for automatic texture classification and basically two sets of terrain samples were used to classify [43]. Texture features were extracted by the various feature extraction models like Fourier Power Spectrum, First Order Statistics of Gray Level and Second Order Gray Level Statistics differences. In this study, work was done to find feature sets with respect to their orientation and size sensitivity. The author used a set of fifty-four aerial photographic terrain samples that belong to nine land use classes and also a larger-scale study has been done by using 180 LANDSAT non-imagery samples from 3 geological terrains. In a result it has been found that the FPS features did not performed well while the other additional feature sets all performed comparably and this was also the limitation of the paper.

Kadah et al. proposed tissue classification algorithm for diffuse liver classification from ultrasound images [115]. The data set consists of total 120 images and these 120 were divided into two equal size training and testing dataset. The performance of several classifiers like Statistical classifier and neural classifier are evaluated which provide good results. This paper has proposed feature extraction algorithms for extraction of parameters such as First and Second Order Gray Level, Backscattering Coefficient and Attenuation and Backscattering from liver images. The results obtained from the neural network classifier gave 100% sensitivity of fatty liver images. The hardware implementation was demanded to be made simple for easier tissue analysis of ultrasound images.

Badawi et al. made use of Fuzzy logic-based algorithm for classification of tissue in diffuse liver diseases from ultrasound images [44]. In this paper, a fuzzy approach

is applied for automatic segregation of diffuse liver diseases. It extracted numerical quantitative features from the ultrasound images. There were 140 cases of normal, cirrhotic, fatty liver from which fuzzy rules are generated for differentiation of cirrhotic liver from normal liver. In this study, the fuzzy system outcome is obtained on the basis of three main categories: normal cirrhotic or fatty and the steps were taken for differentiating the pathologies by dividing the input spaces of the data into fuzzy sets. This approach demands expert knowledge for generation of fuzzy rules and the fuzzy inference procedures for pathology determination. As a result, the sensitivity and specificity is much higher than the statistical methods which is also as good as the neural networks techniques.

Palvopoulos et al. proposed a Fuzzy Neural Network based texture analysis [124]. The dataset of total 150 images were used and the 32 by 32 pixel ROI were selected from each images. In this study two main steps is performed firstly, tissue characterization features extraction basically five techniques and models like Spatial GLCM were used for feature extraction. Secondly, the classification of fatty and normal liver is done by using a fuzzy neural network classifier. The Voronoi diagram obtained from the training patterns were used for the creation of fuzzy sets and building of class boundaries. In this due to large number of different subset combinations the result leads to accuracy rate of greater than 75% of correct classification.

Chen et al. proposed an Automatic Diagnostic System (ADS) for CT Liver Images Classification that classify liver diseases by finding CT liver boundary automatically [125]. In this paper, the system contains a Detect-Before-Extract (DBE) for liver boundary identification. A neural network classifier was applied to distinguish two liver tumors namely hemangioma and hepatoma. In this study, normalized Brownian motion model in DBE system is applied liver boundaries and deformable contour model was used to outline the liver boundary. The proposed system consists the dataset of 30 liver cases. As a result, the classifier Multi-Probabilistic Neural Network (MPNN) is not always produce optimal results in every application and can be replaced by a better system. The limitation of this paper was it is not necessary that MPNN provides optimal results in all applications.

Mukherjee et al. proposed a classification of normal and fatty ultrasound liver images which relied on spatial pattern of echogenicity and echoes [126]. This was a subjective method for classification. A dataset of 100 ultrasound human liver images have been taken from hospital in this work. To generate profile plots a Self-Organizing Map (SOM) was used as a classifier. In this paper, the author analyzes the pattern content in both fatty and normal livers diagnosis with the help SOM algorithm. In this study each individual feature Student's t test is calculated to differentiate among the results obtained from fatty and normal livers. Based upon the statistical distribution, the two components such as maximum probability and uniformity of the feature vector are identified to be most distinguishing. In this work, the best results for classification after statistical texture analysis were obtained by using "Maxp" and "Uni" of the ultrasound human images.

Li et al. proposed a Support Vector Machine (SVM) based CAD system for Fatty Liver Ultrasonic Images [26]. A database of total 95 ultrasound images was used. Out of these 95 ultrasound images, 25 normal liver and 68 fatty liver cases were used for training and testing purposes. This study presented classification of normal and fatty livers with high recognition rate. In this paper, Near-Field Light-Spot Density, Near-Far-Field Grayscale Ratio, Neighborhood Gray-Tone Difference Matrix (NGTDM) and Grayscale Co-occurrence Matrix features were extracted. RBF kernel was used in SVM classifier and the accuracy obtained from the classification rate of normal 87% and fatty liver 97.1%.

Ribeiro et al. presented a Quantitative Tissue Characterization Technique (QTCT) technique for detection of FLD in ultrasound liver images [34]. All images were stored in DICOM format. In this study features were selected in such a way that as same characteristics are selected by the physicians in the diagnosis of the disease. For the diagnosis of the liver steatosis from ultrasound images, the author presented an automatic classification algorithm that applied Naive Bayes classifier for fatty liver characterization and the overall accuracy leads to 95% and 100% sensitivity.

Sriraam et al. has presented a performance evaluation of CAD tool for diagnosis of Ultrasound Liver Disease [127]. The proposed CAD tool applied Gabor wavelet transform to compute statistical features for segmentation of image into sub block for

proper analysis. In this study, out of 42 images, 20 training images and 22 were used for testing. Classification was performed using a Back Propagation Neural Network (BPNN). With BPNN classifier, accuracy of 96.8% was obtained.

Afsar et al. proposed a novel automatic method for classification of liver tissue [118]. The proposed system selects a characteristic Region of Interest (ROI) from an image automatically. In this study, total 88 cases ultrasound images were acquired from MINAR. Statistical features were extracted by using Wavelet Transform (WT) and also ROI of an image was analyzed. In this study an effective method, WT with multi-scale analysis capability is used for FLD detection using features that measure variations in echogenicity, homogeneity and granularity of ultrasound. Classification process was carried out by v-Linear Support Vector Classifier (v-LSVC). The proposed system produced a 95% accuracy. In future, work on larger database of liver images needs to be done. The work can be extended in future by using features that are based upon the differences in echogenicity of the liver from renal and spleen cortex.

Singh et al. presented a new metric of classification of Liver Ultrasound Images [128]. A set of 30 ultrasound images were taken to evaluate the performance of proposed metric. Out of which 15 images are used as normal liver and rest of the 15 images were taken as fatty liver images. A ROI of size  $30 \times 30$  was selected along the central line of the image. In this study, five texture models were used for extraction of texture features. Fisher's linear discriminative analysis was applied to extract the best features. Furthermore, the selected features are then aggregated into a single metric by taking into consideration the weightage identical to the visual principal that is used for liver classification. The proposed method gave 92% accuracy and 100% sensitivity. The main drawback of the proposed study is that the criterion used for characterization is very much machine dependent.

Acharya et al. presented a fatty liver classification framework by taking three feature models into account for feature extraction and also used directly B-mode ultrasound images for feature extraction [116]. The author used total 35 ultrasound liver images for classifier development and evaluation. In this paper, Probabilistic Neural Network (PNN) and K-Nearest Neighbor (K-NN) classifiers were used that gave 93.3% accuracies with a small sample size, balanced sensitivity 94.4% and the specificity

91.7%. The proposed classifier has some advantages like easy to implement, less complex, faster diagnosis and no additional cost required to build classifier. The main drawback was that the type of distortion was chosen manually by physician and hence the process was not completely automated.

Singh et al. presented a method based on fusion of information using texture analysis of ultrasound images [21]. In this study, seven models are used to extract texture features. By using these seven models total 35 texture features were extracted. Out of these 35 features the best 7 features selected. The process of categorizing the fatty and normal liver are carried out in two steps firstly the best texture features are identified and secondly the information fusion of these best features, a new classification method is proposed and a linear classifier is used for fusion of selected feature. In this paper, whole process contains less time and low complexity and as a result the accuracy and sensitivity leads to 95% and 100%. In future, sub-classification of fatty liver as 'low', 'moderate' and 'severe' needs to be explored with the proposed method. Further, application to other general classification problems can also be done for an annotated dataset.

Acharya et al. proposed a classification technique of fatty and normal liver [129]. Discrete Cosine Transform and Radon Transform were used in this method. The extracted features are then fed to minimum Redundancy and Maximum Relevance (mRMR) ranking method. The dataset included images of both normal and fatty livers that were acquired by expert in University of Malaya Hospital, Malaysia.

Saba et al. proposed a computer-based detection system for the Fatty Liver Diseases [130]. For carrying out the experiments the authors have selected 124 images from a ultrasound database consisting of cancerous and normal images of 62 patients. 6 sets of features namely Basic geometric, Fourier transform, Haralick, Gupta transform, Discrete Cosine Transform and Gabor transform were used. Back Propagation Network (BPN) classifier was for classification of images as normal and abnormal.

Acharya et al. proposed an approach for the classification and detection of steatosis from ultrasound images [45]. For feature extraction the authors have used



GIST descriptor models. In order to identify the highly discriminating features, Marginal Fisher Analysis (MFA) along with Wilcoxon Rank test has been used. Finally features are fused together by using variety of classifiers such as Linear Discriminant Analysis (LDA), Support Vector Machine (SVM), AdaBoost, K-Nearest Neighbor (K-NN), Probabilistic Neural Network (PNN), Decision Tree (DT), and Naïve Bayes (NB) for classification of liver images.

Singh et al. [21] proposed a method based on an information fusion for liver classification using texture analysis of ultrasound images. Seven different models have been used in this paper to extract 35 texture features. On the basis of Linear Discriminative Analysis (LDA) and Pearson's Correlation Coefficient (PCC) feature selection techniques best seven features were extracted. The process of categorizing the fatty and normal liver are carried out in two steps firstly the best texture features are identified and secondly the information fusion of these best features, a new classification method is proposed and then by using a linear classifier, fusion of selected features take place. In this paper the accuracy and sensitivity lead to 95% and 100%.

Acharya et al. [116] presented a data mining framework for classification of ultrasound fatty liver diseases. In this study, author takes three feature models into account for feature extraction and also used directly B-mode ultrasound images for feature extraction. The author used total 35 ultrasound liver images for classifier development and evaluation. In this paper K-Nearest Neighbour (K-NN) and Probabilistic Neural Network (PNN) classifiers are used that gave 93.3% accuracies with a small sample size, balanced sensitivity 94.4% and the specificity 91.7%.

Li et al. [26] proposed CAD of Fatty Liver Ultrasonic Images which is based on SVM. The database of total 95 ultrasound images were obtained from the local hospital. This study presented categorization of fatty and normal livers at immense recognition rate and also SVM is used as classifier for characterization of fatty and normal ultrasound livers images. In this paper features were extracted from Near-Field Light-Spot Density (NFLSD), Grayscale Co-occurrence Matrix and Near-Far-Field Grayscale Ratio, Neighborhood Gray-Tone Difference Matrix (NGTDM). As a result, the classification accuracy rate obtained by the normal liver is 84% and fatty liver is 97.1%.

Ribeiro et al. [34] presented characterization and classification of FLD by ultrasound. In this paper Quantitative Tissue Characterization Technique (QTCT) is used for significant features and for detection of FLD in ultrasound liver images. In this study, to select different features the physicians used similar characteristics in the diagnosis of the disease. For the diagnosis of the FLD from ultrasound images, the author presented an automatic classification algorithm. Naive Bayes classifier is used for fatty liver characterization and classification and the overall accuracy leads to 95% and 100% sensitivity.

Singh et al. [128] has presented Liver Classification from Ultrasound Images based on new quantitative metric. A set of 30 ultrasound images were taken to calculate the performance of proposed metric. In this study, author selected ROI of size 30×30 onward the middle line of the image. In this work, five different texture models are used to extract various texture features and the best features are then selected on the basis of fisher's linear discriminative (FLD) analysis. The overall accuracy obtained 92%.

Mukherjee et al. [126] proposed the subjective classification of fatty and normal ultrasound liver images on the basis of spatial pattern of echoes and echogenicity. A dataset of 100 ultrasound human liver images have been taken from hospital in this work. To generate profile plots a Self-Organizing Map (SOM) was used as a classifier. In this work the best results obtained from the statistical texture analysis by using “Maxp” and “Uni” of the ultrasound human images.

Sabih et al. [118] proposed a novel method for Automated Classification of Liver Disorders using Ultrasound Images. In this work, the proposed system automatically choose an illustrative Region of Interest (ROI) in a liver ultrasound for diagnosis. In this study total 88 cases were taken for classification of liver disorder. A number of statistical features are achieved by using Wavelet Packet Transform (WPT) and also ROI was analyzed by the author. The overall accuracy of 95% is obtained by the system.

Sriraam et al. [127] presented a CAD Tool for Detection of Ultrasound Liver Disease. The proposed CAD tool contain Gabor wavelet transform to compute statistical features. In this study out of 42 images, 20 images are taken for training and another 22 images are used for testing. Classification is done by a Back Propagation Neural Network

(BPNN) and feed-forward neural network model. By using BPNN classifier 96.8% accuracy obtained and 94% accuracy obtained by multi classification.

Krishnan et al. have proposed a classification system for liver Ultrasound images based on Grey Level Run Length Matrix based features [131]. For classifying the images, the Support Vector Machine Classifier has been used. The authors have also analyzed the performance of linear, non-linear and diffusion filters for improving the quality of images.

Virmani et al. proposed a system to characterize liver ultrasound images into normal liver, cirrhotic liver and hepatocellular carcinoma [132]. The authors have used multiresolution wavelet packet texture descriptors for texture representation of Region of Interest and feature selection has been done with Genetic Algorithm. For classifying the images, Support Vector Machine classifier has been used.

Jeon et al. have proposed a new multiple Region of Interest based liver ultrasound image classification [133]. The authors have extracted features to represent the various characteristics in the image. For classification purpose, Support Vector Machine with Sigmoid Function has been used.

Singh et al. presented a classification approach based on texture analysis of Liver ultrasound images in which they have used seven different texture models to represent the texture of Region of Interest [134]. Feature selection has been done by Linear Discriminant Analysis (LDA) and Pearson Correlation Coefficient (PCC). Finally, the authors have classified the images using the proposed information fusion-based classifier.

Acharya et al. proposed a novel approach to classify normal, FLD and cirrhotic liver based on Curvelet Transform and different entropy features [135]. Probabilistic Neural Network (PNN) classifier has been used for the classification purpose.

Saba et al. have used six set of features comprising of 128 features in total for the classification of liver ultrasound images into normal and abnormal categories [136].

Back Propagation Neural Network (BPNN) has been used for the classification purpose.

An integrated index to classify the liver ultrasound images has been proposed by Acharya et al. [137]. For feature extraction the authors have used Radon Transform (RT) and Discrete Cosine Transform (DCT). Further, Locality Sensitive Discriminant Analysis (LSDA) has been applied to reduce the number of features. Afterwards, the highly ranked features are fused by means of Probabilistic Neural Network (PNN), Decision Tree (DT), Support Vector Machine (SVM), Fuzzy Sugeno (FS), K-Nearest Neighbour (K-NN) and AdaBoost classifiers for getting the better performance.

Xu et al. proposed a CAD system to distinguish liver ultrasound images in two categories based on texture features and SVM classifier [138]. For feature extraction the authors have employed GLCM model and GLRLM model to extract 96 features in total.

Amin et al. proposed a computationally efficient technique for the classification of liver images [139]. For extraction of features Wavelet Packet Transform (WPT) has been used and classification has been done with several classifiers that include kNN, linear SVM, kernel-based SVM and LDA.

Krithiga et al. have proposed an automated classification technique based on the texture and wavelet domain features [140]. For feature selection the authors have employed Correlation based feature selection method and finally classification is done using random forest-based learning.

Recent studies for the classification of fatty and normal liver ultrasound images using different texture features and classifiers can be found in [141-145].

## **2.5 Performance Evaluation Metrics**

The performance of classification methods is evaluated by Receiver Operating Characteristics (ROC) analysis through *Specificity, Sensitivity and Accuracy* [123-125]. This analysis is based on the number of correct instances in each class out of total instances. The True Positive (TP) is the number of instances when the disease is correctly detected. The False Positive (FP) is the number of instances when the patient

does not have the disease but it was detected as disease. False Negative (FN) is the number of instances when the patient has the disease but it was not detected. In medical related classification methods, this number is very critical, because if some method has even a single instance in FN then it means the method may miss the detection of disease, which is not at all desirable in medical imaging. The True Negative (TN) is the number of instances when the disease is not present and the method also recommend the same. All these terms are represented in Table 2.3. On the basis of this formulation, the following terms are used to indicate the performance of classification method.

“*True Positive (TP)*: Ultrasound Image classified as fatty that proved to be fatty.”

“*False Positive (FP)*: Ultrasound Image classified as fatty that proved to be normal.”

“*True Negative (TN)*: Ultrasound Image classified as normal that proved to be normal.”

“*False Negative (FN)*: Ultrasound Image classified as normal that proved to be fatty.”

**Table 2.3: Evaluation of Classification Accuracy**

		Is the liver ultrasound fatty?	
		Yes	No
Did the test indicate the Presence of dense tissue?	Yes	True Positive (TP)	False Positive (FP)
	No	False Negative (FN)	True Negative (TN)

**Sensitivity**, also called True Positive Fraction (TPF) is defined as the ratio of “number of correct positive assessments to the number of truly positive cases”.

$$Sensitivity = \frac{TP}{TP+FN} \quad (2.1)$$

**Specificity** or True Negative Fraction (TNF) is defined as the ratio of the number of correct negative assessments to the number of truly negative cases.

$$Specificity = \frac{TN}{TN+FP} \quad (2.2)$$

**Accuracy** is defined as the ratio of “number of correct assessments” to the “total number of cases”.

$$Accuracy = \frac{TP + TN}{TP + FP + TN + FN} \quad (2.3)$$

“ROC-AUC is a good indicator for evaluating efficiency of the classifier. AUC reflects the overall accuracy of a test, with an average value of 1.0 suggesting a high sensitivity and specificity. The AUC value 0.5 does not implies any discrimination. 100 per cent sensitivity means that all positive images are classified as positive, i.e. fatty images are recognised as fatty. Specificity is related to the capacity of the classifier to distinguish the negative cases.”

## 2.6 Research Gaps

In the medical field, images, and especially digital images, are produced in enormous quantities and are used for diagnostics and therapy. Due to non-ionizing property, portable, real time imaging and low-cost Ultrasound Imaging has been widely used.

A review of related work in processing and analysis of ultrasound images has been done. From the literature survey it has been found that in recent years many approaches have been proposed for the analysis of ultrasound images and major work has been done in the area of Computer Aided Diagnosis of fatty liver (Steatosis). From the literature survey it has been found that the subjective evaluation of liver ultrasound images is less accurate and highly dependent on the experience of radiologist.

The visual criteria for separating fatty liver and normal liver are usually subjective. Diagnosis primarily relies on the radiologists' ability to analyse and compare differences in textural properties in the image. Homogeneity and echogenicity are examples of these characteristics. It has been found that different radiologist's sometimes have different interpretation for the same image.

However, the echogenicity concept was widely discussed by experienced radiologists, particularly in marginal cases, through visual analysis of pictures. Diagnostic accuracy is currently estimated at approximately 72 percent by visual interpretation [2]. The low precision of visual perception further raises the need for objective methods for the liver classification based on quantitative texture analyses.

Much research was carried out in the field of liver characterization using ultrasound imaging. There are numerous methods of quantitative liver characterization, such as back-scatter Radio Frequency (RF) and an analysis of attenuation, elastography etc. but the most reliable technique is texture analysis. A large number of texture models have been used for Ultrasound Tissue Characterization including the “Spatial Gray Level Co-occurrence Matrix (SGLCM), Law's Texture Energy Measure (TEM), Grey Level Difference Statistics (GLDS), Fourier Power Spectrum (FPS), Statistical Feature Matrix (SFM), First Order Statistics (FOS) and Grey Level Run Length Matrices (GLRLM).”

The features extracted by above-mentioned texture models are used with various classifiers. Each classifier exhibits its own merits and demerits. The more precise methods are computationally expensive, whereas methods that are easier are not very much accurate. It has been found that main issues are involved in the processing and analysis of ultrasound images that includes extraction of Region of Interest, feature extraction, selection of highly discriminating features and type of classifier. In view of the above, a quantitative, improved method needs to be established that gives reasonably high accuracy with less computational load.

## **2.7 Objectives of the Proposed Work**

Keeping in view of the above research gaps, the following objectives are defined:

1. To study and analyze various speckle reduction methods and quantitative texture analysis methods for Ultrasound liver tissue characterization.
2. To propose a speckle suppression filter that enhances the edges and fine details in the ultrasound images.
3. To propose a method to help the radiologists in characterizing the fatty liver more accurately and fast.
4. Performance evaluation of the proposed speckle suppression filter and liver tissue characterization method on Ultrasound images through visual analysis by the expert radiologists as well as through quantitative metrics.

## **2.8 Conclusion**

In the domain of medical imaging informatics, a large amount of image data is being produced from different medical imaging modalities. Effective methods are required to manage these complex images. In the recent years, a lot of work has already been done to improve the performance of Computer Aided Diagnosis methods. Each method has its own advantages and limitations.

In this chapter a comprehensive survey of related work and a description of the mathematical models used to achieve the proposed goals has been done. Various speckle reduction techniques have been studied to identify the best method. Different texture domain models have also been studied and analyzed to find the optimal set of features for liver tissue characterization.



## **Chapter-3**

### **Material and Methods**

#### **3.1 Introduction**

The present research work has focused on liver ultrasound images for the classification of fatty liver images and normal images. Among all the liver diseases, fatty liver disease (steatosis) is a highly prevalent illness of all liver problems in India and Western countries. Radiologists primarily measure the fatty tissue by a highly subjective visual interpretation of the ultrasound image of the liver. Automatic methods of image classification seek to emulate such a visual decision and classify images based on the underlying characteristics of the textures. With widespread acceptance of ultrasound imaging as a tool, there is a need to process images efficiently using techniques of computer vision. In this chapter, four different methods have been proposed for the classification of liver ultrasound images. The present research work is likely to contribute significantly in the area of ultrasound imaging.

#### **3.2 Proposed Method I**

**(Based on Decision Tree Classifier with Principal Component Analysis)**

##### **3.2.1 Image Dataset Used**

In this research work, 90 ultrasound liver images are collected from Delta Diagnostic Centre Patiala, India. Out of 90 images, half of the images are of fatty liver. To create this medical image dataset, 90 patients (within the age group of 25 – 60 years) has been examined by experienced radiologists. The ultrasound images are collected by the ultrasonic system Voluscan730 PRO (General Electric Medicare) with a curved array probe of 68 mm at a frequency of 3.6 MHz. In order to keep the background grey level same across the whole range, the Time Gain Compensation (TGC) setting has been done accordingly. All the patients were advised to take at least eight hours fast before ultrasound scan so that increasing liver glycogen and water concentration does not effect the quality of ultrasound imaging. Experienced radiologists are requested to acquire the images and to label them as per the standard procedure.

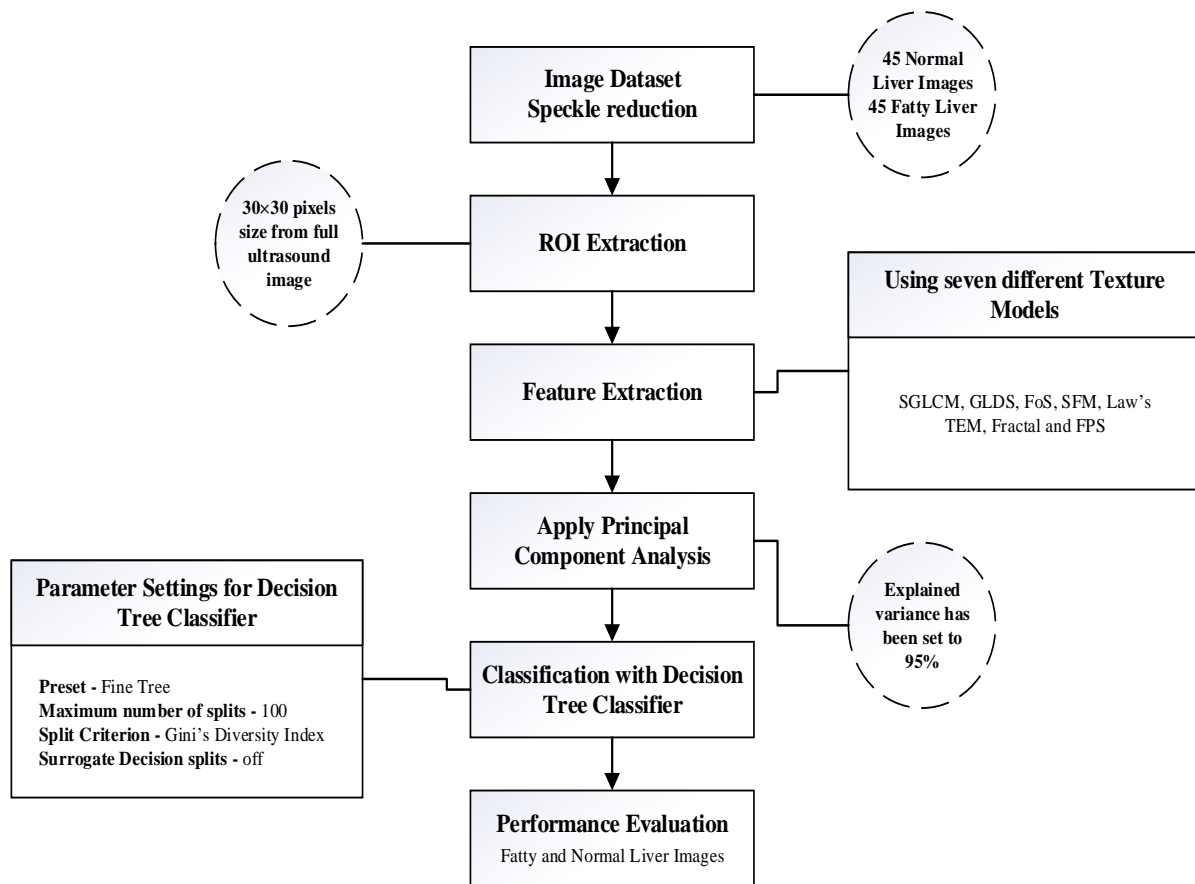


**Figure 3.1: Steps carried out in Proposed Method I**

### 3.2.2 Speckle Reduction

Speckle is a locally correlated multiplicative noise that has granular pattern, and this makes the visual quality of ultrasound image poor. Speckle also hinders the automatic image analysis task very difficult. Therefore, it is important to suppress the speckle noise in the pre-processing stages. A modified fourth order partial differential equation-based filter as proposed by Singh et al. [151] was used to accomplish this work. The proposed filter is adaptive to the local 'variance coefficient' in the 3x3 space window. Proposed method employs the local statistics in a moving window, to flatten or preserve the central pixel. In order to enhance the fine details and edges in the ultrasound image 'edge-map' technique has been used. To further increase the efficacy, after feature extraction from the region of interest all the features have been normalized. The visual analysis done by the radiologists indicate that the method is suitable for

computer aided analysis of ultrasound images, as it preserves the diagnostically significant information in the image.

### **3.2.3 Region of Interest (ROI) Extraction**

In medical image processing, to identify the ultrasound image characteristics quantitatively, a “Region of Interest” (ROI) is extracted [128, 148, 151]. ROI is a selected significant part of an image which represent the whole image and also helps the users to avoid unnecessary calculations. Different authors have used different ROI sizes in their research work but for reliable statistics, a 30×30 fixed square size ROI (900 pixels) [21] is selected by the experienced radiologists from each image in the present research work. The sample ROIs contain tissue pattern only. The ROI size (30 × 30 pixels) of an image is chosen diagonally to avoid effect of liver glycogen, fat, blood vessels and water storage [125, 152]. The main reason for choosing square shape is that most of the texture models are based on calculations of matrices, which can be easily done for square matrices. Thus, the square-shaped ROIs were chosen for this analysis. This size of ROI also decreases the computational cost in extracting the texture features. In earlier studies researchers have proved that ROI extracted from the full image should have sufficient number of pixels so that better analysis can be done and moreover parameters of texture are considered sensitive to sample size. \**Kadah et al.* stated that a 30x30 square sized ROI (900 pixels) provides a suitable sample size for reliable statistics. Furthermore, conversations with the radiologists also indicate that a size of 30x30 pixels is ideal, and that ROI should be extracted from or near the centre line of image. Therefore, a ROI of size 30x30 pixels is selected for the present study.

### **3.2.4 Feature Extraction**

The next step in the present methodology is to extract texture features from ROI selected from each ultrasound liver image in the database. As per the literature survey done by authors, various texture feature extraction models have been extensively explored in medical applications, which extract different features from an image in different ways for different purposes. In [21], seven different texture feature extraction models i.e. SGLCM, FoS, FPS, GLDS, TEM, SFM and FF have been used to extract total 35 features. In the present study, same models (as shown in Table 3.1 and Figure

3.3) have been used to extract total 45 features in order to improve the classifier accuracy of existing CAD systems.

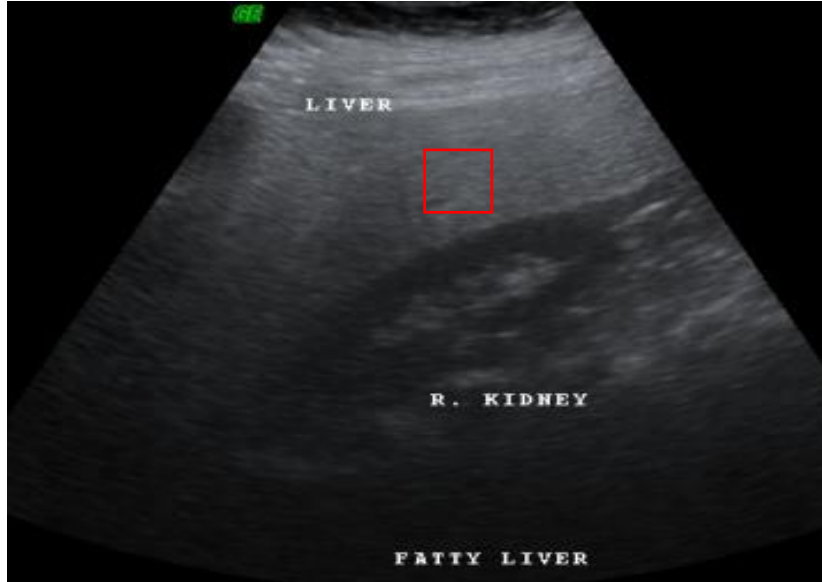


**Figure 3.2: Region of Interest Extraction from full image**

**Table 3.1: Various models used for feature extraction**

Models used	Feature Extraction
SGLCM	“Angular Second Moment, Contrast, Correlation, Inverse difference moment, Sum of square, Difference Entropy, Entropy, Sum Variance, Sum Average, Sum Entropy, Maximal Correlation Coefficient, Difference Variance, information measure of correlation 1, information measure of correlation 2.
FOS	Mean, Variance, Skewness, Kurtosis
GLDS	Homogeneity, Contrast, Mean, Energy, Entropy
SFM	Coarseness, Contrast, Periodicity, Roughness
Law’s TEM	Spot_Level, Edge_Level, Wave_Level, Ripple_Level, Spot_Edge, Wave_Edge, Wave_Spot, Ripple_Edge, Ripple_Spot, Ripple_Wave, Spot_Spot, Edge_Edge, Wave_Wave, Ripple_Ripple
Fractal	Hurst Coefficient at Resolution 1, Hurst Coefficient at Resolution 2.
FPS	Radial Sum, Angular Sum”

### Proposed Algorithm

**Input:** Liver Ultrasound Image

**Output:** Class of Image (Normal/Fatty)

1. For each image  $I$  in  $N$ , obtain
  - ii)  $r_i = \text{Extract } 30 \times 30 \text{ pixels ROI from } I$
  - ii)  $R = R \cup r_i$ , where  
 $R$  is a set of all extracted  $30 \times 30$  pixels ROI,  
 $N$  is the total no of images.
2. For each  $r_i$  in  $R$ , Obtain
  - i)  $F_{1-14} = \text{Extract GLCM based Haralick Features}$
  - ii)  $F_{15-19} = \text{Extract GLDS Features}$
  - iii)  $F_{20-23} = \text{Extract FoS Features}$
  - iv)  $F_{24-27} = \text{Extract SFM Features}$
  - v)  $F_{28-41} = \text{Extract Law's TEM Features}$
  - vi)  $F_{42-43} = \text{Extract Fractal Features}$
  - vii)  $F_{44-45} = \text{Extract FPS Features}$
3.  $S = \{F_{1-14} \cup F_{15-19} \cup F_{20-23} \cup F_{24-27} \cup F_{28-41} \cup F_{42-43} \cup F_{44-45}\}$
4. Apply Principal Component Analysis on  $S$ .
  - (i) Standardized  $d$ -dimensional dataset.
  - (ii) Create the covariance matrix.
  - (iii) Decompose the covariance matrix into its eigenvalues and eigenvectors.
  - (iv) Sort your own values to define the corresponding vectors by decreasing order.
  - (v) Choose  $k$  eigenvectors that match the  $k$  's largest eigen values, where  $k$  is the dimension of the new subspace function.
  - (vi) Create the projection matrix  $W$  from top  $k$  eigenvectors
  - (vii) To obtain the new  $k$ -dimensional feature subspace, transform the  $d$ -dimensional data set  $X$  using the projection matrix  $W$ .
5. For each  $r_i$  in  $R$ 
  - i) Apply Decision Tree based Classification using PCA.
6. End

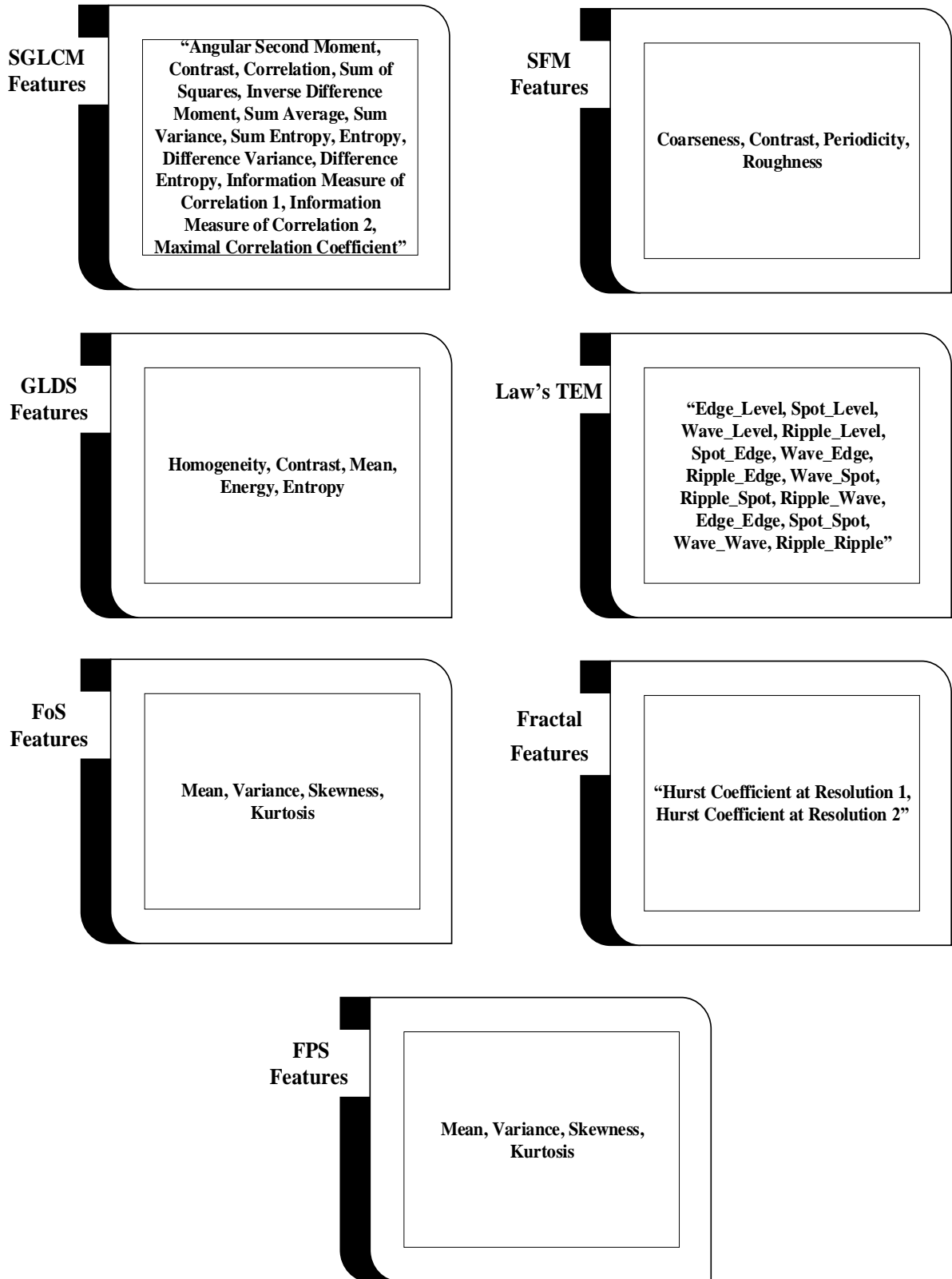


**Figure 3.3: Different texture models used in the proposed work**

**(i). Haralick's Gray Level Cooccurrence Matrix based Features**

“A set of 14 texture features are used in this study, and these are defined on a single co-occurrence matrix. In GLCM model the selection of distance  $d$  and angle plays a crucial role. In the proposed work, for a chosen distance  $d=1$  and for angles  $\theta = 0^\circ, 45^\circ, 90^\circ, \text{ and } 135^\circ$ , we have calculated four values for each feature and their average is taken for further analysis.

The various representations used to compute these texture features are given as follows:

<i>Notations</i>	<i>Description</i>
$P(i, j)$	<i>Probability that the <math>i</math> and <math>j</math> grey level combination occurs in sequence</i>
$p(i, j)$	<i><math>(i, j)</math>th entry in a normalized co – occurrence matrix,</i> $= \frac{P(i, j)}{R}$ where, $R$ is a normalizing constant.
$p_x(i)$	$= \sum_{j=1}^{N_g} P(i, j)$ , obtained by summing the rows of $p(i, j)$ .
$N_g$	Number of distinct gray levels in the quantized image.
$p_y(j)$	$= \sum_{i=1}^{N_g} P(i, j)$ , obtained by summing the columns of $p(i, j)$ .
$p_{(x+y)}(k)$	$= \sum_{i=1}^{N_g} \sum_{j=1}^{N_g} p(i, j)$ , $k = 2, 3, \dots, 2N_g$ .
$p_{(x-y)}(k)$	$= \sum_{i=1}^{N_g} \sum_{j=1}^{N_g} p(i, j)$ , $k = 0, 1, 2, \dots, N_g - 1$ .
$\sum_i$	$= \sum_{i=1}^{N_g}$ and $\sum_j = \sum_{j=1}^{N_g}$

$\mu_x, \mu_y, \sigma_x$  and  $\sigma_y$  are the means and standard deviations of  $p_x$  and  $p_y$ .

The Haralick features calculated in this thesis work are detailed in the following section [153].

(a) *Angular Second Moment (ASM)*: It is measure of uniformity or energy of texture.

It is computed as summation of squared elements of SGLCM.

$$ASM = \sum_i \sum_j \{p(i,j)\}^2 \quad (3.1)$$

A homogeneous image has a few gray level values so SGLCM contains few but high values of  $P(i,j)$ . So, value of ASM will be high.

(b) *Contrast (CNT)*: It is measure of intensity contrast between pixel and its neighborhood over the entire image and is difference moment of SGLCM.

$$CNT = \sum_{n=0}^{Ng-1} n^2 \left\{ \sum_{i=1}^{Ng} \sum_{j=1}^{Ng} \Big|_{|i-j|=n} p(i,j) \right\} \quad (3.2)$$

High contrast value provides clear separation between objects in an image.

(c) *Correlation (CRC)*: It is measure of how correlated a pixel is to its neighbor over the entire image.

$$CRC = \frac{\sum_i \sum_j (ij)p(i,j) - \mu_x \mu_y}{\sigma_x \sigma_y} \quad (3.3)$$

(d) *Inverse Difference Moment (IDM)*: It is measure of closeness of distribution of elements in co-occurrence matrix to main diagonal.

$$IDM = \sum_i \sum_j \frac{1}{1 + (i-j)^2} p(i,j) \quad (3.4)$$

This feature has relatively high value when high values of matrix are near the main diagonal. High value indicates homogeneity of image.

(e) *Variance (VAR)*: It provides measure of deviation from mean value of SGLCM.

$$VAR = \sum_{i=1}^{Ng} (i-j)^2 p_{x+y}(i) \quad (3.5)$$

(f) *Sum Average (SAVG)*: It indicates brightness of image. Sum average is high if image is bright.

$$SVAG = \sum_{i=2}^{2Ng} ip_{x+y}(i) \quad (3.6)$$

(g) *Entropy (ENT)*: It is statistical measure of randomness in image. Homogeneous image have high entropy while inhomogeneous image have low entropy.

$$ENT = - \sum_i \sum_j p(i,j) \log(p(i,j)) \quad (3.7)$$



(h) *Sum Entropy (SENT)*: It measure entropy of vector  $P_{x+y}$ . Its value is lower than entropy.

$$SENT = - \sum_{i=2}^{2N_g} p_{x+y}(i) \log\{p_{x+y}(i)\} \quad (3.8)$$

(i) *Sum Variance (SVAR)*: It is measure of deviation of elements of  $P_{x+y}$  from sum entropy. It has high value for low contrast image.

$$SVAR = \sum_{i=2}^{2N_g} (i - SENT)^2 p_{x+y}(i) \quad (3.9)$$

(j) *Difference Entropy (DENT)*: It is measure of entropy of vector  $P_{x-y}$ . Its weight increases as we move away from main diagonal.

$$DENT = - \sum_{i=0}^{N_g-1} p_{x-y}(i) \log\{p_{x-y}(i)\} \quad (3.10)$$

(k) *Difference Variance (DVAR)*: It is measure of deviation of elements of  $P_{x-y}$  vector from difference entropy. Sum variance and difference variance are opposite to each other.

$$DVAR = \sum_{i=0}^{N_g-1} (i - DENT)^2 p_{x-y}(i) \quad (3.11)$$

(l) *Information Measures of Correlation 1 (IMC1)*: Homogeneous image has low value for information measures of correlation 1.

$$IMC1 = \frac{HXY - HXY1}{\max\{HX, HY\}} \quad (3.12)$$

where,  $HX$  and  $HY$  are entropies of  $p_x$  and  $p_y$  and

$$HXY = - \sum_i \sum_j p(i, j) \log(p(i, j)),$$

$$HXY1 = - \sum_i \sum_j p(i, j) \log\{p_x(i)p_y(j)\},$$

$$HXY2 = - \sum_i \sum_j p_x(i)p_y(j) \log\{p_x(i)p_y(j)\}.$$

(m) *Information Measures of Correlation 2 (IMC2)*: Image with more energy has low value of information measures of correlation 2.”

$$IMC2 = (1 - \exp[-2.0(HXY2 - HXY)])^{1/2} \quad (3.13)$$

**Table 3.2: Description of Features**

Feature	Name of Feature	Texture Model
F1	ASM	GLCM Model
F2	Contrast	
F3	Correlation	
F4	Sum_Squares	
F5	Inverse_Diff_Moment	
F6	Sum_Average	
F7	Sum_Variance	
F8	Sum_Entropy	
F9	Entropy	
F10	Diff_Variance	
F11	Diff_Entropy	
F12	Info_Measure1	
F13	Info_Measure2	
F14	Max_Corr_Coff	
F15	Homogeneity	GLDS Model
F16	Contrast	
F17	Mean	
F18	Energy	
F19	Entropy	
F20	Mean	FoS Model
F21	Variance	
F22	Skewness	
F23	Kurtosis	
F24	Coarseness	SFM Model
F25	Contrast	
F26	Periodicity	
F27	Roughness	

**Table 3.2: Description of Features (Continued)**

<b>Feature</b>	<b>Name of Feature</b>	<b>Texture Model</b>
<b>F28</b>	EE	Law's TEM Model
<b>F29</b>	SS	
<b>F30</b>	WW	
<b>F31</b>	RR	
<b>F32</b>	EL	
<b>F33</b>	SL	
<b>F34</b>	WL	
<b>F35</b>	RL	
<b>F36</b>	SE	
<b>F37</b>	WE	
<b>F38</b>	RE	
<b>F39</b>	WS	
<b>F40</b>	RS	
<b>F41</b>	RW	
<b>F42</b>	H1	Fractal Model
<b>F43</b>	H2	
<b>F44</b>	Sr	FPS Model
<b>F45</b>	Stheta	

**Table 3.3: Feature values of Region of Interest obtained by Haralick’s GLCM Model for Fatty Liver Ultrasound Images**

<b>Image</b>	<b>F1</b>	<b>F2</b>	<b>F3</b>	<b>F4</b>	<b>F5</b>	<b>F6</b>	<b>F7</b>	<b>F8</b>	<b>F9</b>	<b>F10</b>	<b>F11</b>	<b>F12</b>	<b>F13</b>	<b>F14</b>
<b>ROI 1</b>	0.4510	0.1103	0.7709	18.5568	0.9448	8.6161	52.9274	1.3995	1.5038	0.2507	0.5010	-0.4917	0.7924	0.7718
<b>ROI 2</b>	0.5317	0.0862	0.7787	18.2463	0.9569	8.5299	55.0911	1.1544	1.2406	0.1927	0.4237	-0.5122	0.7582	0.7787
<b>ROI 3</b>	0.5610	0.1034	0.7144	14.4415	0.9483	7.6000	41.7237	1.1887	1.2900	0.2344	0.4798	-0.4273	0.7112	0.7311
<b>ROI 4</b>	0.6927	0.0701	0.7234	15.0331	0.9649	7.7667	47.3915	0.9141	0.9816	0.1530	0.3664	-0.4524	0.6709	0.7301
<b>ROI 5</b>	0.8834	0.0264	0.7105	15.5228	0.9868	7.9046	56.6059	0.3912	0.4168	0.0482	0.1762	-0.4711	0.4881	0.7105
<b>ROI 6</b>	0.7257	0.0759	0.6500	25.6797	0.9621	10.1471	86.4324	0.8695	0.9453	0.1672	0.3874	-0.3911	0.6076	0.6502
<b>ROI 7</b>	0.7511	0.0736	0.6220	16.3359	0.9632	8.0851	53.0453	0.8235	0.8945	0.1615	0.3791	-0.3594	0.5807	0.6543
<b>ROI 8</b>	0.4043	0.1103	0.8455	16.6930	0.9448	8.1816	43.1183	1.7124	1.7933	0.2507	0.5010	-0.5880	0.8818	0.8487
<b>ROI 9</b>	0.9772	0.0080	0.4706	15.8112	0.9960	7.9851	62.1851	0.1007	0.1076	0.0115	0.0675	-0.2498	0.1923	0.4706
<b>ROI 10</b>	0.5696	0.0989	0.7109	22.8338	0.9506	9.5632	72.3331	1.0927	1.1906	0.2234	0.4653	-0.4215	0.6902	0.7109

**Table 3.4: Feature values of Region of Interest obtained by Haralick’s GLCM Model for Normal Liver Ultrasound Images**

<b>Image</b>	<b>F1</b>	<b>F2</b>	<b>F3</b>	<b>F4</b>	<b>F5</b>	<b>F6</b>	<b>F7</b>	<b>F8</b>	<b>F9</b>	<b>F10</b>	<b>F11</b>	<b>F12</b>	<b>F13</b>	<b>F14</b>
<b>ROI 11</b>	0.4455	0.1253	0.7496	13.9737	0.9374	7.4655	36.7325	1.4769	1.5974	0.2852	0.5444	-0.4505	0.7825	0.7540
<b>ROI 12</b>	0.4268	0.0862	0.8791	9.6093	0.9569	6.1115	21.0134	1.6758	1.7599	0.1927	0.4237	-0.6396	0.9023	0.8942
<b>ROI 13</b>	0.5519	0.0632	0.8440	7.5736	0.9684	5.4908	19.6729	1.1388	1.1889	0.1359	0.3401	-0.6090	0.8131	0.8564
<b>ROI 14</b>	0.4202	0.0885	0.8277	6.2177	0.9557	4.9345	13.6084	1.3745	1.4598	0.1983	0.4315	-0.5750	0.8326	0.8281
<b>ROI 15</b>	0.5817	0.1023	0.7065	8.1460	0.9489	5.6678	20.7979	1.1730	1.2740	0.2317	0.4762	-0.4300	0.7096	0.7202
<b>ROI 16</b>	0.9548	0.0092	0.7515	3.8763	0.9954	3.9632	14.3740	0.1802	0.1877	0.0135	0.0754	-0.5265	0.3767	0.7515
<b>ROI 17</b>	0.7275	0.0517	0.7686	4.5831	0.9741	4.2563	12.6081	0.7616	0.8132	0.1076	0.2937	-0.5232	0.6647	0.7686
<b>ROI 18</b>	0.8918	0.0264	0.6796	3.8081	0.9868	3.9138	12.7053	0.3688	0.3952	0.0482	0.1762	-0.4536	0.4575	0.6796
<b>ROI 19</b>	0.7319	0.0575	0.7318	4.5260	0.9713	4.2437	12.5364	0.7557	0.8126	0.1217	0.3173	-0.4712	0.6335	0.7318
<b>ROI 20</b>	0.4357	0.1057	0.7751	5.7882	0.9471	4.7540	12.5456	1.3318	1.4369	0.2399	0.4870	-0.4950	0.7830	0.7751

**(ii) GLDS Features**

“The GLDS algorithm uses first-order local property value statistics based on the absolute differences between pairs of grey or average grey levels to extract the following 5 texture measurements: homogeneity, contrast, mean, energy and entropy [43]. These characteristics are based on the absolute difference between pairs of grey levels separated from each other at distance  $\delta = (\Delta x, \Delta y)$ . For a given displacement  $\delta = (\Delta x, \Delta y)$ , the difference image  $f_\delta(x, y)$  is defined as:

$$f_\delta(x, y) = |f(x, y) - f(x + \Delta x, y + \Delta y)| \quad (3.14)$$

and  $p_\delta$  is the probability density (gray-level histogram) of  $f_\delta(x, y)$  for  $m$  gray levels. Various texture features extracted from  $p_\delta$  are:

(a) *Homogeneity (HOMG)*: It is a measure of similarity in grey level intensities.

$$HOMG = \frac{\sum p_\delta(i)}{1 + i} \quad (3.15)$$

(b) *Contrast (CNTG)*: It is a measure of grey level intensity difference between neighboring pixels.

$$CNTG = \sum i^2 p_\delta(i) \quad (3.16)$$

(c) *Mean (MENG)*: It is the average value of the grey level intensities within a given area.

$$MENG = \frac{1}{m} \sum i p_\delta(i) \quad (3.17)$$

(d) *Energy (ENGG)*: It represents amplitude of grey level values.

$$ENGG = \sum p_\delta(i)^2 \quad (3.18)$$

(e) *Entropy (ENTG)*: It measures the randomness in grey level intensities within the given area.”

$$ENTG = - \sum p_\delta(i) \log p_\delta(i) \quad (3.19)$$

**Table 3.5 Feature values of Region of Interest obtained by GLDS Model for Fatty Liver Ultrasound Images**

<b>Image</b>	<b>F15</b>	<b>F16</b>	<b>F17</b>	<b>F18</b>	<b>F19</b>
<b>ROI 1</b>	0.6326	35.5529	3.1779	0.3142	2.7975
<b>ROI 2</b>	0.6733	19.1893	2.2538	0.3488	2.4972
<b>ROI 3</b>	0.6577	24.9423	2.6319	0.3375	2.5946
<b>ROI 4</b>	0.6510	16.9390	2.2314	0.3149	2.5602
<b>ROI 5</b>	0.7094	7.1701	1.4011	0.3782	2.1450
<b>ROI 6</b>	0.6304	46.5952	3.5548	0.3127	2.8721
<b>ROI 7</b>	0.6309	38.2433	3.2693	0.3112	2.8246
<b>ROI 8</b>	0.6926	18.4772	2.1168	0.3881	2.3682
<b>ROI 9</b>	0.7033	9.9344	1.6131	0.3749	2.2359
<b>ROI 10</b>	0.6750	17.9035	2.1601	0.3479	2.4727

**Table 3.6: Feature values of Region of Interest obtained by GLDS Model for Normal Liver Ultrasound Images**

<b>Image</b>	<b>F15</b>	<b>F16</b>	<b>F17</b>	<b>F18</b>	<b>F19</b>
<b>ROI 11</b>	0.6271	35.7759	3.2157	0.3037	2.8330
<b>ROI 12</b>	0.5878	55.5478	4.1237	0.2656	3.0965
<b>ROI 13</b>	0.6674	16.6915	2.1454	0.3442	2.4573
<b>ROI 14</b>	0.6271	26.5061	2.8453	0.3023	2.7497
<b>ROI 15</b>	0.6389	27.1022	2.7616	0.3112	2.7212
<b>ROI 16</b>	0.6968	7.4150	1.4710	0.3621	2.1902
<b>ROI 17</b>	0.6342	23.7009	2.6217	0.3016	2.6982
<b>ROI 18</b>	0.6856	8.5964	1.5894	0.3492	2.2711
<b>ROI 19</b>	0.6777	13.3591	1.8987	0.3470	2.4033
<b>ROI 20</b>	0.6539	21.6069	2.4569	0.3242	2.6027

**(iii) FOS Features**

“In this model, the statistics of first order describing the distribution of the gray-level image (histogram) are used. These characteristics are obtained from a normalised image histogram. Assuming pixel values of the image to be random variables that can take discrete values  $i = 0, 1, \dots, N_g - 1$  where,  $N_g$  is the number of gray levels, the normalized histogram is defined as:

$$p(i) = \frac{\text{number of pixels with intensity } i}{\text{total number of pixels}} \quad \text{where,}$$

$$= 0, 1, \dots, N_g - 1 \quad (3.20)$$

For characterising the image's texture, key moments derived from the histogram are used. Based on the grey value of pixels in the image, the following statistical features are calculated: mean value, variance, skewness and Kurtosis [154].

(a) *Mean (MENF or  $\mu$ )*: Mean provides the measure of average intensity level of image.

$$\mu = \sum_{i=0}^{N_g-1} ip(i) \quad (3.21)$$

(b) *Skewness (SKWF or  $\mu_3$ )*: Skewness is a measure of lack of symmetry in the histogram.

$$\mu_3 = \sigma^{-3} \sum_{i=0}^{N_g-1} (i - \mu)^3 p(i) \quad (3.22)$$

(c) *Kurtosis (KRTF or  $\mu_4$ )*: Kurtosis is variability of grey level intensity around the mean value.

$$KRTF = \mu_4 = \sigma^{-4} \sum_{i=0}^{N_g-1} (i - \mu)^4 p(i) - 3 \quad (3.23)$$

The constant value 3 is used in equation 2.27 to normalize  $\mu_4$  to 0 for Gaussian shaped histogram.”

**Table 3.7: Feature values of Region of Interest obtained by FoS Model for Fatty Liver Ultrasound Images**

<b>Image</b>	<b>F20</b>	<b>F21</b>	<b>F22</b>	<b>F23</b>
<b>ROI 1</b>	119.7256	197.7969	-0.0755	2.2735
<b>ROI 2</b>	121.2811	110.7288	0.2145	3.0158
<b>ROI 3</b>	99.4000	93.3511	0.5310	3.5198
<b>ROI 4</b>	103.1711	103.2641	-0.0143	2.8543
<b>ROI 5</b>	103.6778	47.1895	-0.3827	2.9529
<b>ROI 6</b>	148.8867	111.9760	0.0672	2.5750
<b>ROI 7</b>	110.6178	117.4383	0.1531	2.8682
<b>ROI 8</b>	112.1944	329.4722	0.1870	2.1612
<b>ROI 9</b>	105.3222	28.3828	-0.1623	3.7349
<b>ROI 10</b>	133.8322	65.7419	0.4326	2.9584

**Table 3.8: Feature values of Region of Interest obtained by FoS Model for Normal Liver Ultrasound Images**

<b>Image</b>	<b>F20</b>	<b>F21</b>	<b>F22</b>	<b>F23</b>
<b>ROI 11</b>	99.2733	177.5631	0.2771	2.8682
<b>ROI 12</b>	75.3122	371.6925	0.4482	2.9307
<b>ROI 13</b>	63.4444	128.5825	0.0250	2.5583
<b>ROI 14</b>	56.0133	159.6465	0.4024	2.8474
<b>ROI 15</b>	64.2789	109.3656	0.6664	3.6631
<b>ROI 16</b>	30.6533	34.7732	0.1180	3.3407
<b>ROI 17</b>	44.4144	99.4382	0.7437	4.2553
<b>ROI 18</b>	28.5589	42.9799	0.5244	3.5160
<b>ROI 19</b>	43.8089	85.3057	0.5131	2.7458
<b>ROI 20</b>	52.7467	95.9914	0.3079	2.9827



**(iv) Laws' TEM Features**

“Another approach to texture quantification that uses convolution with different filters is based on the masks of the Laws [121]. These are constructed using three simple vectors in one dimension, corresponding to centre-weighted local average, Edge detection with first symmetric differentiation, and Spot detection with second differentiation. These steps are measured first by adding small kernels of convolution to a digital image and then performing a nonlinear windowing operation.

$$L5 = [ 1 \quad 4 \quad 6 \quad 4 \quad 1] \quad (3.24)$$

$$E5 = [ -1 \quad -2 \quad 0 \quad 2 \quad 1] \quad (3.25)$$

$$S5 = [ -1 \quad 0 \quad 2 \quad 0 \quad -1] \quad (3.26)$$

9 distinct two-dimensional kernels are obtained from these one-dimensional convolution kernels by combining a vertical 1-d kernel with a horizontal 1-d kernel. A list of all names for the 5x5 kernels is given below:

$$\begin{array}{lll} L5L5 & E5L5 & S5L5 \\ L5E5 & E5E5 & S5E5 \\ L5S5 & E5S5 & S5S5 \end{array}$$

Subsequently, the texture energy measures are computed by applying convolution kernels: The digital image (or regions) of size  $N$  rows and  $M$  columns is convoluted with each of these 9 kernels. The result is a set of 9  $N \times M$  grayscale images. The windowing operation is performed in a local neighborhood as follows:

$$NEW(x, y) = \sum_{i=-7}^7 \sum_{j=-7}^7 |OLD(x + i, y + j)| \quad (3.27)$$

All convolution kernels except L5L5 are zero-mean. Thus, L5L5T is used as normalizing image. Normalizing any TEM image pixel-by-pixel with the L5L5T image will normalize that feature for contrast. After the normalization L5L5T image is discarded. The similar features in vertical and horizontal directions can be combined to create rotation invariant features. The following 6 TEM features are used in this study: LL Texture Energy from L5\*L5 kernel; EE Texture energy from E5\*E5 kernel, SS Texture energy from S5\*S5 kernel, LE average texture energy from L5\*E5 and E5\*L5 kernels, ES average texture energy from E5\*S5 and S5\*E5 kernels, and LS average

texture energy from L5\*S5 and S5\*L5 kernels. When the image is transformed with the masks of Laws, metrics which quantify the texture of a region of interest are obtained from the filtered image by computing statistics. Usually these measurements are the sum of the absolute or squared pixel values determined by the number of pixels thus called energy measures.”

(v) **FPS Features**

“This texture model includes details about the image's texture orientation, grain size and texture contrast. The Discrete Fourier Transform (DFT) method is used here for texture quantification because it is difficult to explain repetitive global patterns with spatial techniques but relatively easy to represent with peaks in the spectrum [155]. To define texture, the DFT's Radial sum and Angular sum were computed. The FPS functions in the frequency domain are determined from the power spectrum.

$$|F(u, v)|^2 = F(u, v)F^*(u, v) \quad (3.28)$$

where,  $F(u, v)$  is the Fourier transform of the image and  $F^*(u, v)$  is the complex conjugate of Fourier transform of the image.

Spectral features are expressed in polar coordinates to yield a function  $S(r, \theta)$ . For each direction  $\theta$ ,  $S(r, \theta)$  can be expressed as  $S_\theta(r)$  and similarly for each frequency  $r$ ,  $S(r, \theta)$  can be expressed as  $S_r(\theta)$ . Analyzing  $S_\theta(r)$  for a fixed value of  $\theta$  gives the behavior of spectrum along a radial direction from the origin and is called wedge analysis whereas analyzing  $S_r(\theta)$  for a fixed value of  $r$  gives the behavior of spectrum along a circle centered on the origin and is called ring analysis. A global interpretation is obtained by summing over discrete variables:

$$S_\theta = \sum_{\theta=0}^{\pi} S_\theta(r) \quad (3.29)$$

and

$$S_r = \sum_{r=1}^{R_0} S_r(\theta) \quad (3.30)$$

where,  $R_0$  is the radius of circle centered at origin. In this texture model, two features:  $S_r$  and  $S_\theta$  are calculated and these are measure of the orientation of the texture.”

**Table 3.9: Feature values of Region of Interest obtained by Law’s TEM Model for Fatty Liver Ultrasound Images**

Image	F28	F29	F30	F31	F32	F33	F34	F35	F36	F37	F38	F39	F40	F41
ROI 1	0.8484	1.0119	1.0456	1.0790	1.0866	0.9830	0.9194	0.8681	0.9277	1.0648	1.2480	1.0367	1.1036	1.1165
ROI 2	1.0030	1.0352	1.0604	1.1555	0.9817	1.0846	0.8560	0.7560	1.0713	1.0459	1.1486	0.9297	1.1006	1.0646
ROI 3	1.2011	1.2611	1.1073	0.9035	0.8345	1.0053	1.1491	1.1742	1.1136	1.0253	0.9936	1.1211	1.0216	1.0451
ROI 4	1.0554	0.7860	1.0115	0.7187	0.8981	0.8867	0.8748	1.0130	0.8567	0.8460	0.9453	0.8649	1.0746	0.9555
ROI 5	1.3267	1.1514	1.2012	1.2934	1.0586	1.0448	0.8482	0.9748	1.1840	0.9511	1.0090	1.1026	1.0988	1.1374
ROI 6	0.9881	1.0399	1.0601	0.7887	1.1825	1.0668	0.8752	0.8587	0.9238	0.9956	0.8878	0.9294	1.0091	1.0672
ROI 7	0.9503	0.6517	1.0665	1.0301	0.8796	0.7117	0.9429	0.7479	0.6509	0.7251	0.6810	0.7931	0.7948	0.9308
ROI 8	0.5127	0.8832	0.8699	1.1143	0.9059	0.8190	0.7426	0.9197	0.7902	0.8796	0.8266	1.0080	0.8221	0.9403
ROI 9	0.6560	0.9244	0.6860	0.8610	0.6238	0.7208	0.8951	0.9900	0.9085	0.9046	0.8862	0.7409	0.7567	0.8890
ROI 10	1.0833	1.1872	1.1093	1.1041	0.9797	0.9692	0.9520	0.8979	1.0644	1.0159	0.9672	1.1479	1.1336	1.0553

**Table 3.10: Feature values of Region of Interest obtained by Law’s TEM Model for Normal Liver Ultrasound Images**

Image	F28	F29	F30	F31	F32	F33	F34	F35	F36	F37	F38	F39	F40	F41
ROI 11	1.1442	1.1129	0.9634	0.7693	1.1542	0.9815	0.9613	1.0986	1.0025	1.0093	1.1245	1.0827	1.0628	0.9628
ROI 12	1.0249	0.9309	0.8915	1.0455	1.3023	1.1209	0.9592	0.8166	1.0105	0.7902	0.7437	0.9452	0.8685	0.9683
ROI 13	0.6902	0.9760	1.0223	0.8098	0.8889	0.8952	0.7929	0.8867	0.7178	0.7199	0.6948	0.9309	0.8232	0.7967
ROI 14	0.6586	0.8527	1.0151	0.9367	0.9807	1.0451	1.0525	0.9465	0.7827	0.9330	1.0168	0.8607	0.9596	1.0348
ROI 15	0.9749	0.9731	0.9613	0.9147	0.9884	1.1141	1.1851	1.2335	0.8934	0.9098	0.8961	0.9377	0.8850	1.0266
ROI 16	0.7340	0.7449	0.6774	0.5920	1.0179	1.0993	1.0552	0.8016	0.8192	0.8092	0.7585	0.6190	0.6982	0.7657
ROI 17	1.0840	0.8042	0.9218	0.9477	0.9966	0.7525	0.9003	0.9796	0.7143	1.0107	1.0565	1.1344	0.9225	0.9224
ROI 18	0.8015	0.5986	0.7255	0.6169	0.8718	1.0174	1.0300	0.9234	0.9339	0.9621	0.9749	0.8838	0.8172	0.6401
ROI 19	1.1115	1.0064	0.9853	0.7783	1.2463	1.1562	1.2613	1.1572	1.0453	0.9668	0.9299	0.9695	1.0371	1.0038
ROI 20	0.5498	0.8324	0.9488	1.1073	0.8456	0.9589	1.0046	0.9993	0.9118	0.8674	0.7697	0.8819	0.8718	1.0178

**Table 3.11: Feature values of Region of Interest obtained by FPS Model for Fatty Liver Ultrasound Images**

<b>Image</b>	<b>F44</b>	<b>F45</b>
<b>ROI 1</b>	877104.06	20531396.00
<b>ROI 2</b>	703251.25	20504478.00
<b>ROI 3</b>	799946.25	16935822.00
<b>ROI 4</b>	616353.25	17576676.00
<b>ROI 5</b>	476110.06	17400360.00
<b>ROI 6</b>	865238.75	24929916.00
<b>ROI 7</b>	905153.56	18833874.00
<b>ROI 8</b>	850841.38	19445278.00
<b>ROI 9</b>	488563.44	17492136.00
<b>ROI 10</b>	598449.50	22396142.00

**Table 3.12: Feature values of Region of Interest obtained by FPS Model for Normal Liver Ultrasound Images**

<b>Image</b>	<b>F44</b>	<b>F45</b>
<b>ROI 11</b>	844629.13	17257552.00
<b>ROI 12</b>	1147602.63	13758881.00
<b>ROI 13</b>	676986.00	11229438.00
<b>ROI 14</b>	828404.81	10202119.00
<b>ROI 15</b>	734314.38	11344594.00
<b>ROI 16</b>	386824.66	5482707.00
<b>ROI 17</b>	702693.19	8042051.00
<b>ROI 18</b>	459252.56	5190159.00
<b>ROI 19</b>	590917.81	7920410.50
<b>ROI 20</b>	739893.69	9291179.00

**(vi) SFM Features**

“The SFM tests the statistical properties of pixel pairs within an image at different distances which are used for statistical analysis. The texture features such as Coarseness, Contrast, Periodicity, and Roughness are measured based on the SFM [122]. In this model a matrix  $M_{sfm}$  of size  $(L_r + 1) \times (2L_c + 1)$  is constructed whose  $(i, j)$  element is the  $d$  statistical feature of the image, where  $d = (j - L_c, i)$  is an intersample spacing distance vector for  $i = 0, 1, \dots, L_r$  and  $j = 0, 1, \dots, 2L_c$  and  $L_r$  and  $L_c$  are the constants which determine the maximum inter-sample spacing distance. In this method, two such matrices constructed are the contrast matrix ( $M_{con}$ ) and the dissimilarity matrix ( $M_{dss}$ ) whose  $(i, j)$  elements are ‘change in contrast’ and ‘change in dissimilarity’ respectively.

A  $\delta$  statistical feature is the statistical feature of an image  $I$  with inter-sample spacing distance vector  $\delta = (\Delta x, \Delta y)$ .  $\delta contrast$  and  $\delta dissimilarity$  are defined as:

$$\delta contrast: CON(\delta) \equiv E\{[I(x, y) - I(x + \Delta x, y + \Delta y)]^2\} \quad (3.31)$$

$$\delta dissimilarity: DSS(\delta) \equiv E\{|I(x, y) - I(x + \Delta x, y + \Delta y)|\} \quad (3.32)$$

where,  $E\{\cdot\}$  denotes the expectation operation.

The four texture features extracted from image are:

(a) *Coarseness (CRCC)*: It is a measure of the ‘size’ of primitives. It represents occurrence of similar grey levels in a given area.

$$CRSS = c/m_{crs} \quad (3.33)$$

where  $c$  is a normalizing factor and  $c = 100$  and  $m_{crs}$  is the mean of all elements of the matrix  $M_{dss}$

$$m_{crs} = \sum_{(i,j) \in N_r} DSS(i, j)/n \quad (3.34)$$

where  $N_r$  is the set of displacement vectors and  $n$  is the number of elements in the matrix  $M_{dss}$ .

(b) *Contrast (CNTS)*: It is a measure of difference in the grey level intensities for a specified neighborhood.

$$CNTS = \left[ \sum_{(i,j) \in N_r} CON(i,j)/4 \right]^{1/2} \quad (3.35)$$

(c) *Periodicity (PER)*: The feature is a measure of the repetition of a specific pattern in the image.

$$PER = \frac{\bar{M}_{dss} - M_{dss}}{\bar{M}_{dss}} \quad (3.36)$$

where  $\bar{M}_{dss}$  is the mean of all elements of  $M_{dss}$  and  $M_{dss}$  is the deepest valley in the matrix.

(d) *Roughness (RGH)*: It measures the dissimilarity between the neighboring pixels

$$RGH = (D_f^{(h)} + D_f^{(v)})/2 \quad (3.37)$$

where  $D_f^{(h)}$  and  $D_f^{(v)}$  are the estimated fractal dimensions in the horizontal and vertical directions by considering the displacement vector of the forms  $(\Delta x, 0)$  and  $(0, \Delta y)$  respectively.  $D_f$  is obtained from the equation:

$$D_f = 3 - H \quad (3.38)$$

and  $H$  can be evaluated from the dissimilarity matrix since the  $(i, j + L_c)$  element of the dissimilarity matrix is  $E\{|\Delta I|\}$  with  $\delta = (j, i)$ .  $H$  and  $E\{|\Delta I|\}$  are related as:

$$E\{|\Delta I|\} = C|\delta|^H \quad (3.39)$$

Thus, first of all  $H$  is estimated separately for horizontal and vertical directions from dissimilarity matrix as per equation (2.43) by considering displacements of  $(\Delta x, 0)$  and  $(0, \Delta y)$  respectively. Then  $D_f^{(h)}$  and  $D_f^{(v)}$  are evaluated according to equation (2.42) and finally roughness is calculated according to equation.

In this thesis work SFM features are calculated for  $L_r = 4$  and  $L_c = 4$ .”

### (vii) Fractal Features

“The Hurst coefficients ( $H(k)$ ) are calculated for different image resolutions, where a smooth texture surface is represented by a large value of parameter  $H(k)$ , while a rough texture surface is indicated by the lower value [120].

In this model, Hurst coefficient is calculated at two image resolutions: Original image of size  $N \times M$ ; termed as  $H_1$  and original image scaled by a factor of  $1/2$  and of size  $N/2 \times M/2$ ; termed as  $H_2$ .

For a given image  $I$  Hurst coefficient  $H$  is estimated from the relationship:

$$E(|\Delta I|) = k(\Delta r)^H \quad (3.40)$$

where,  $E(\cdot)$  denotes the expectation operator,  $\Delta I \equiv I(x_2, y_2) - I(x_1, y_1)$ ,

$\Delta r \equiv \|(x_2, y_2) - (x_1, y_1)\|$  is the spatial distance and  $k = E(|\Delta I|)_{\Delta r=1}$

Hurst coefficients for the two resolutions are evaluated from equation (3.41) as the texture features.”

$$\log E(|\Delta I|) = \log k + H \log(\Delta r) \quad (3.41)$$

**Table 3.13: Feature values of Region of Interest obtained by SFM Model for Fatty Liver Ultrasound Images**

<b>Image</b>	<b>F24</b>	<b>F25</b>	<b>F26</b>	<b>F27</b>
<b>ROI 1</b>	29.0379	19.9756	0.6082	2.5488
<b>ROI 2</b>	27.1024	20.4235	0.6567	2.3724
<b>ROI 3</b>	24.7214	21.4303	0.7306	2.3371
<b>ROI 4</b>	31.7511	18.7044	0.6398	2.4361
<b>ROI 5</b>	49.6692	12.7042	0.5473	2.4754
<b>ROI 6</b>	19.0376	24.8473	0.6648	2.3931
<b>ROI 7</b>	18.7656	25.0191	0.5945	2.3963
<b>ROI 8</b>	54.8398	13.4467	0.6420	2.6128
<b>ROI 9</b>	42.2134	14.6586	0.6405	2.4355
<b>ROI 10</b>	33.9778	17.5713	0.6391	2.4693

**Table 3.14: Feature values of Region of Interest obtained by SFM Model for Normal Liver Ultrasound Images**

<b>Image</b>	<b>F24</b>	<b>F25</b>	<b>F26</b>	<b>F27</b>
<b>ROI 11</b>	25.9393	21.2929	0.5799	2.5039
<b>ROI 12</b>	13.5109	27.8508	0.7380	2.2725
<b>ROI 13</b>	37.2484	16.9168	0.7568	2.4153
<b>ROI 14</b>	23.5672	22.0033	0.6931	2.3357
<b>ROI 15</b>	20.5469	23.9247	0.6292	2.3281
<b>ROI 16</b>	43.3335	14.3528	0.6479	2.3322
<b>ROI 17</b>	20.8680	23.4555	0.6839	2.2671
<b>ROI 18</b>	37.3123	16.1793	0.6492	2.2799
<b>ROI 19</b>	38.7623	16.2259	0.6623	2.3483
<b>ROI 20</b>	22.4244	22.5875	0.7142	2.2444



**Table 3.15: Feature values of Region of Interest obtained by Fractal Model for Fatty Liver Ultrasound Images**

<b>Image</b>	<b>F42</b>	<b>F43</b>
<b>ROI 1</b>	0.4126	0.1672
<b>ROI 2</b>	0.5548	0.3277
<b>ROI 3</b>	0.5912	0.3583
<b>ROI 4</b>	0.5271	0.1475
<b>ROI 5</b>	0.4334	0.2395
<b>ROI 6</b>	0.5543	0.3709
<b>ROI 7</b>	0.5591	0.3926
<b>ROI 8</b>	0.3101	-0.3383
<b>ROI 9</b>	0.5336	0.3299
<b>ROI 10</b>	0.4787	0.2569

**Table 3.16: Feature values of Region of Interest obtained by Fractal Model for Normal Liver Ultrasound Images**

<b>Image</b>	<b>F42</b>	<b>F43</b>
<b>ROI 11</b>	0.4429	0.1543
<b>ROI 12</b>	0.6435	0.5150
<b>ROI 13</b>	0.5276	0.1844
<b>ROI 14</b>	0.5966	0.3822
<b>ROI 15</b>	0.6189	0.4217
<b>ROI 16</b>	0.6044	0.3490
<b>ROI 17</b>	0.6575	0.5605
<b>ROI 18</b>	0.6301	0.4397
<b>ROI 19</b>	0.5890	0.2327
<b>ROI 20</b>	0.6549	0.4747

### 3.2.5 Principal Component Analysis

Dimensionality reduction decreases the model's complexity and prevents overfitting. There are two methods to reduce the dimensionality. One is feature selection in which highly discriminating features are selected from the initial feature vector on the basis of some algorithm. The other method is feature transformation in which the initial extracted feature set is transformed into some another subspace that is used for classification purpose. In the literature, the PCA algorithm is widely used to compress a dataset into a smaller dimensional space to preserve most of the data concerned.

“PCA operates on a condition that, while data in a higher-dimensional space is mapped to data in a lower-dimensional space, there should be a maximum variance or distribution of data in the lower-dimensional space [156]”.

The function of PCA is based on the full variance or distribution of data in the lower dimension space while the data in a higher dimension space is compared to data in a lower measured space in view of the restriction that new axes are orthogonal to each other, the orthogonal axes (main elements) of the new subspaces can be interpreted as directions of maximum variance as shown in this figure:

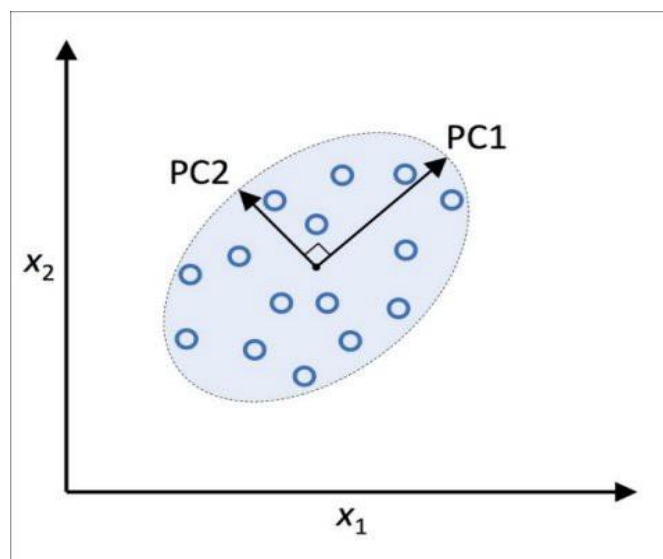


**Figure 3.4: Directions of Maximum Variance**

In the above diagram, the original function axes are  $x_1$  and  $x_2$ , and the key components are PC1 and PC2.

“If we use PCA to minimise dimensionality, we construct a  $d \times k$  – dimensional transformation matrix  $W$  that allows us to map a sample vector  $x$  to a new  $k$  – dimensional subspace with less dimensions than the original  $d$  – dimensional function space:

As a result of translating the original  $d$ -dimensional data into this new  $k$ -dimensional subspace (typically  $k \ll d$ ), the first main component will have the greatest possible variance and all consequent main components will have the greatest variance provided that these components are uncorrelated (orthogonal) to the other main components — even though the input features are co-related. Figure 3.5 describes steps taken in the proposed study.”

**Algorithm:**

1. Standardized dataset of  $d$ -dimensions.
2. Create the covariance matrix.
3. Decompose the covariance matrix into its eigenvalues and eigenvectors.
4. Sort your own values to define the corresponding vectors by decreasing order.
5. Choose  $k$  eigenvectors that match the  $k$  's largest eigen values, where  $k$  is the dimension of the new subspace function.
6. Create the projection matrix  $W$  from top  $k$  eigenvectors
7. To obtain the new  $k$ -dimensional feature subspace, transform the  $d$ -dimensional data set  $X$  using the projection matrix  $W$ .

**3.2.6 Classification with Decision Tree Classifier**

Decision tree classifiers have an accurate, readable classification model in several different application contexts [36, 158]. By constructing a decision tree, the Decision Tree Classifier tree node sets a test in an attribute, and any branch that falls out of that node corresponds to one of the possible attribute values. Leaf is associated with class labels of the case. The training collection shall be graded according to the results of the track tests, by sailing from the root of the tree to a leaf.

Each node divides the instance space into two or more sub-spaces according to the test condition of an attribute starting from the tree root node. Then a new node will be generated as you travel down the tree branch that is the attribute value. This process

is repeated until all records in the training set are listed for the subtree rooted in the new node. The decision tree building method typically operates top-down by selecting a test status at each stage to better divide the records.

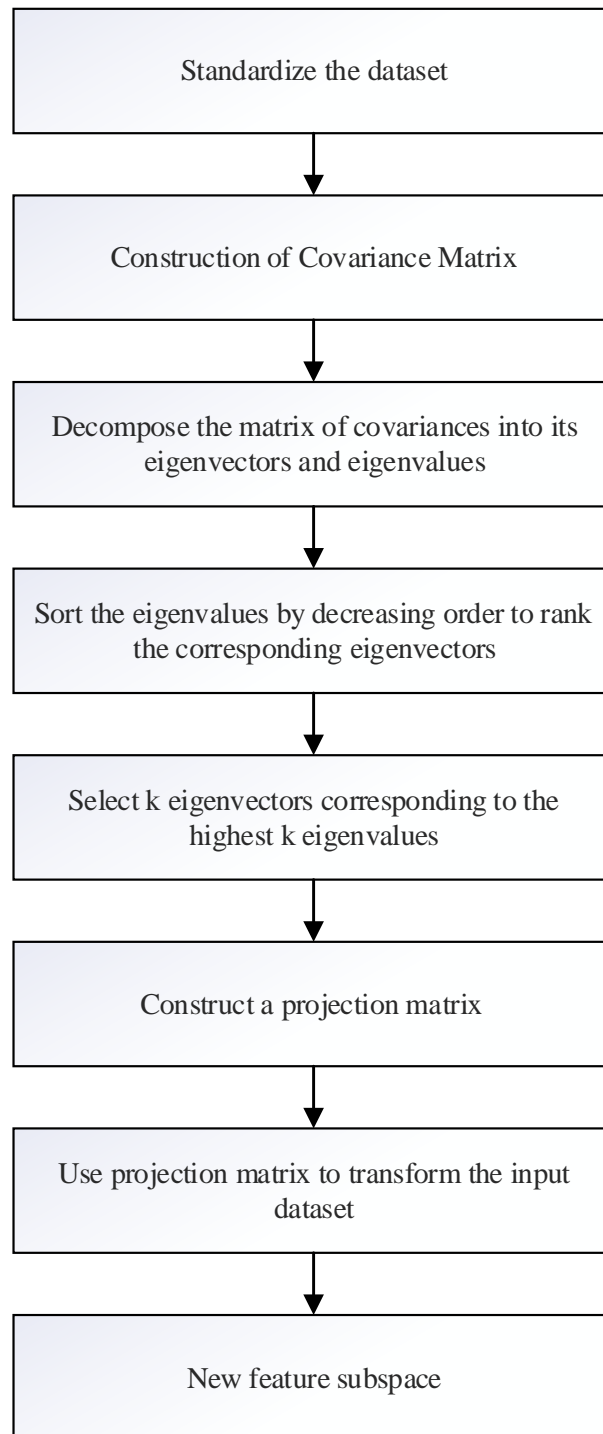


**Figure 3.5: Steps performed in Principal Component Analysis**

### 3.3 Proposed Method II

(Based on K-Nearest Neighbors' Algorithm)

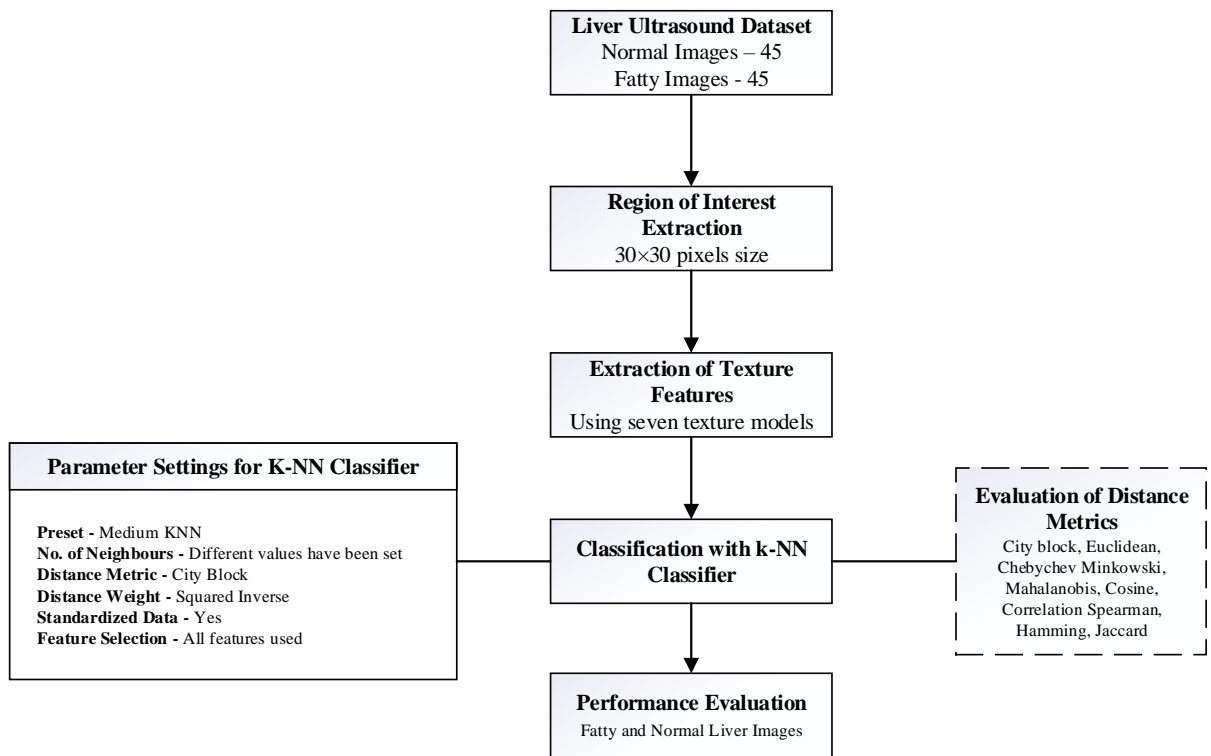


**Figure 3.6: Flowchart of proposed methodology used in Proposed Method II**

The main aim of this work is to identify a subset of features that improves the model performance and enhances the semantic interpretability.

See Figure 3.6 for the flowchart of the proposed technique. The proposed technique consists of various steps such as extraction of the ROI, extraction of the Texture Feature, selection of features and classification.

#### 3.3.1 Extraction of Region of Interest and Features

In the proposed method, for ROI Extraction the similar process as mentioned in proposed method I has been used. The ROI's of size  $30 \times 30$  pixels are extracted from the Liver Ultrasound dataset. Texture analysis is a significant and valuable area of study in many computer imaging and machine vision applications. The tonal variations make the fatty liver and normal image different. Over the last few years, the researchers have suggested several models for texture analysis. We can categorize these models into

structural, statistical, model-based and transform-based models. Each model visualizes texture in a different way and it is always a challenging task to determine the optimal texture model for liver tissue classification. Various texture models like “Haralick's Spatial Gray Level Co-occurrence Matrix (SGLCM), First-order Statistics (FoS), Statistical Feature Matrix (SFM), Gray Level Difference Statistics (GLDS), Fourier Power Spectrum (FPS), Law Texture Energy Measures (TEM), Fractal” were used in the proposed work to extract the features from ROI.

The details of these texture models are given in section 3.2.3. The extracted features using different texture models are given in Table 3.1.

<b>Proposed Algorithm</b>
<p><b>Input:</b> Liver Ultrasound Image</p> <p><b>Output:</b> Class of Image (Normal/Fatty)</p> <ol style="list-style-type: none"> <li>1. For each image I in N, obtain           <ol style="list-style-type: none"> <li>ii) <math>r_i = \text{Extract } 30 \times 30 \text{ pixels ROI from } I</math></li> <li>iii) <math>R = R \cup r_i</math>, where R is a set of all extracted <math>30 \times 30</math> pixels ROI, N is the total no of images.</li> </ol> </li> <li>2. For each <math>r_i</math> in R, Obtain           <ol style="list-style-type: none"> <li>(viii) <math>F_{1-14} = \text{Extract GLCM based Haralick Features}</math></li> <li>(ix) <math>F_{15-19} = \text{Extract GLDS Features}</math></li> <li>(x) <math>F_{20-23} = \text{Extract FoS Features}</math></li> <li>(xi) <math>F_{24-27} = \text{Extract SFM Features}</math></li> <li>(xii) <math>F_{28-41} = \text{Extract Law's TEM Features}</math></li> <li>(xiii) <math>F_{42-43} = \text{Extract Fractal Features}</math></li> <li>(xiv) <math>F_{44-45} = \text{Extract FPS Features}</math></li> </ol> </li> <li>3. <math>S = \{F_{1-14} \cup F_{15-19} \cup F_{20-23} \cup F_{24-27} \cup F_{28-41} \cup F_{42-43} \cup F_{44-45}\}</math></li> <li>4. For each <math>r_i</math> in R           <ol style="list-style-type: none"> <li>(viii) Apply kNN based Classification using S.</li> <li>(ix) Evaluate different values of k.</li> <li>(x) Evaluate different similarity metrics</li> </ol> </li> <li>5. End</li> </ol>

### 3.3.2 Classification with K-Nearest Neighbour Classifier

Given two classes: Fatty and Normal, a feature vector 'x' of liver ultrasound image whose class label is unknown. The main task is to classify 'x' in one of the two classes given above. In order to classify the feature vectors of testing data, K-Nearest Neighbor (*k*-NN) classifier [159] is used. The algorithm is given below:

<b><i>k</i>-NN Algorithm</b>
1. Among the $N$ training points, search for the $K$ nearest neighbours closest to $x$ using a distance measure. The parameter $k$ is user defined. For two class problem $k$ should be odd.
2. Out of the $k$ closest neighbours, identify the number $k_i$ of the points that belongs to class $w_i$ . Obviously,
$\sum_{i=1}^c k_i = k$
3. Assign $x$ to class $w_i$ , for which $k_i > k_j, j \neq 1$ . In other words, $x$ is assigned to the class in which the majority of the $k$ -closest neighbors belong.
4. End

The key advantage of the *k*-NN classifier is its simplicity, lack of parameter assumptions and intuitive existence (i.e. it is presumed that new samples belong to the same class as the training samples in the feature space that are nearest to them). As a classifier, *k*-NN is used as the simplest and most commonly used machine learning algorithm.

Suppose we are given  $c$  classes,  $w_i, i = 1, 2, 3, \dots, c$ , and a point  $x \in R^l$ , and  $N$  Training points,  $x_i, i = 1, 2, 3, \dots, N$ , in the  $l$ -dimensional space, with the corresponding class labels. Given a point,  $x$ , whose class label is unknown, the task is to classify  $x$  in one of the  $c$  classes.

Further in this work, different distance metrics have been used.

“One of the simplest and most common classifications is the K-Nearest Neighbour (K-NN) classification [160-161]. Its quality however competes with the most complex literature classifiers. The centre of this classifier is largely based on calculating the difference or similarity between the examples tested and the examples of the training. The question arises as to the distance metric should be used for the KNN classifier from a great number of available distance and similarity measures?”

In KNN classifier, different methods are used to classify the distances between the test sample and the training data samples. Distance measurements therefore play a crucial role in deciding the final performance for the classification. Very few studies explored the impact of various distance metrics on KNN 's results, which used a limited number of distances. Such experimental shortage does not prove which distance to use with the KNN classifier is better.

‘Best distance metric’ is the one that gives best performance of the KNN in terms of overall accuracy [162]. In this thesis work, 10 different distance metrics available in the literature have been explored. The details of the distance metrics used are given in Table 3.2.

**Table 3.17: Distance Metrics used in the Proposed Method II**

<b>Sr. No.</b>	<b>Distance Metric Used</b>
1	City block
2	Euclidean
3	Chebychev
4	Minkowski
5	Mahalanobis
6	Cosine
7	Correlation
8	Spearman
9	Hamming
10	Jaccard



### 3.4 Proposed Method III

(Based on a two-layer feedforward Neural Network)

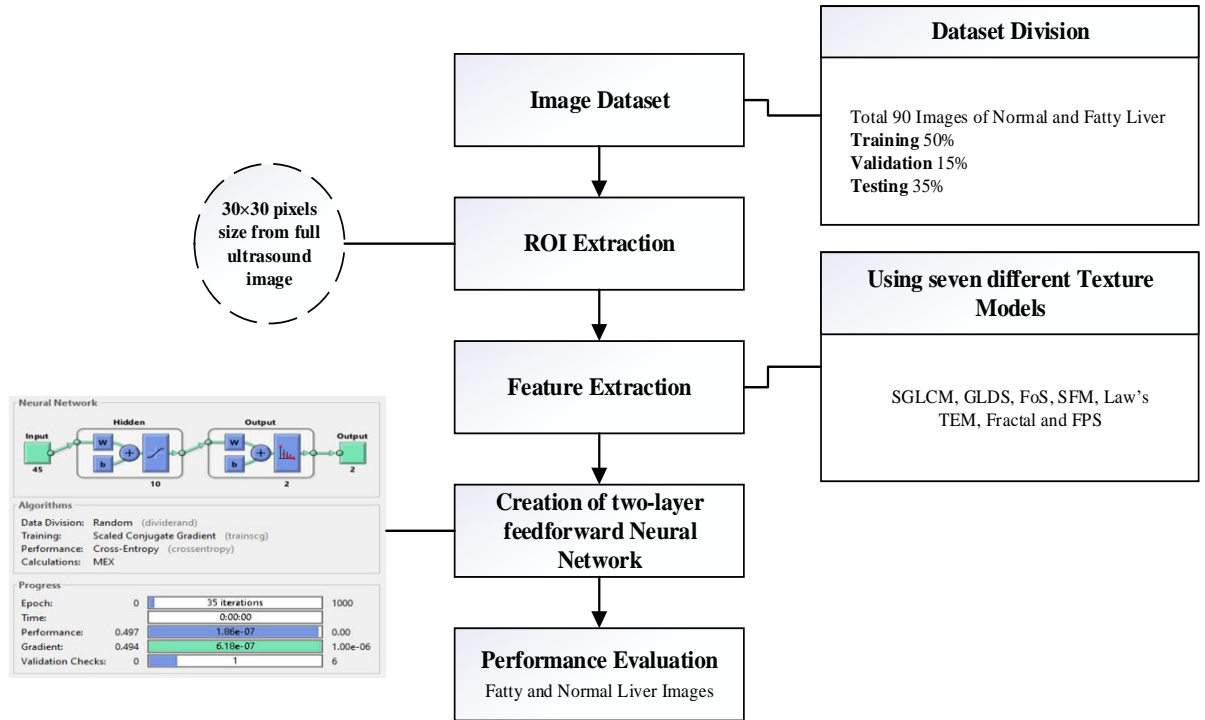


**Figure 3.7: Steps carried out in Proposed Method III**

#### 3.4.1 ROI Extraction and Feature Extraction

In the proposed method, for ROI Extraction the similar process as mentioned in proposed method I has been used. Size 30x30-pixel ROIs are derived from the dataset of Liver Ultrasound. Texture features are extracted using different texture models such as “Haralick's Spatial Gray Level Co-occurrence Matrix (SGLCM), Gray Level Difference Statistics (GLDS), First-order Statistics (FoS), Law's Texture Energy Measures (TEM), Fourier Power Spectrum (FPS), Statistical Feature Matrix (SFM), and fractal features” are extracted from each ROI selected from the entire ultrasound picture. Figure 3.7 indicates the measures carried out in the Proposed Method III.

The details of these texture models are given in section 3.2.3. The extracted features using different texture models are given in Table 3.1.

### **3.4.2 Creation of two-layer feedforward neural network**

A two-layer feedforward neural network [163-165] was modelled in the Proposed Method III. For the creation of a neural network classification system a three-stage (training – validation – test) approach is used. Sigmoid transfer function was used in the hidden layer of the neural network and a SoftMax transfer function was used as a standard network for the classification of liver ultrasound images in the output layer. The value of the hidden neurons is set as 10 for conducting the experiments. Since the number of categories to be listed in is two, the output neuron value is set as 2.

#### **(i) Division of Dataset**

A total of 90 images are randomly divided into Training, Validation and Testing. Training data set is the data set that has been provided to the network for the training purpose and accordingly network is adjusted on the basis of its error rate [166]. Validation data set is basically used to measure the generalization capability of network and further to halt the process of training when there is no improvement in the generalization. Testing data set is independent of the training data set and validation data set that has no effect on training. This data set is used to measure the network performance after training.

In the proposed work, the neural network has been trained with scaled conjugate gradient backpropagation. As the cross-entropy error of the validation sample increases that shows the generalization has stopped improving and ultimately training stops.

#### **(ii) Training of designed network**

In the proposed work, the neural network has been trained with scaled conjugate gradient backpropagation. As the cross-entropy error of the validation sample increases that shows the generalization has stopped improving and ultimately training stops. Figure 3.8 shows the neural network has been trained with scaled conjugate gradient backpropagation.

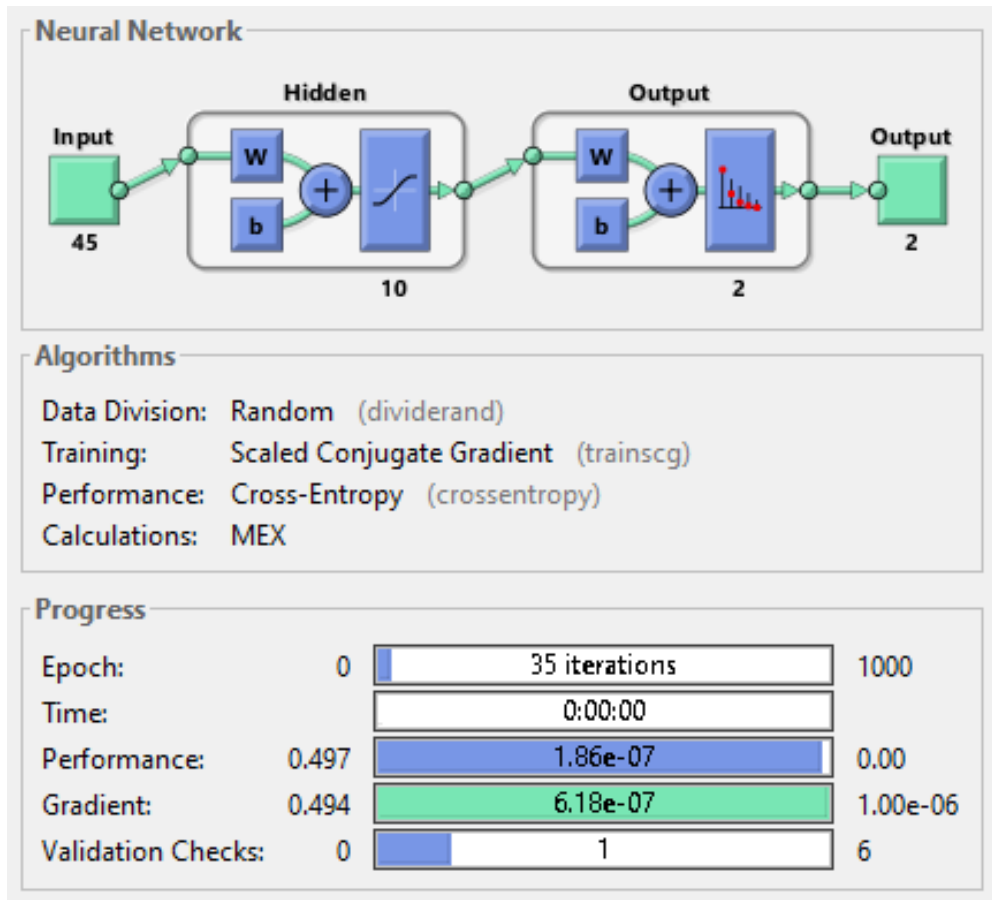


Figure 3.8: Training of Designed Neural Network

### 3.5 Proposed Method IV

(Based on Sequential Minimal Optimization and Mutual Information Feature Selection)

It is clear from the literature that many researchers have done work on the classification of fatty and normal liver ultrasound images and to the best of author's knowledge, very less work is done on feature selection techniques in this domain. Furthermore, the researchers have focused more upon the accuracy rate instead of Miss Rate. But it is well known that classifying fatty liver as normal is more harmful than classifying normal liver as fatty. With regard to this, in this thesis, we have worked upon above issues deeply. Figure 3.9 shows the flowchart of Proposed Method IV. The proposed method consists of various steps like ROI Extraction, Feature Extraction,

Feature Selection and Classification. The details of these steps are mentioned in subsequent sections.

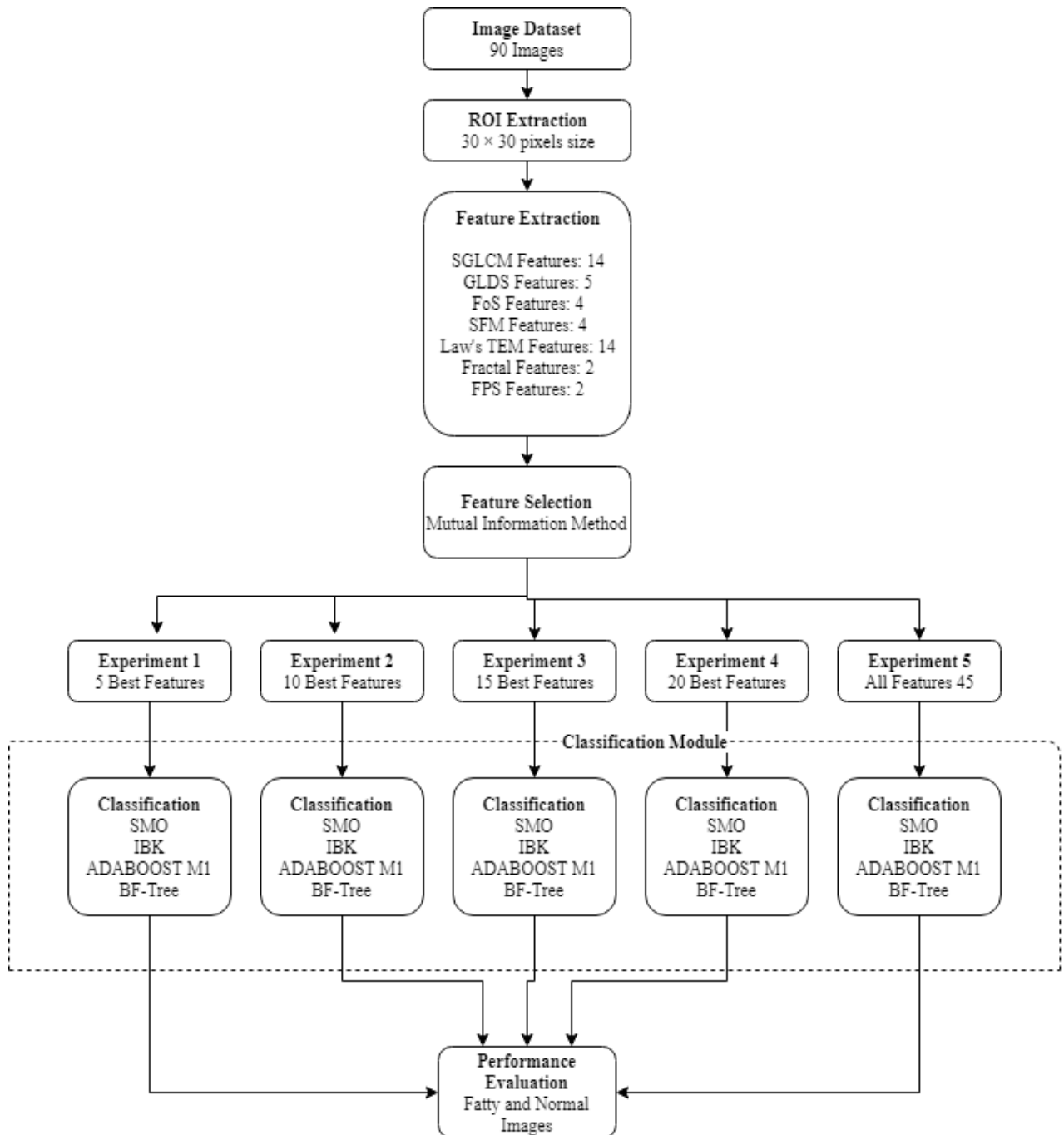


Figure 3.9: Flowchart depicting the working of Proposed Method IV

### **3.5.1 ROI Extraction**

In medical image processing, to identify the ultrasound image characteristics quantitatively, a “Region of Interest” (ROI) is extracted. ROI is a selected significant part of an image which represent the whole image and also helps the users to avoid unnecessary calculations. Different authors have used different ROI sizes in their research work but for reliable statistics, a  $30 \times 30$  fixed square size ROI (900 pixels) [21] is selected by the experienced radiologists from each image in the present research work. The sample ROIs contain tissue pattern only. The ROI size ( $30 \times 30$  pixels) of an image is chosen diagonally to avoid effect of liver glycogen, fat, blood vessels and water storage.

### **3.5.2 Texture Feature Extraction**

The next step in the present methodology is to extract texture features from ROI selected from each ultrasound liver image in the database. As per the literature survey done by authors, various texture feature extraction models have been extensively explored in medical applications, which extract different features from an image in different ways for different purposes. In [21], seven different texture feature selection models i.e. “SGLCM, FPS, GLDS, FoS, SFM, TEM and FF” have been used to extract total 35 features. In the present study, same models have been used to extract total 45 features in order to improve the classifier accuracy of existing CAD systems.

### **3.5.3 Feature Selection using Mutual Information (MI)**

From the past few years, it has been found that data analysis task is one of the major difficulties in case of very high dimensional dataset. To overcome this problem, feature selection methods are used. Selection is basically an extensive method for identifying the best characterizing features. In this work, total 45 texture features are extracted. Out of which, the best features are selected by the Mutual Information (MI) method [167], which is based on information theory and is used to evaluate the amount of information achieved between two random variables. If value of MI is zero, both variables are independent and contain no information about each other. As seen from Algorithm 1, this method finds out the relevant and redundant features from the dataset, and this subset of features  $S \in F$  produces equal or better classification accuracy as compared to original feature set  $F$ . In the present work, five different experiments are carried out based on the required

number of features (k) to be selected, i.e. 5 best features (k=5), 10 best features (k=10), 15 best features (k=15), 20 best features (k=20) and in last 45 features all together.

---

Algorithm 1. Mutual Information

---

*(Initialization)*

1. Set  $F \leftarrow$  set of all image features of dataset  $D$
2. Set  $S \leftarrow$  empty set

*(Computation of Mutual Information)*

3. For  $\forall f_i \in F$

Compute  $I(C; f_i)$ ;

where  $I(C; f_i) = \sum_{c \in C, f_i} P(c; f_i) \log \frac{P(c, f_i)}{P(c)P(f_i)}$

4. Find the feature  $f_i$  that maximizes  $I(C; f_i)$

$S \leftarrow S \cup \{f_i\}, F \leftarrow F / \{f_i\}$ ;

Repeat until  $|S| = k$ ;

where  $k$  is the required no. of features to be selected

*(Output)*

5. Output the set  $S$  with the selected features.
- 

### 3.5.4 Classification with Sequential Minimal Optimization

For classifying the ultrasound images on the basis of feature selection, different binary classifiers i.e. SMO [26], IBk [168], AdaboostM1 [169] and BF Tree [170] are evaluated to achieve high recognition rate. In this paper, the binary classification is taken into account because ultrasound liver images can be classified either fatty or normal liver. The choice of classifier for evaluation purpose is made keeping in view their respective advantages. SMO classifier (also known as Support Vector Machine (SVM) classifier) outperforms in high dimensional space, avoids local convergence and provides optimal solutions. This classifier uses kernel trick and helps in solving the problems of overfitting. On the other hand, IBk works as K-Nearest Neighbour (K-NN) classifier which is fast, easy to implement and gives effective outcome. The AdaBoost M1 Classifier is a productive classification algorithm with boosting features and enhances the characterization rate, whereas BF Tree helps in removing impurity and examining new pruning techniques by deciding the quantity of developments. The parameter settings for different classification algorithms is done with the help of WEKA [171]

tool, to perform extensive experiments for the selection of optimal values of different parameters for different classifiers.

### **3.6 Conclusion**

Fatty Liver Disease (FLD) is one of the most critical diseases that should be detected and cured at the earlier stage in order to decrease the mortality rate. To identify the FLD, ultrasound images have been widely used by the radiologists. However, due to poor quality of ultrasound images, they found difficulties in recognizing FLD. To resolve this problem, many researchers have developed various Computer Aided Diagnosis (CAD) systems for the classification of fatty and normal liver ultrasound images. However, the performance of existing CAD systems is not good in terms of sensitivity while classifying the FLD. In this chapter, four different methods have been proposed for the classification of liver ultrasound images.





## Chapter-4

### Results and Discussion

#### 4.1 Introduction

The findings of the proposed methods are introduced and discussed in this chapter with reference to the study purpose, which is the processing and analysis of ultrasound images for diagnosis of disease. The main objective of this research work is to determine the accuracy of the classification of fatty and normal ultrasound images of the liver. As described in Chapter 3, the present work has used seven different texture feature extraction models to extract texture features and different classifiers to distinguish fatty and normal liver images. In this analysis, different values for parameters were set to obtain good results for the classification. To assess efficiency of the methods proposed, 5-fold cross-validation has been performed. The exploratory results revealed that the methods proposed could be used with higher accuracy to distinguish fatty and normal liver ultrasound images.

#### 4.2 Performance Evaluation of Proposed Method I

**(Based on Decision Tree Classifier with Principal Component Analysis)**

For evaluating the performance of the proposed method, the extracted 45 features are passed to the Decision Tree Classifier and parameter setting has been done to obtain the maximum accuracy.

Table 4.1 shows the parameter settings done for Decision Tree classifier. The preset used is Fine Tree with maximum no. of splits as 100. Further, Gini's Diversity Index has been used as split criteria for evaluating the performance.

**Table 4.1: Parameter Settings for Decision Tree Classifier**

<b>Preset</b>	Fine Tree
<b>Max. no. of splits</b>	100
<b>Surrogate Decision splits</b>	off
<b>Criterion used for split</b>	Gini's Diversity Index

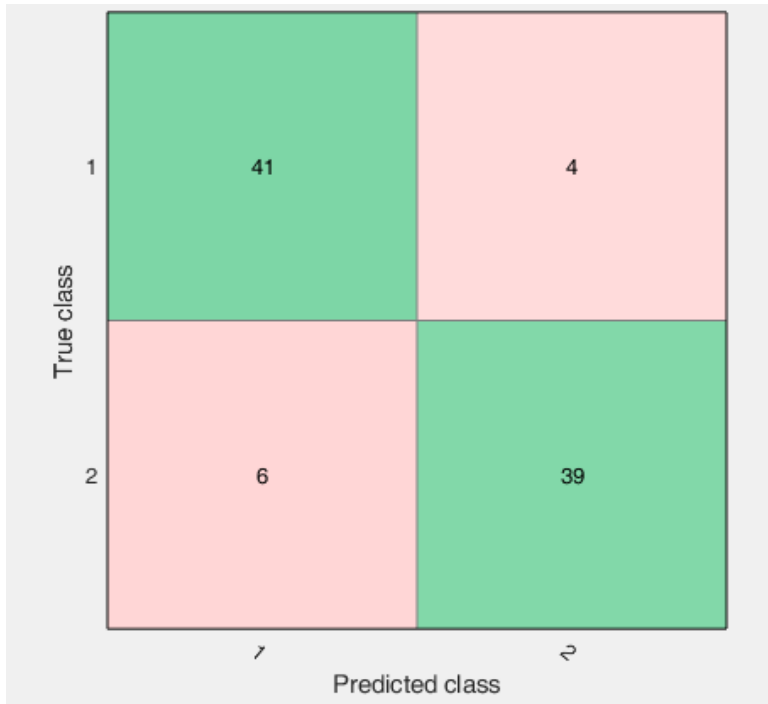


**Figure 4.1: Plot of number of observations with Decision Tree classifier**

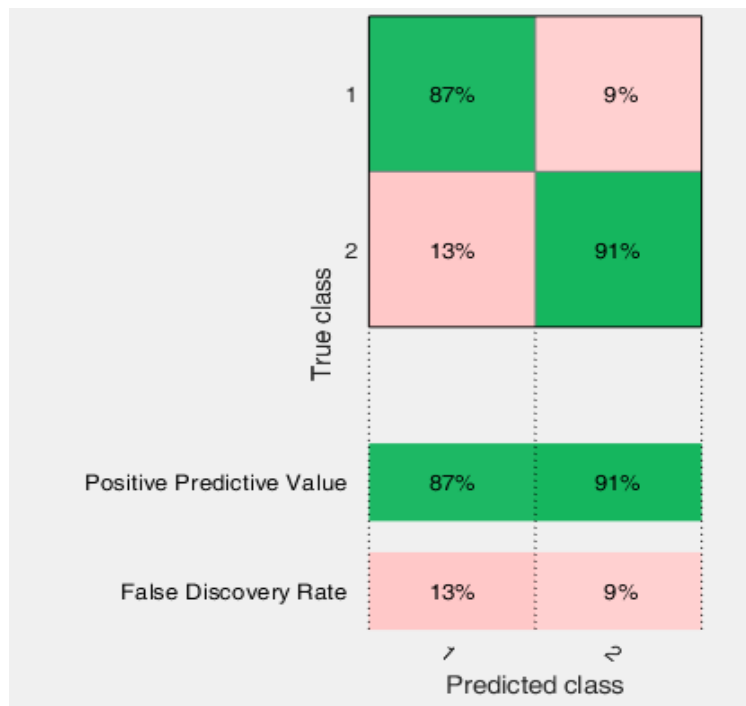


**Figure 4.2: Positive Predictive Value and False Discovery Rate when Decision Tree classifier used**

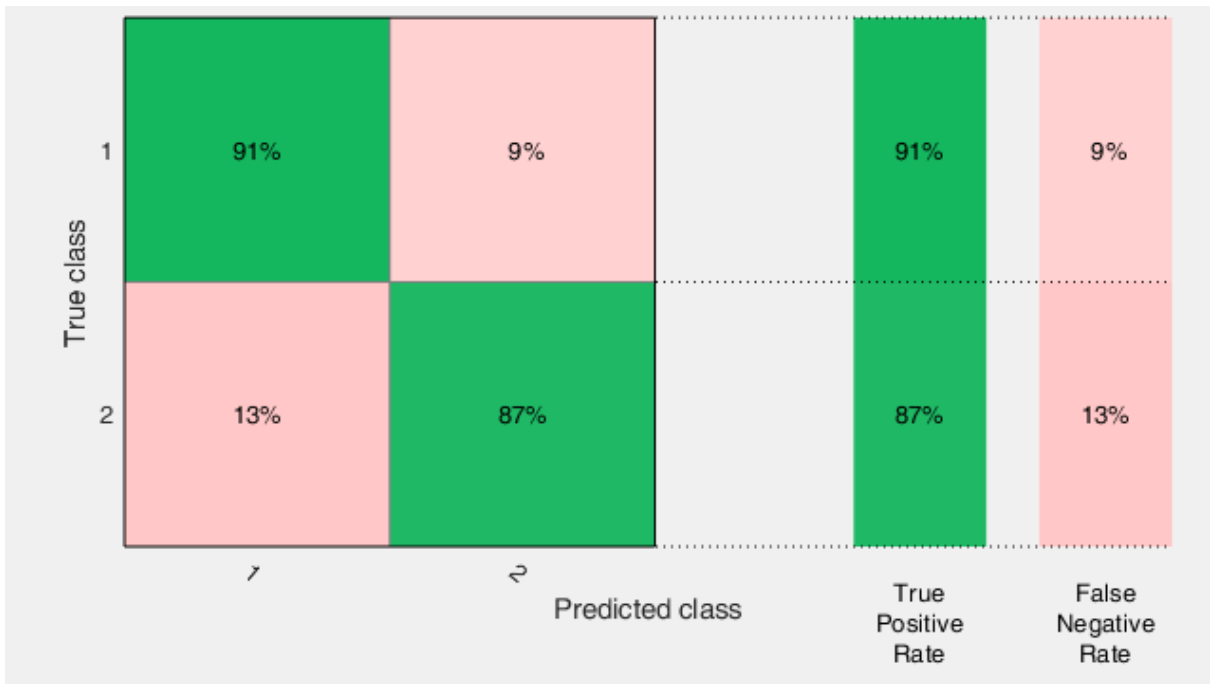


**Figure 4.3: True Positive Rate and False Negative Rate when Decision Tree classifier used**

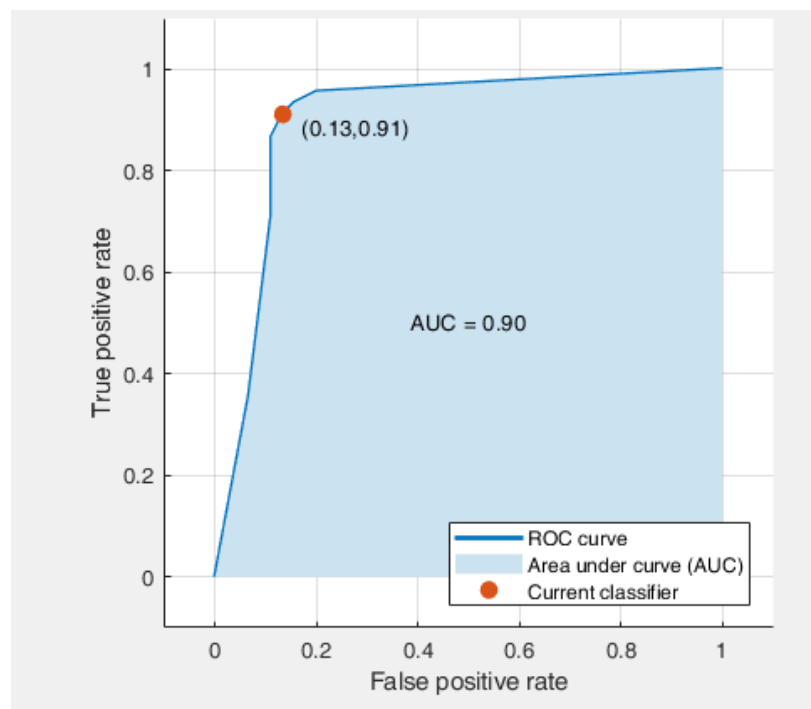


**Figure 4.4: ROC curve when Decision Tree classifier used**

From the figure 4.1, it is clearly shown that when extracted forty-five features have been passed to Decision Tree classifier with the above parameter settings, then classifier is able to make predictions as shown in above Figure 4.1 in terms of TP, TN, FP and FN. Figure 4.2 shows Positive Predictive Value and False Discovery Rate when Decision Tree classifier has been used. Figure 4.3 presents True Positive Rate (TPR) and False Negative Rate (FNR) when Decision Tree classifier has been used. Here, TPR refers to the fraction of correctly graded results per true class and the FNR is the fraction of erroneously classified results per true class. In the last two columns on the right the plot shows summaries per true class.

The receiver operating characteristic (ROC) curve as shown in Figure 4.4 showing true and false positive rates. The ROC plot represents true positive vs. false positives rate for the already identified trained classifier. The good outcome without incorrectly classified points is a right angle to the top left of the curve. A 45-degree line depicts a poor outcome and is no better than chance. The Area Under Curve number is a measure of classifier's overall efficiency. An overall accuracy of 88.9% has been achieved in case of decision tree classifier when all forty-five extracted features have been used. The area under ROC curve is found to be 0.90.

The use of Principal Component Analysis (PCA) has been widely studied in the literature for the dimensionality reduction process. Therefore, in the proposed work, PCA has been used for projecting original data into a new coordinate space. Principal Component Analysis (PCA) was used to lower predictor space dimensionality. In order to prevent overfitting issue, dimensionality in classification must be reduced. To generate new variables which can be termed as principal components, PCA converts predictors linearly to remove redundant measurements. Table 4.2 shows the Parameter Settings done for Decision Tree with PCA. While using PCA the explained variance has been set to 95%. It has been found from the literature survey, the higher value results in overfitting whereas the use of lower value results in removing discriminating dimensions.

**Table 4.2: Parameter Settings for Decision Tree with PCA**

<b>Preset</b>	Fine Tree
<b>Maximum number of splits</b>	100
<b>Criterion used for splits</b>	Gini's Diversity Index
<b>Surrogate Decision splits</b>	off

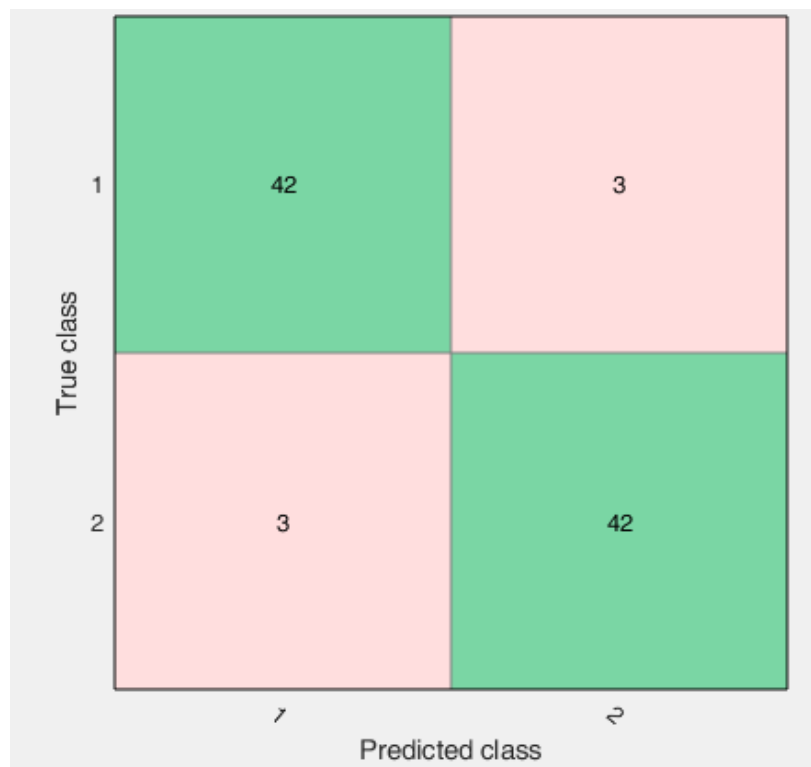


**Figure 4.5: Plot of number of observations when Decision Tree classifier with PCA used**

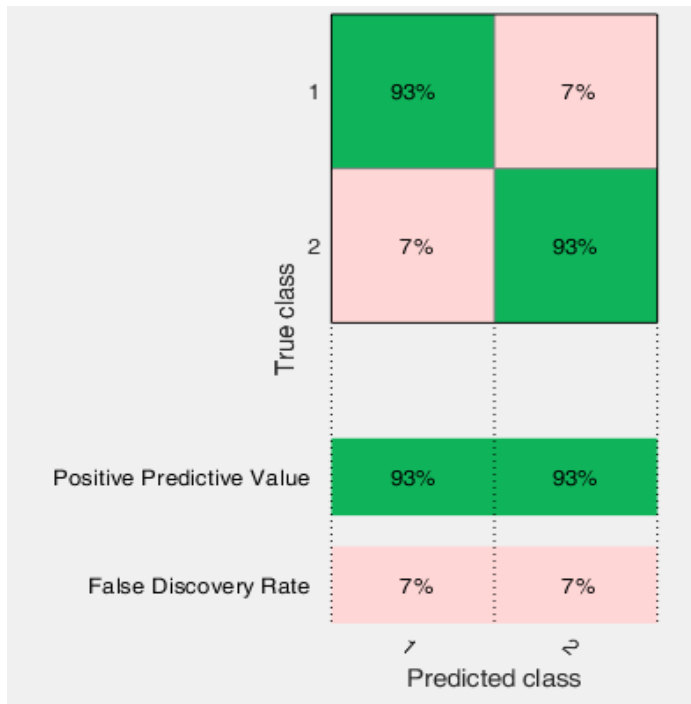


**Figure 4.6: Positive Predictive Value and False Discovery Rate when Decision Tree classifier with PCA used**

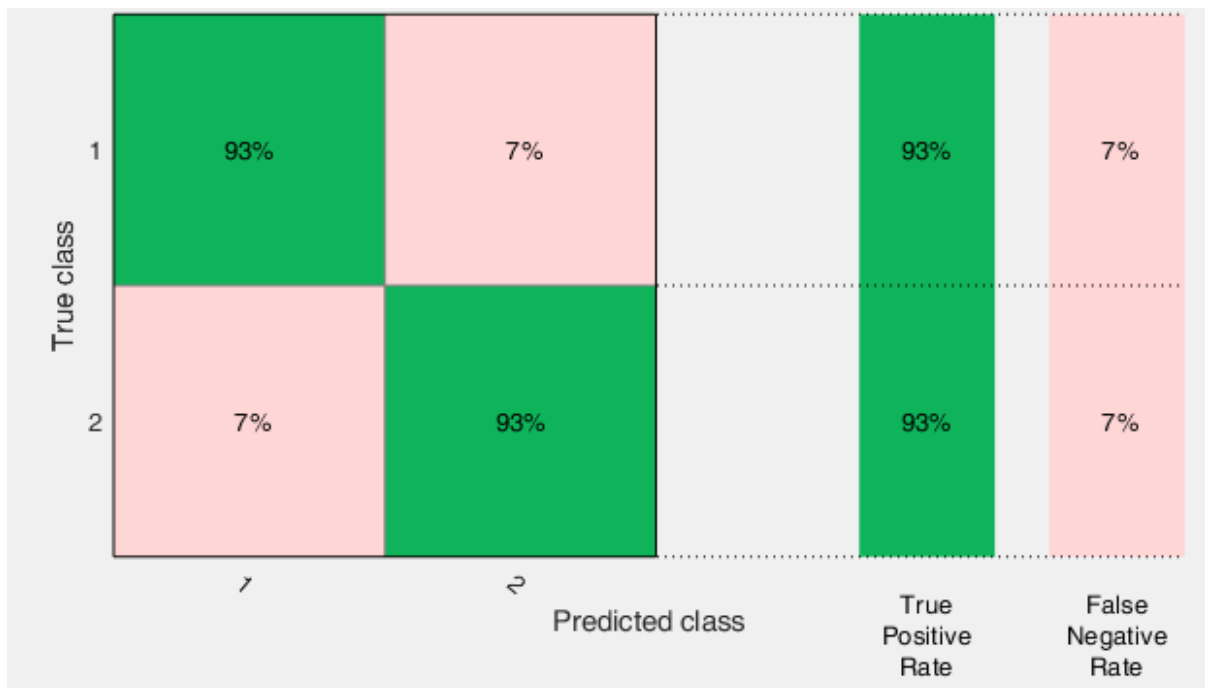


**Figure 4.7: True Positive Rate and False Negative Rate when Decision Tree classifier with PCA used**

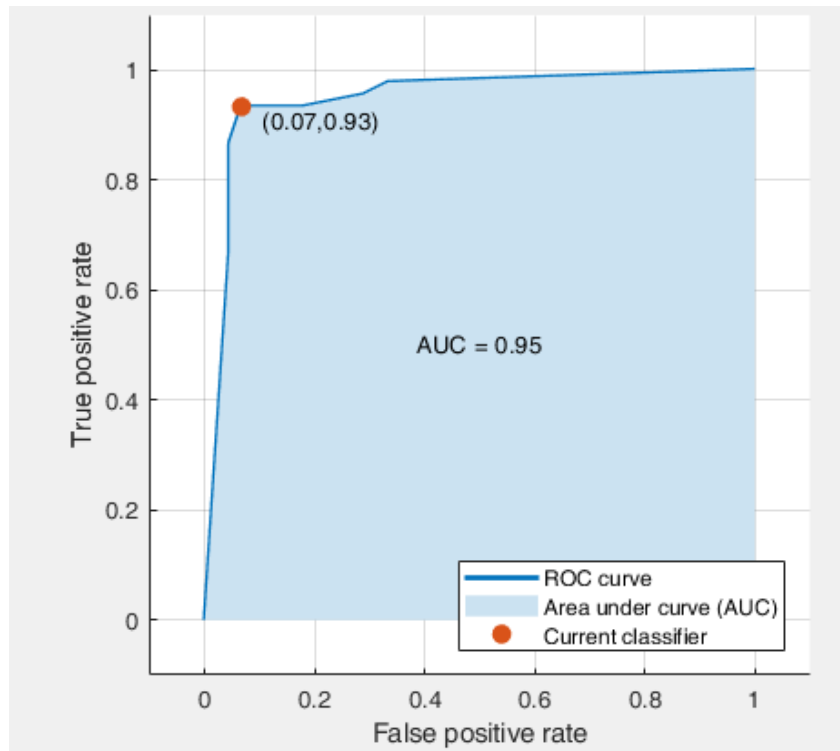


**Figure 4.8: ROC curve when Decision Tree classifier with PCA used**

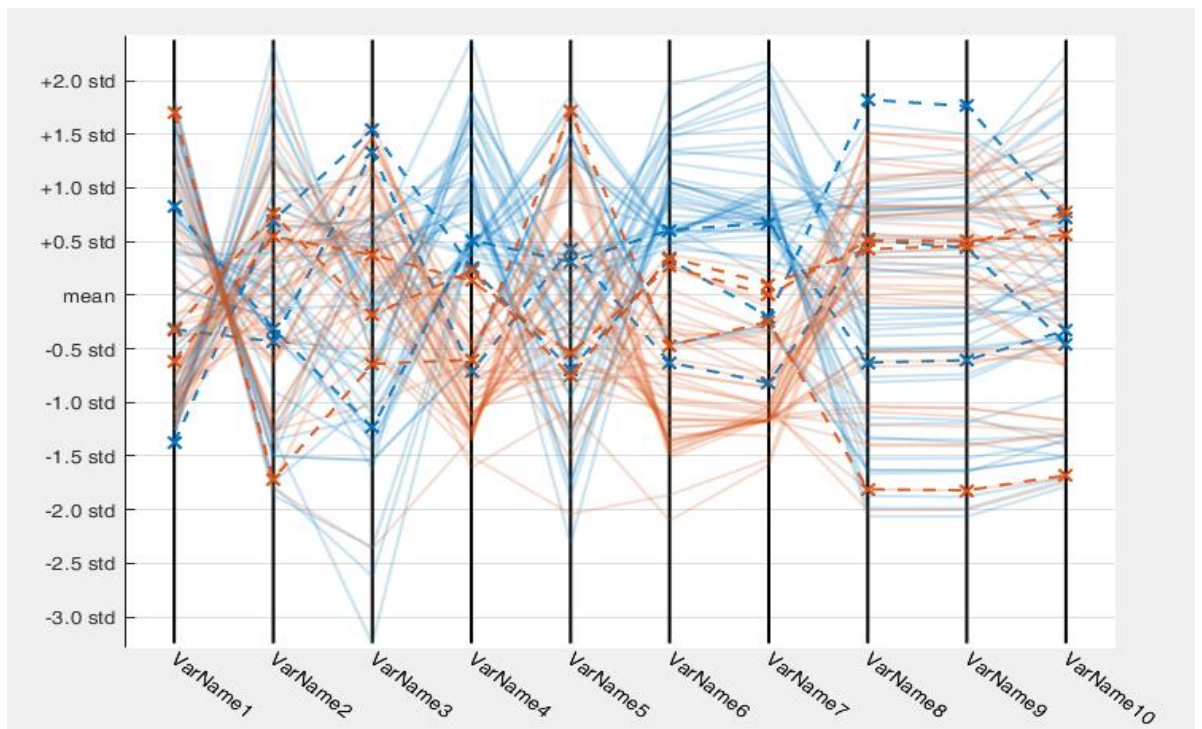


**Figure 4.9: Parallel Coordinate Plot**

In case of PCA, explained variance per component in order is found to be – 99.9%, 0.1%, 0.0 %, 0.0 %, 0.0 %, 0.0 %, 0.0 %, 0.0 %, 0.0 %, 0.0 %. One component was retained during training as the number of components cannot be greater than the number of numerical predictors.

Figure 4.5 shows the observations when Decision Tree classifier with PCA has been used. From the figure it is clearly evident that when PCA has been used with Decision Tree the model is able to make good predictions in terms of TP and TN. Figure 4.6 presents Positive Predictive Value and False Discovery Rate when Decision Tree classifier with PCA has been used. False discovery rate is found to be 7%, which is less than as compared to False Discovery Rate found in the case when Decision Tree classifier alone has been used. Figure 4.7 gives True Positive Rate and False Negative Rate when Decision Tree classifier with PCA has been used. It is clearly evident from the figure that model is able to make good predictions. The Figure 4.8 shows ROC curve when Decision Tree classifier with PCA has been used. The area under ROC curve is found to be 0.95.

Figure 4.9 shows parallel coordinate plot. In order to identify the highly discriminating features that separates two classes this plot plays a crucial role. Further the dashed lines in this plot show misclassified points.

**Table 4.3: Comparison of Accuracy and Area Under ROC for Decision Tree Classifier and Decision Tree with PCA**

<b>Classifier</b>	<b>Features Used</b>	<b>Overall Accuracy</b>	<b>Area Under ROC</b>
Decision Tree	All 45	88.9%	0.90
Decision Tree with PCA	PCA	93.3%	0.95

The Table 4.3 clearly shows the comparison of performance of Decision Tree Classifier and Decision Tree with PCA. From the experimental results, it has been found that Decision Tree with PCA outperforms as compared to Decision Tree. In comparison with the basic decision tree algorithm, the proposed results revealed that Decision Tree with PCA method not only improves the overall accuracy in predicting two classes but also makes the decision tree model simplified.



### 4.3 Performance Evaluation of Proposed Method II

#### (Based on K-Nearest Neighbors' Algorithm)

In this work the feature vectors consist of all the extracted forty-five features from different texture models. These features are used for classification with  $k$ -NN classifier. Given two classes, a feature vector 'x' of liver image whose class label is unknown. The main task is to classify 'x' in one of the two classes. In order to classify the feature vectors of testing data, K-Nearest Neighbour (K-NN) classifier is used. The selection of value of k in KNN plays a significant role. In the proposed work, the K-NN algorithm has been tested with different values of k and that value of k has been selected for further experimentation in which the model is able to make good number of predictions with data that the model has not seen before.

Further in this work an experimental study has been done to evaluate the different distance metrics available to evaluate the performance.

The key advantage of the K-NN classifier is its simplicity, lack of parameter assumptions and intuitive existence (i.e. it is presumed that new samples belong to the same class as the training samples in the feature space that are nearest to them). Being simplest and widely used machine learning algorithm, K-NN is used as a classifier.

Table 4.4 shows parameter setting done to evaluate the performance. The preset used is Medium K-NN. The whole data is standardized to get the best performance. Experiments have been performed with different values of K.

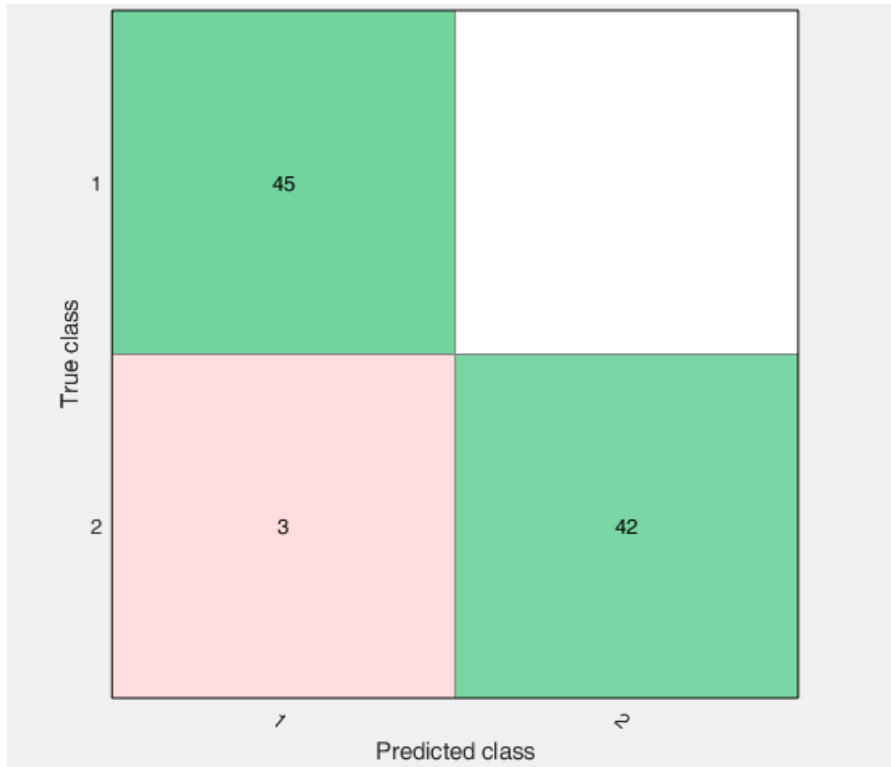
**Table 4.4: Parameter setting of K-NN Classifier**

<b>Preset</b>	Medium KNN
<b>No. of Neighbours</b>	Different values have been set
<b>Distance Metric</b>	City Block
<b>Distance Weight</b>	Squared Inverse
<b>Standardized Data</b>	Yes
<b>Feature Selection</b>	All features used

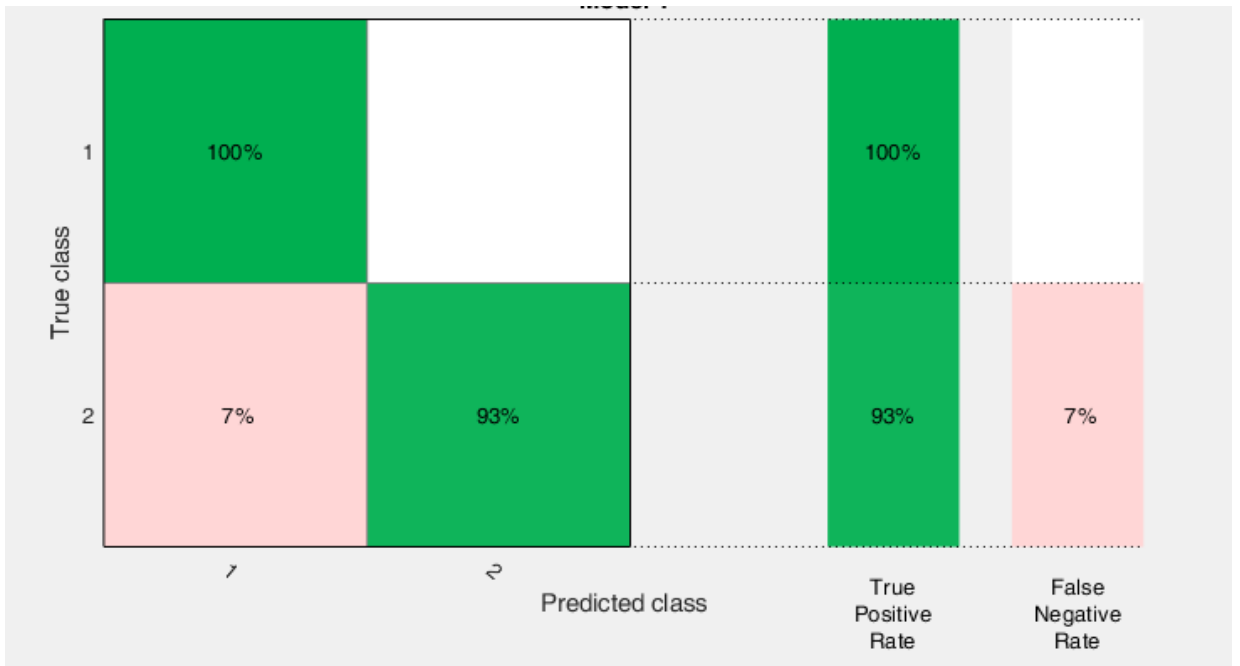
**Table 4.5: Comparison of overall accuracy for different values of K**

<b>Value of k</b>	<b>Overall Accuracy</b>
1	83.3 %
3	93.3 %
5	95.6 %
<b>7</b>	<b>96.7 %</b>
9	95.6 %
11	93.3 %
13	95.6 %

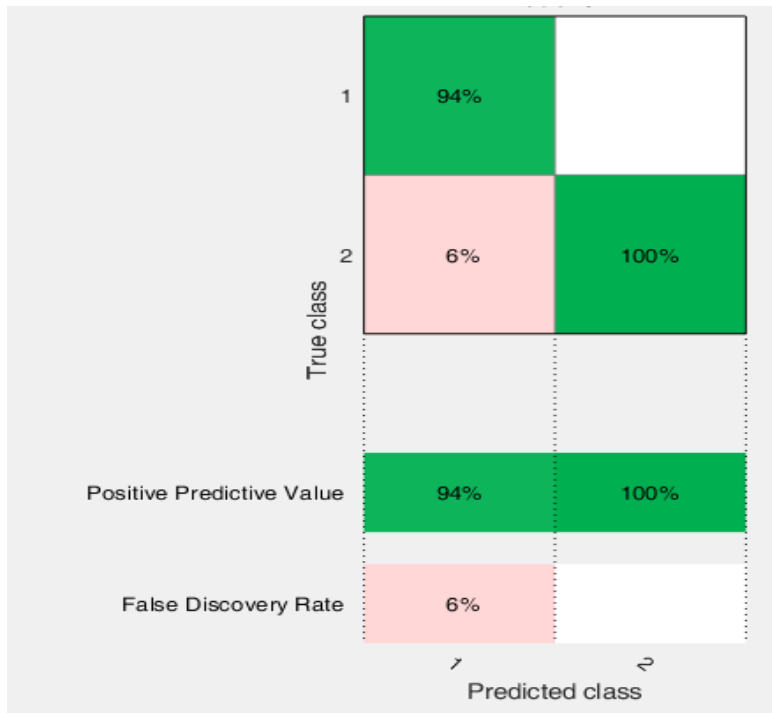
K-NN classification is a nearest-neighbour classification model in which both the distance metric and the number of nearest neighbours can be altered. In this thesis work, an experimental study has been done to identify the best value K. For this different value of K have been used as shown in Table 4.5. From the experimental results it has been found that for value of K as 1, an accuracy of 83.3% has been achieved. As the value of K is increased to 3, there is sharp increase in the overall accuracy and founds to be 93.3%. When value of k is further increased to K=5 an accuracy of 95.6% has been achieved. This clearly shows that value of K has significant effect on the classification accuracy. Further the value of K is set to 7 and an accuracy of 96.7% has been achieved. After that for K=9, 11 and 13, the overall accuracy starts decreasing. From the experimental results it has been found that for K=7 the model gave highest accuracy. Therefore, in the present work the value of K has been set to 7 for further experiments.



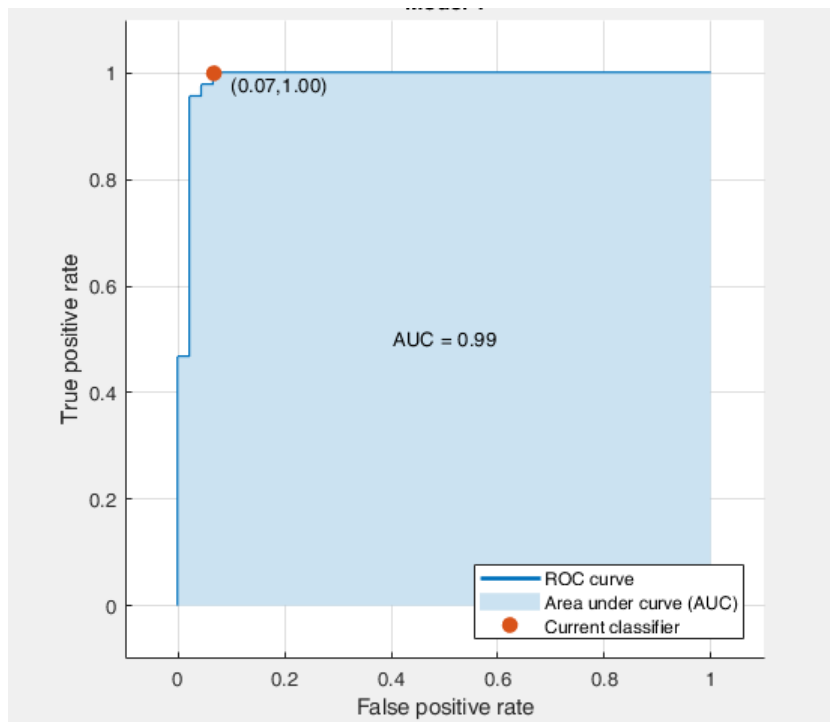
**Figure 4.10: Plot of number of observations with k-NN Classifier**



**Figure 4.11: True Positive Rate and False Negative Rate when k-NN classifier used**



**Figure 4.12: Positive Predictive Value and False Discovery Rate when k-NN Classifier used**



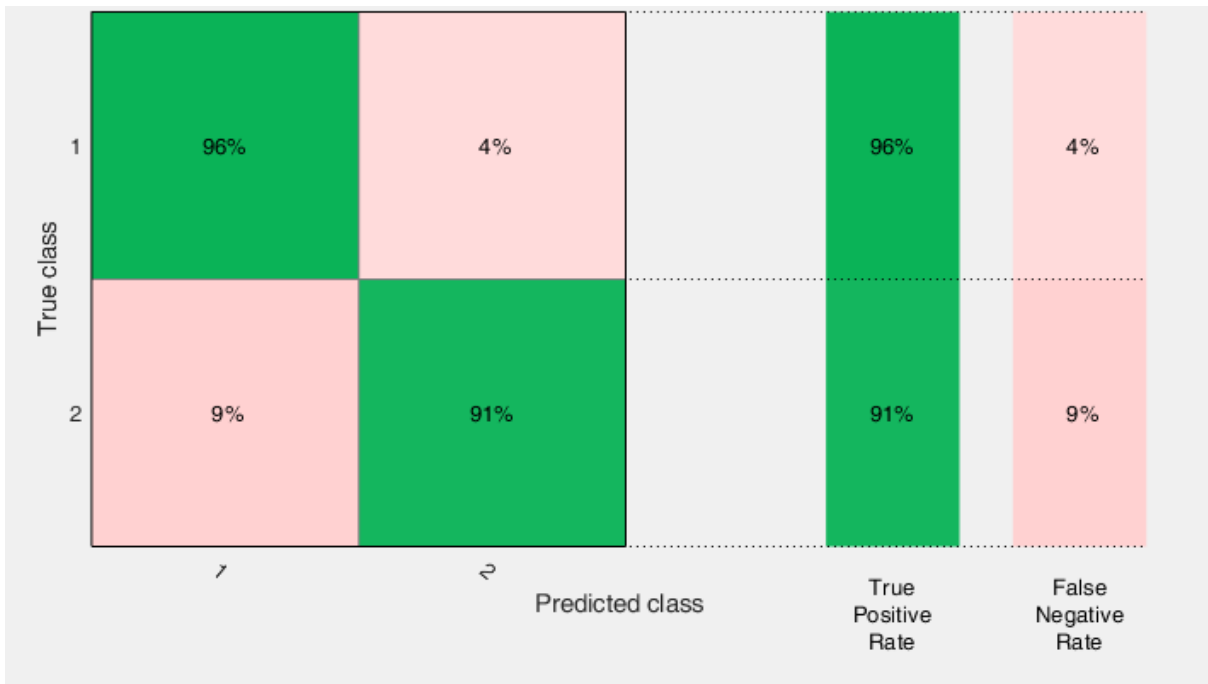
**Figure 4.13: ROC curve when k-NN classifier used**

Figure 4.10 shows the Plot of number of observations with k-NN Classifier has been used. Figure 4.11 presents True Positive Rate and False Negative Rate when k-NN Classifier has been used. Positive Predictive Value and False Discovery Rate are shown in Figure 4.12 when k-NN Classifier has been used. ROC curve has been shown in Figure 4.13. From the figures it is clearly evident that the proposed method based on k-NN classifier gave good results. Area under ROC curve is found to be 0.99 in case of k-NN classifier. The Area Under Curve number is a measure of the overall quality of the classifier.

In the next experiment, the performance of different similarity metrics available in literature have been evaluated for k-NN Classifier. For carrying out the experiments, the value of k is set to 7. Table 4.6 shows the overall accuracy achieved with different distance metrics. From the experimental results it has been found that an accuracy of 96.7% has been achieved with City block distance metric. In case of Euclidean distance, the accuracy obtained is 93.3% where as Chebychev distance metric gave an accuracy of 75.6%. It is clearly evident from the table that Chebychev, Mahalanobis, Hamming, Jaccard distance metric gave an accuracy of less than 80%. The highest accuracy is achieved in case of city block distance metric with value of k as 7. The results show that city block distance metric is good in finding the distance from each query point to every point in X.

**Table 4.6: Comparison of Overall Accuracy with different Distance Metrics**

Sr. No.	Distance Metric Used	Overall Accuracy
1	City block	<b>96.7 %</b>
2	Euclidean	93.3 %
3	Chebychev	75.6 %
4	Minkowski	93.3 %
5	Mahalanobis	73.3 %
6	Cosine	93.3 %
7	Correlation	92.2 %
8	Spearman	92.2 %
9	Hamming	50.0 %
10	Jaccard	50.0 %



**Figure 4.14: True Positive Rate and False Negative Rate with Euclidean Distance Metric**

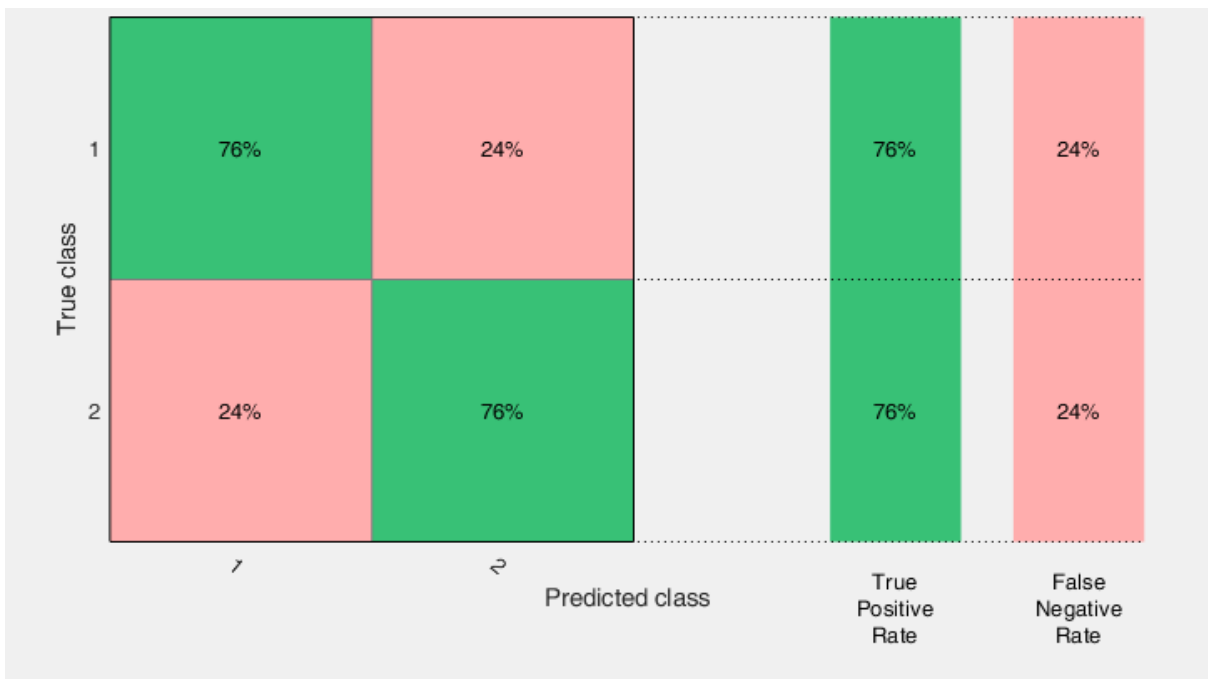


**Figure 4.15: True Positive Rate and False Negative Rate with Chebyshev Distance Metric**

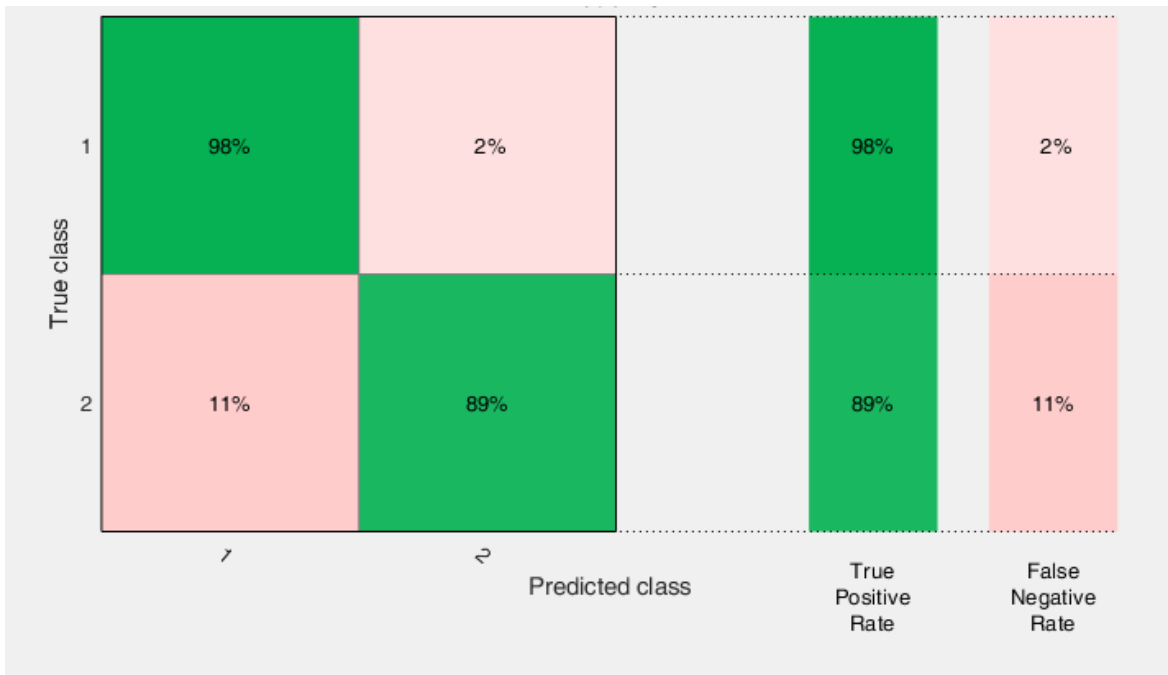


**Figure 4.16: True Positive Rate and False Negative Rate with Minkowski Distance Metric**

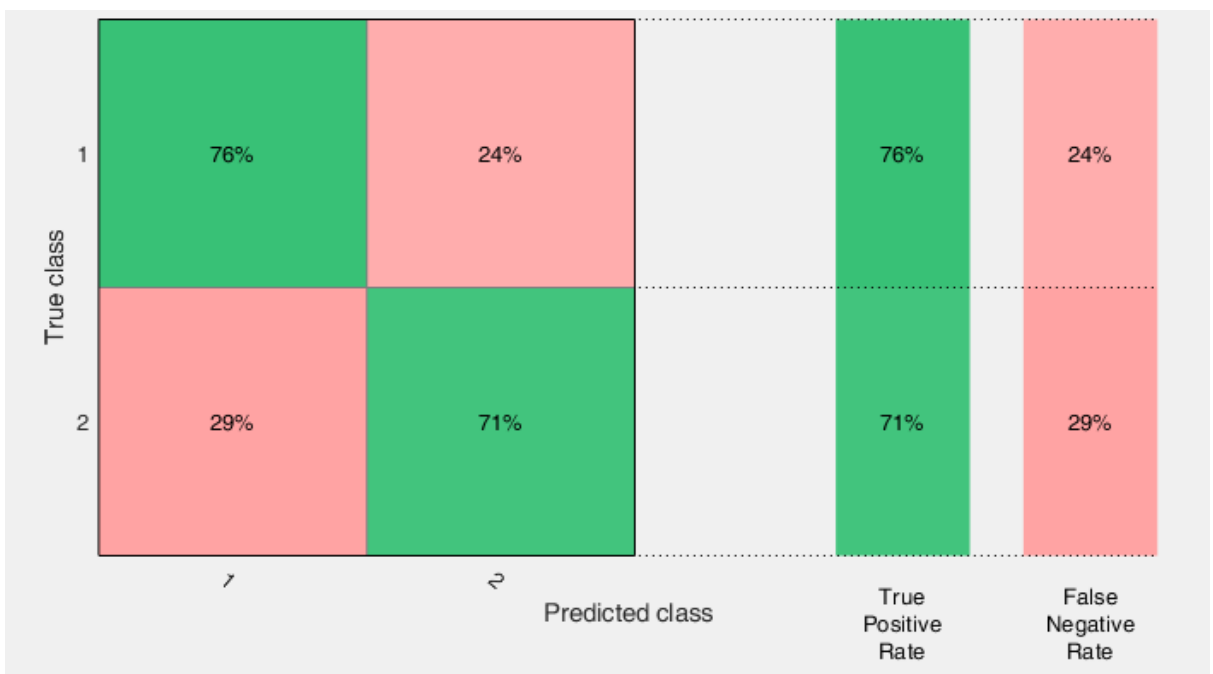


**Figure 4.17: True Positive Rate and False Negative Rate with Mahalanobis distance Metric**

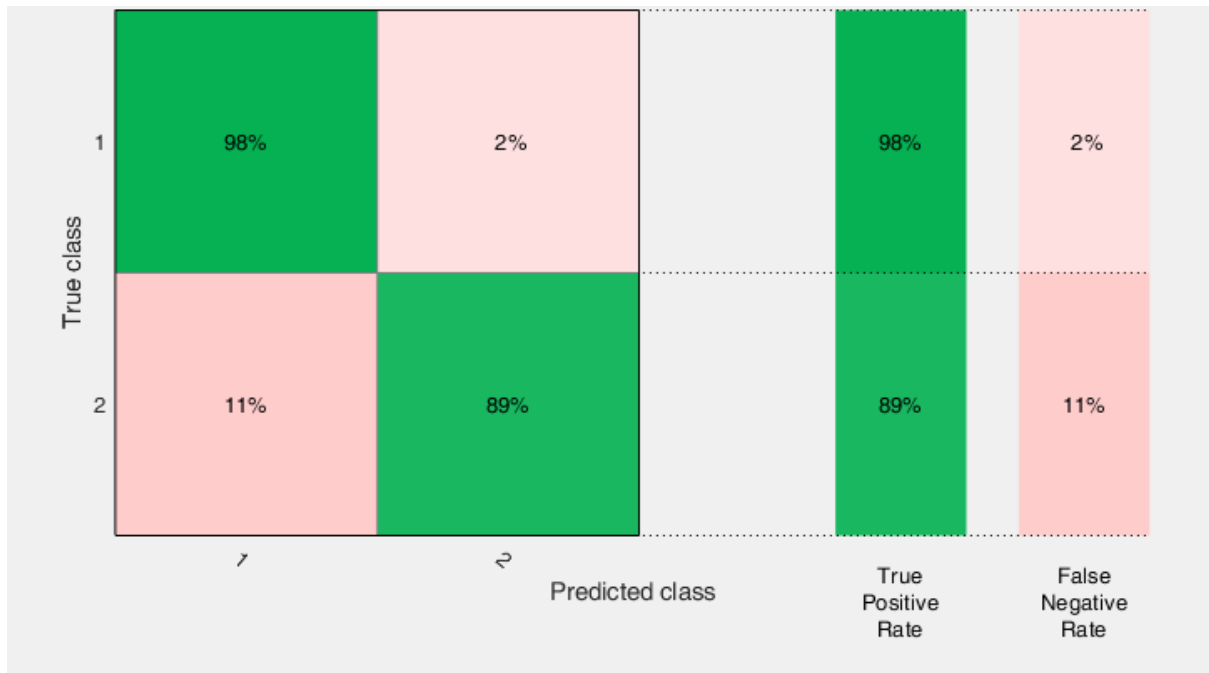


**Figure 4.18: True Positive Rate and False Negative Rate with Cosine Distance Metric**

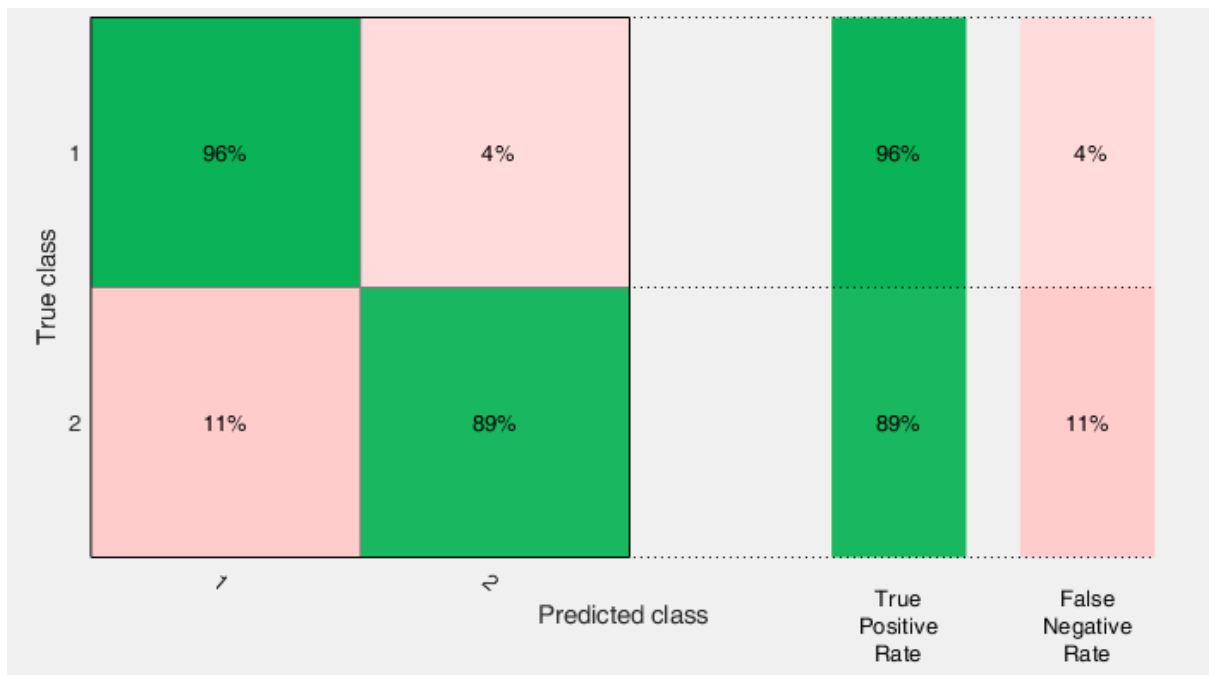


**Figure 4.19: True Positive Rate and False Negative Rate with Correlation Distance Metric**



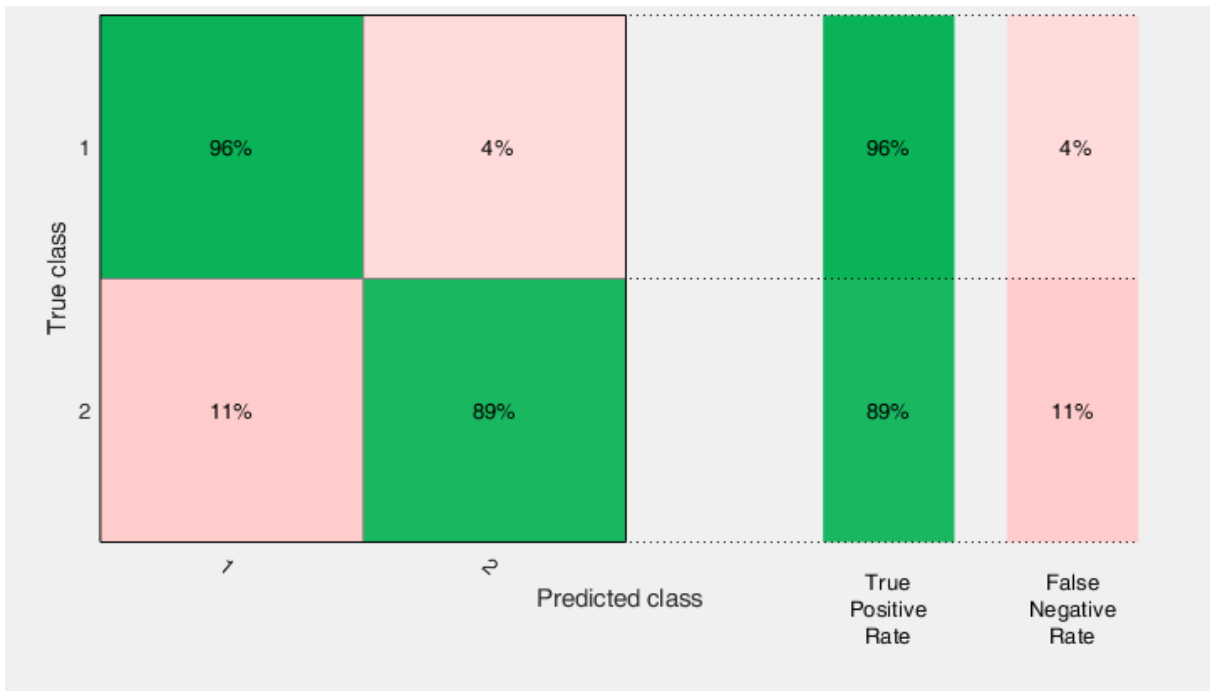


**Figure 4.20: True Positive Rate and False Negative Rate with Spearman Distance Metric**

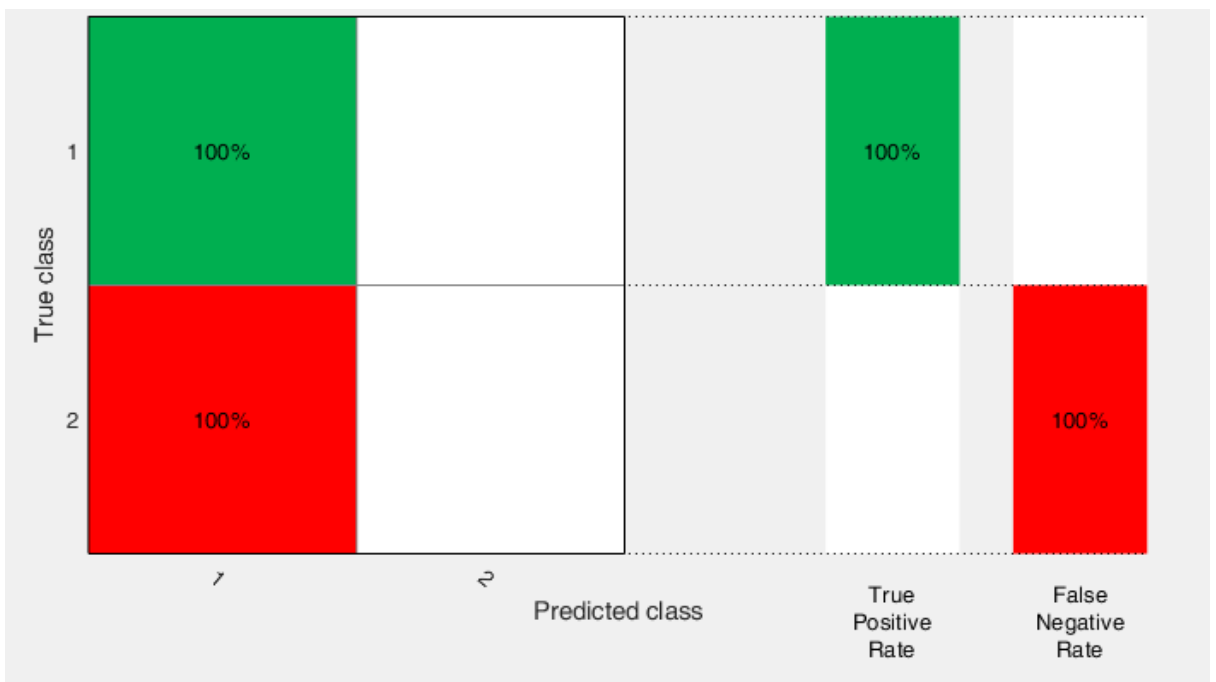


**Figure 4.21: True Positive Rate and False Negative Rate with Hamming Distance Metric**

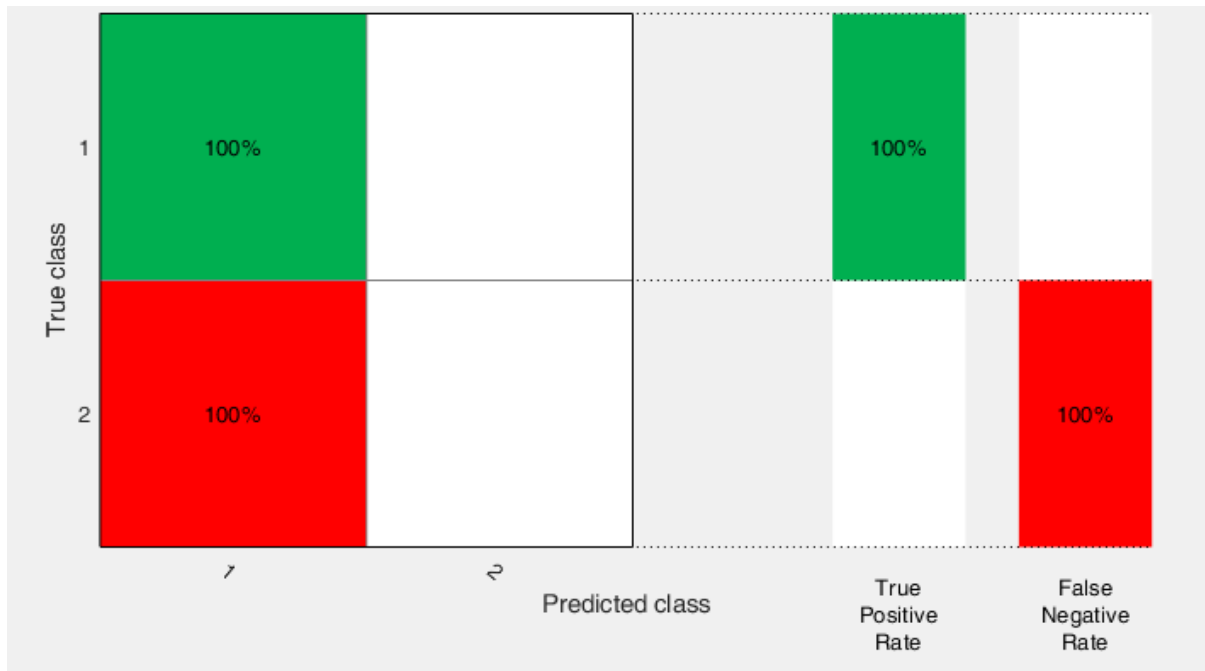


**Figure 4.22: True Positive Rate and False Negative Rate with Jaccard Distance Metric**

Figure 4.14 to Figure 4.22 shows the True Positive Rate and False Negative Rate obtained with different distance metrics.

The experimental results showed that the extracted features are when used with KNN Classifier with city block as distance metric and k value as 7 a highest accuracy of 96.7% has been achieved. It is also observed that in the implementation of algorithm, no additional efforts are required to construct a model and change various specifications which makes algorithm easy to apply.

#### **4.4 Performance Evaluation of Proposed Method III**

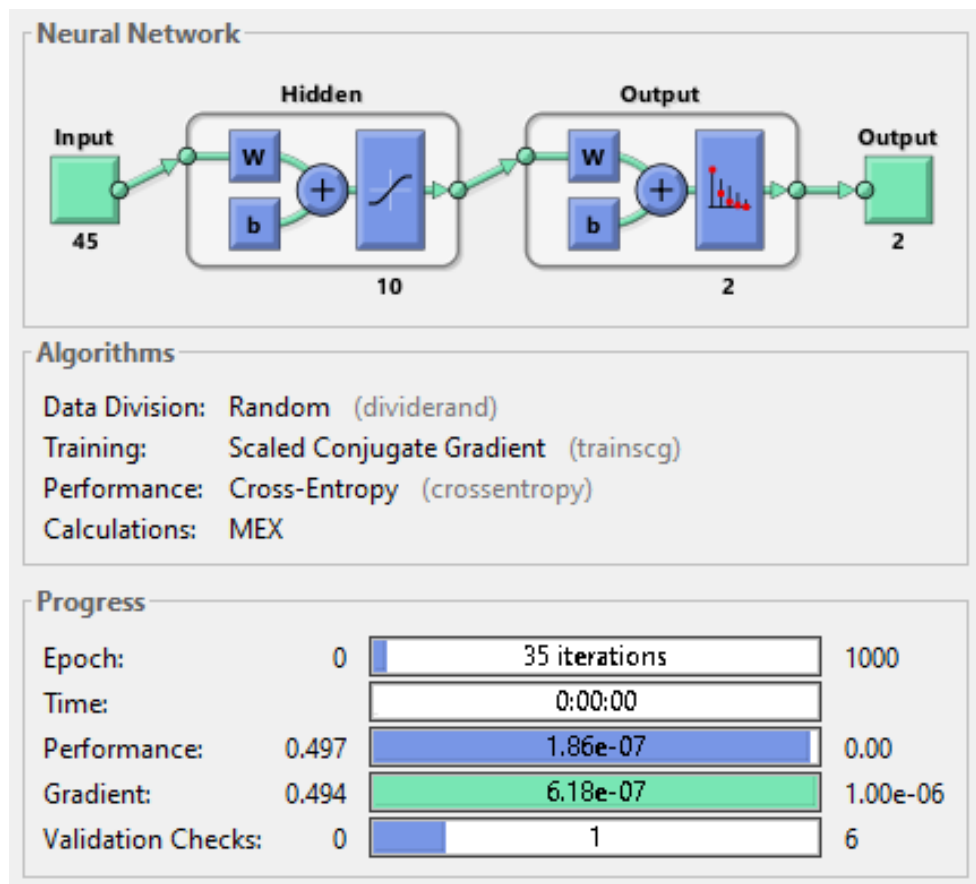
##### **(Based on a two-layer feedforward Neural Network)**

A two-layer feedforward neural network has been modelled in the Proposed Method III. Sigmoid transfer function was used in the hidden layer of the neural network, and a SoftMax transfer function was used in the output layer as a standard network for the classification of hepatic ultrasound. The value of the hidden neurons is set as 10 for conducting the experiments. As the number of categories into which classification has to be done are two so the value of output neurons is set as 2.

A total of 90 images are randomly divided into Training, Validation and Testing set as shown in Table 4.7.

**Table 4.7: Division of dataset into Training, Validation and Testing**

Dataset	Percentage (%)	Number of Images
Training	50%	44
Validation	15%	14
Testing	35%	32
Total		90

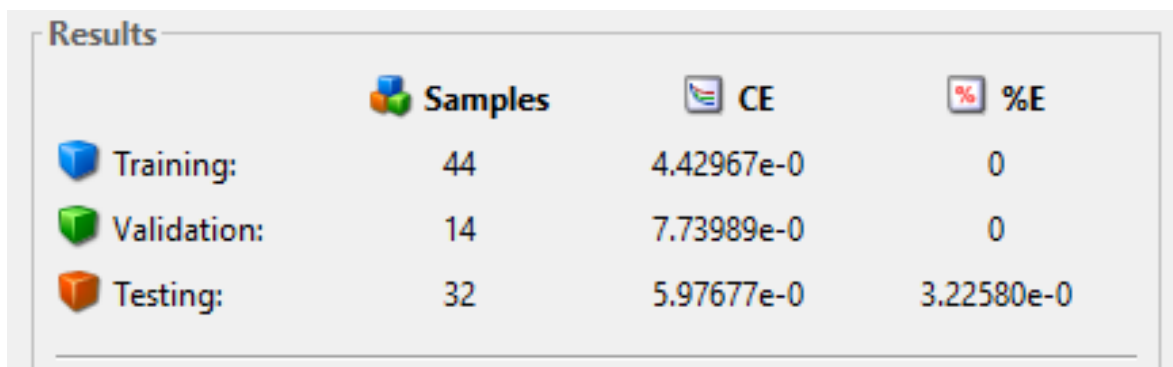








**Figure 4.23: Neural Network parameters used and progress of network**

- Training data set is the data set that has been provided to the network for the training purpose and accordingly network is adjusted on the basis of its error rate.

- Validation data set is basically used to measure the generalization capability of network and further to halt the process of training when there is no improvement in the generalization.
- Testing data set is independent of the training data set and validation data set that has no effect on training. This data set is used to measure the network performance after training.

In the proposed work, the neural network has been trained with scaled conjugate gradient backpropagation. As the cross-entropy error of the validation sample increases that shows the generalization has stopped improving and ultimately training stops. Figure 4.23 shows neural network parameters used and progress of the network.



	 Samples	 CE	 %E
 Training:	44	4.42967e-0	0
 Validation:	14	7.73989e-0	0
 Testing:	32	5.97677e-0	3.22580e-0

**Figure 4.24: Train Network results Cross Entropy CE and Percent Error % E**

In Figure 4.24, training network results that include Cross Entropy and Percent Error are presented.

**Minimizing Cross-Entropy (CE) :** The minimum value of cross entropy results in good classification that means lower values are preferred. There is no error when the value reaches zero.

**Percent Error (%E):** This value of percent error reveals the number of samples that are misclassified in which the value of 100 indicates maximum misclassification and value of zero signifies there is no misclassification.

Figure 4.25 and Figure 4.26 shows statistics related to training; the figures clearly show that we have reached at the bottom of local minima of the goal function. In this figure validation fails are the iterations when the value of validation MSE increases.

Figure 4.27 shows the plot of error histogram. In this figure red bar represents testing data, blue bars represent training data and validation data is represented by green bar. The above histogram provides the data of outliers that are the data points where fit is considerably worse than the most of data. Determination of outliers is found to be a god idea as it tells us whether the data is bad or if those data points differ from the rest of data.

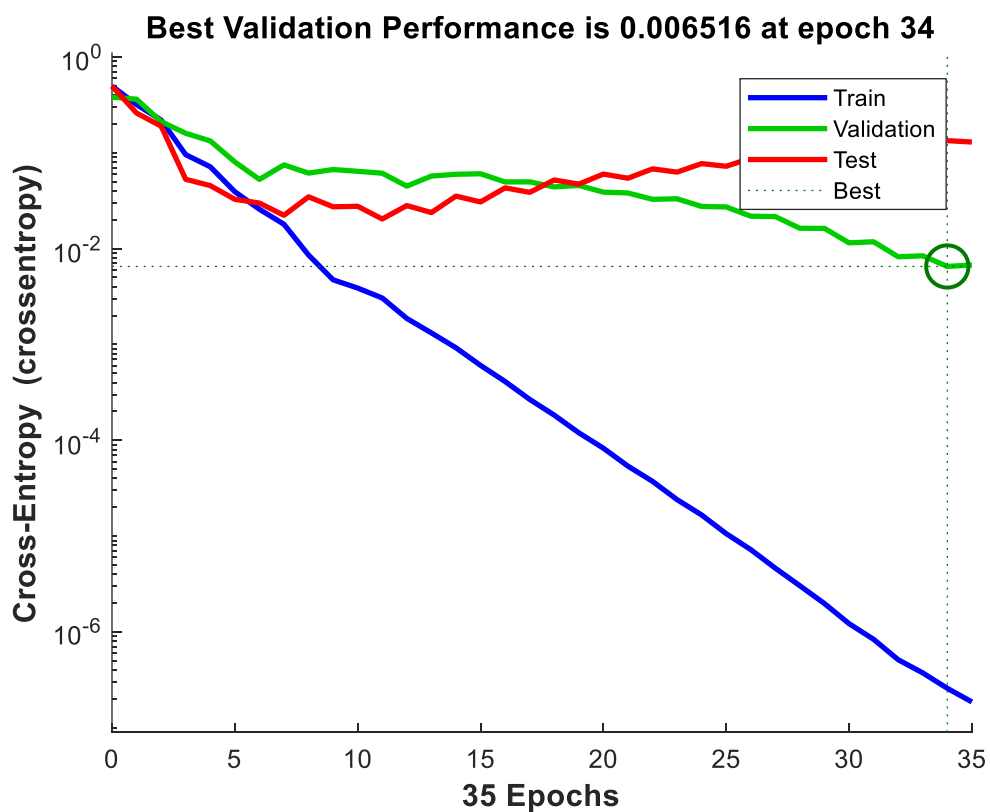


**Figure 4.25: Plot validation performance of network**

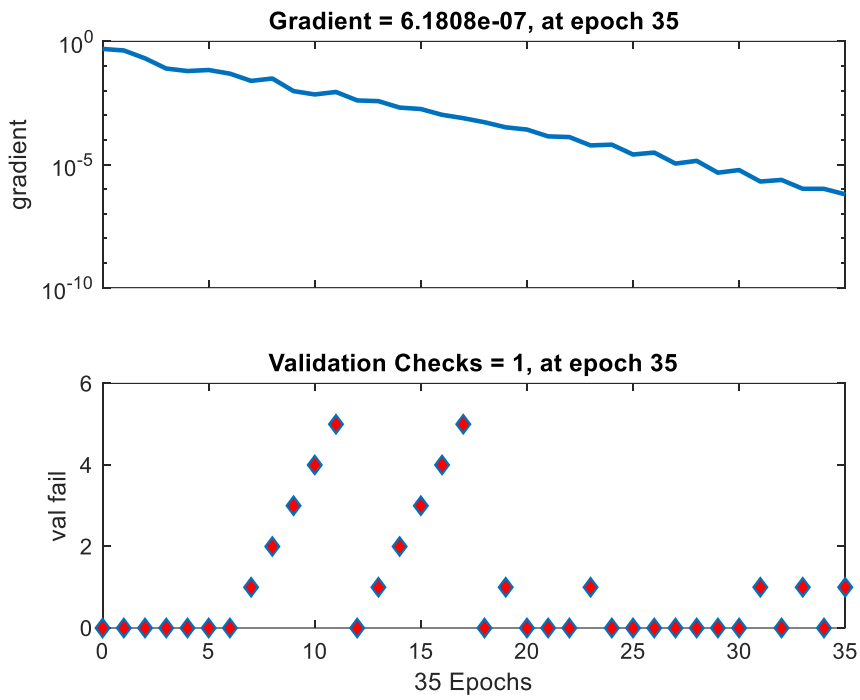


Figure 4.26: Plot of training state values

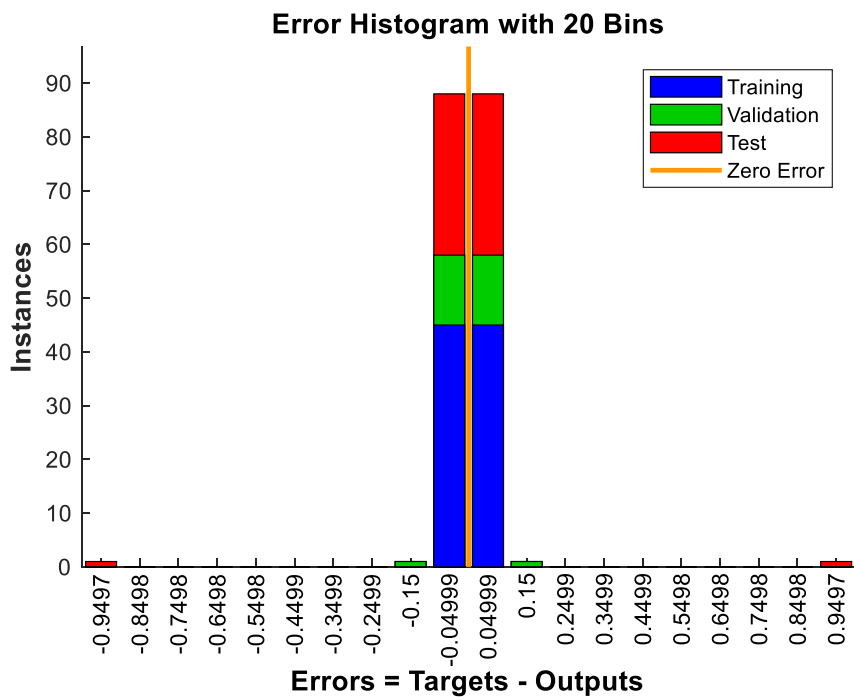


Figure 4.27: Plot of error histogram



**Figure 4.28: Plot of Confusion Matrix**

The above Figure 4.28 clearly shows the confusion matrices that have been generated for the training set, validation set, testing set and combined. From the experimental results it has been found that the results are good in terms of classification as low numbers of incorrect responses are there. In the figure the blue squares show the overall accuracies obtained in the proposed method. From the experimental results it has been found that an overall accuracy of 96.8% has been achieved for test data with very few incorrect classifications. This shows that the proposed method can be used for the classification of liver ultrasound images.

Figure 4.29 shows plot of ROC curves. In the graphs the coloured lines reflect ROC curves. As the threshold varies, “the ROC curve is a plot of the true positive rate (sensitivity) versus the false positive rate (1-specificity)”. A perfect exam, with 100 percent sensitivity and 100 percent accuracy, will show points in the upper-left corner. The network performs very well for that issue.

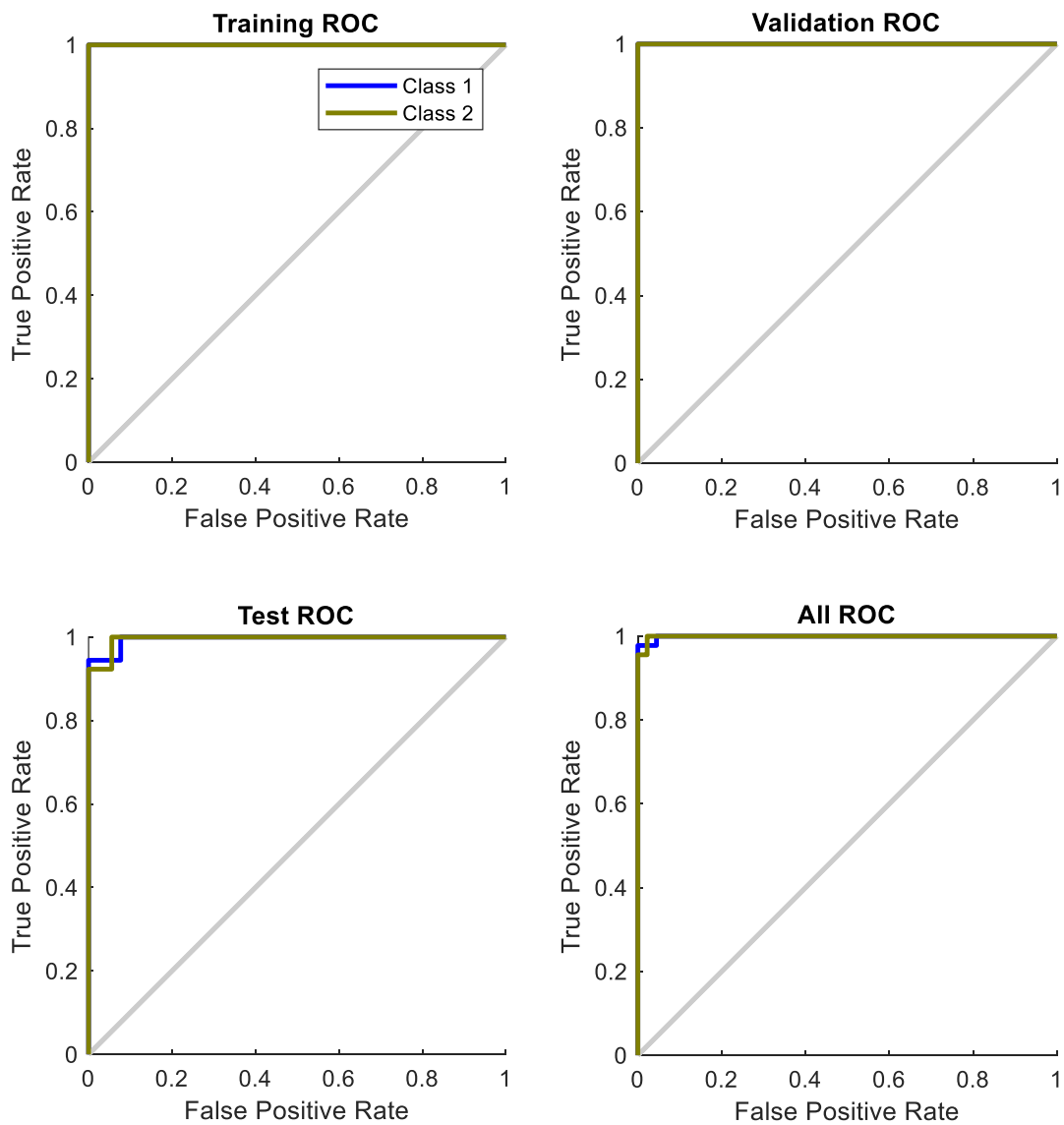


**Figure 4.29: Plot of Receiver Operating Characteristic**



## **4.5 Performance Evaluation of Proposed Method 4**

### **(Based on Sequential Minimal Optimization and Mutual Information Feature Selection)**

In this work, 45 texture features using different texture models i.e. “SGLCM, GLDS, FoS, SFM, Law’s TEM, Fractal and FPS” have been extracted from fixed ROI of size  $30 \times 30$  pixels in order to reduce the Miss Rate to a great extent. The process is further carried out by MI feature selection method and classification algorithms. The performance of 4 classifiers i.e. SMO, IBk, AdaBoostM1 and BF-Tree is evaluated for 5 different experiments based on different number of selected best features. Summarizing the result of all the experiments, SMO is outperforming with accuracy rate of 95.55%, miss rate of 2.22% and sensitivity rate of 97.77% on the present dataset with 20 best features selected by the MI feature selection technique.

The main aim of this research work is to evaluate the classification accuracy of fatty and normal images based on different number of best features, taking Miss Rate into consideration. The present work has used seven different feature extraction models to extract texture features and four different classifiers to classify fatty and normal liver images. In this study, different parameter values have been set to obtain good classification results. In order to evaluate the performance of the classifier, 5-fold cross-validation has been performed. The overall process is frequently performed five-times that involve every fold being chosen arbitrarily. Mutual Information feature selection method has been used for selecting the best features, which gives output on the basis of their weight. The obtained observations for 5 different experiments as follow.

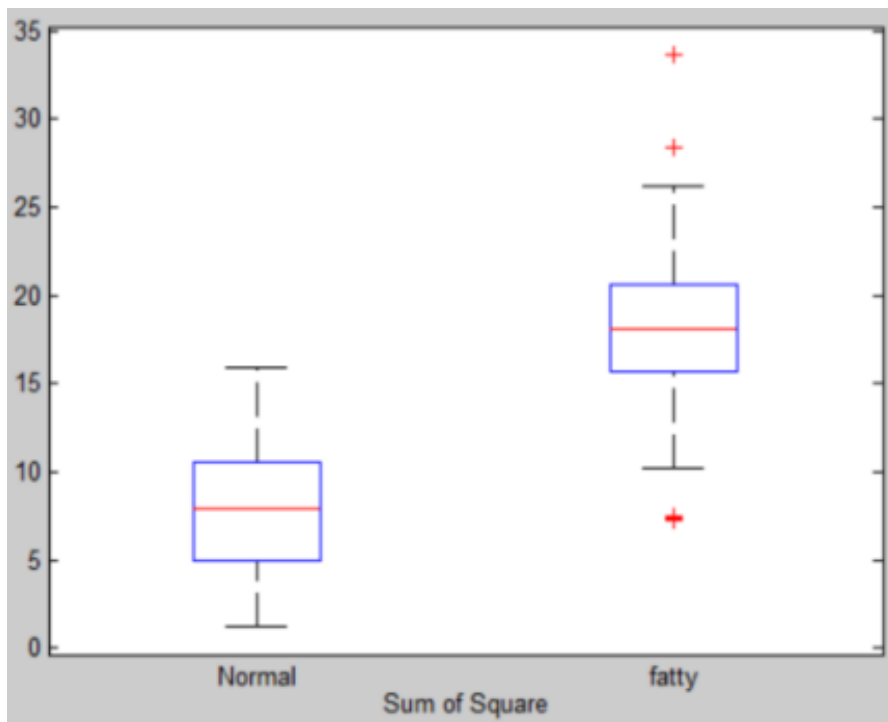
#### **4.5.1 Experiment 1 - Performance Evaluation of 5 Best Features Selected by MI Feature Selection Method.**

The present study evaluates the performance of 5 best features with the help of MI feature selection method by ranking features according to their weights in descending order. For result analysis, overall five experiments have been carried out in this whole process. The first experiment is carried out by using 5 best features out of 45 features, according to the sized vector of feature relevance's (MIs) in the descending order. These features are: Sum Average, Sum variance, Sum of Square, Mean and Angular Sum which are obtained from three models i.e. SGLCM, FOS and FPS. These features show very high discriminating power to classify normal and fatty liver as evidenced from the

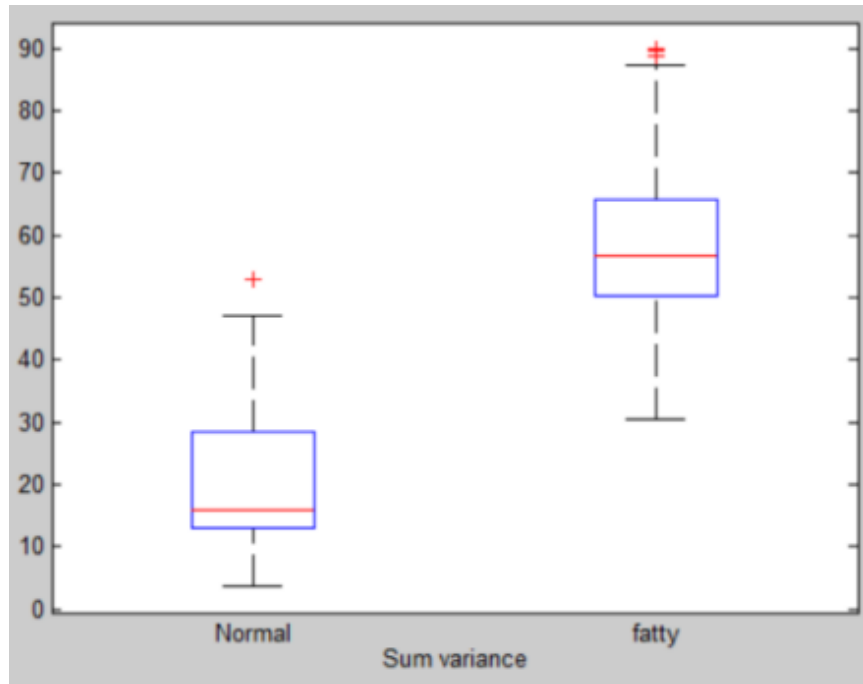
boxplots of best five features (as shown in Figure 4.30 and 4.31), where a clear separation exists between feature values of normal and fatty liver ultrasound images. The highest AUC obtained in this experiment is 0.96 by AdaBoost M1 classifier as shown in Table 4.8.

**Table 4.8: Performance Evaluation of Five Best Features**

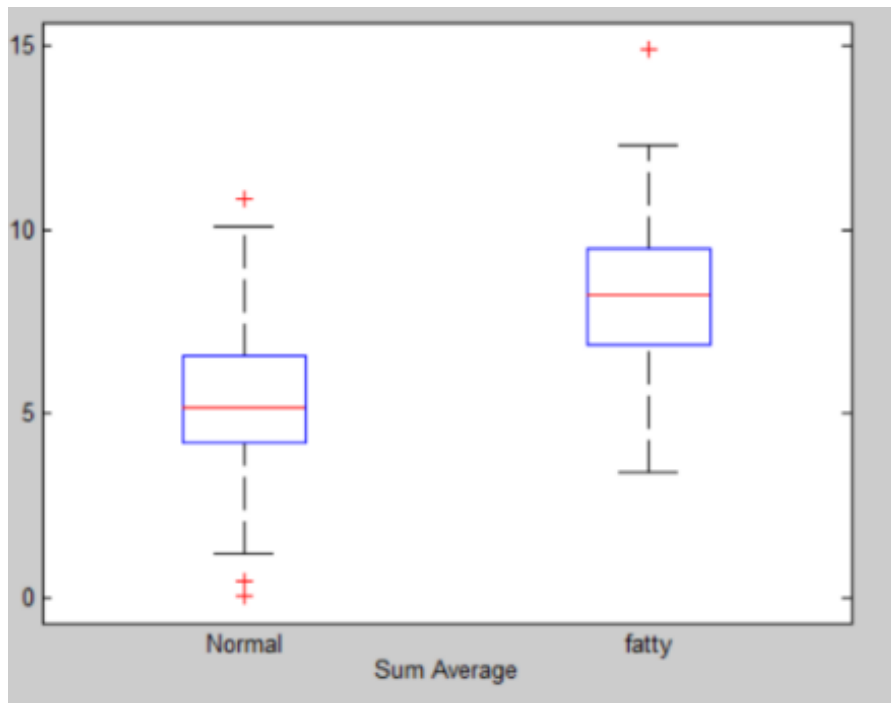
Features Extracted	Classifiers	TP	TN	Sensitivity (%)	Specificity (%)	AUC	Miss Rate (%)	Accuracy (%)
		FP	FN					
<b>5 BEST FEATURES</b>	<b>SMO</b>	41	40	91.11	88.88	0.90	8.88	90.00
		5	4					
	<b>IBK</b>	43	40	95.55	88.88	0.93	<b>4.44</b>	92.22
		5	2					
	<b>ADABOOST M1</b>	43	42	95.55	93.33	<b>0.96</b>	<b>4.44</b>	<b>94.44</b>
		3	2					
	<b>BF-TREE</b>	43	42	95.55	93.33	0.95	<b>4.44</b>	<b>94.44</b>
		3	2					



**(A) Box plot of Sum of Square**

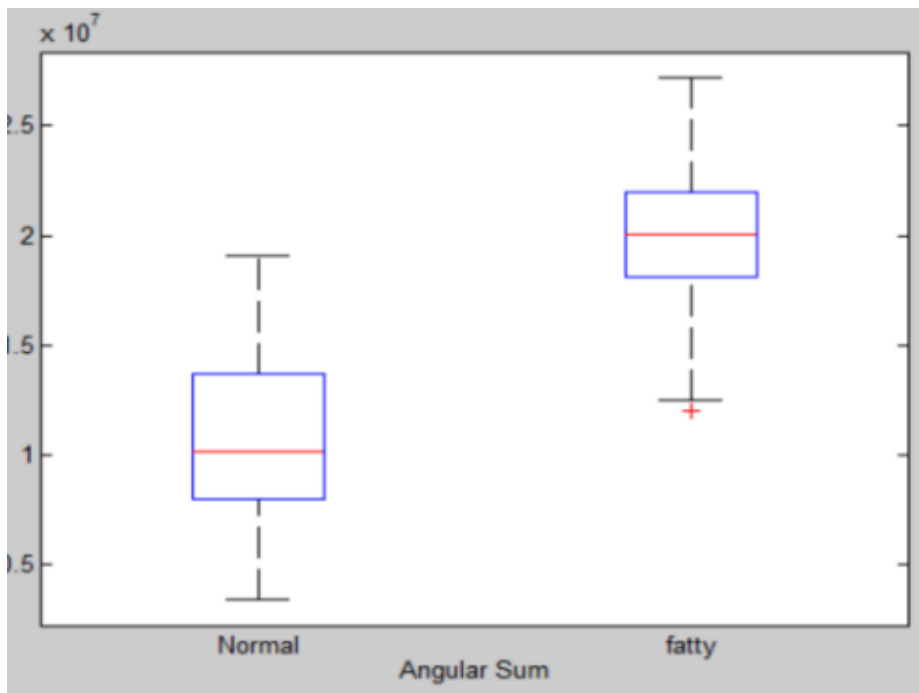


(B) Box plot of Sum Variance

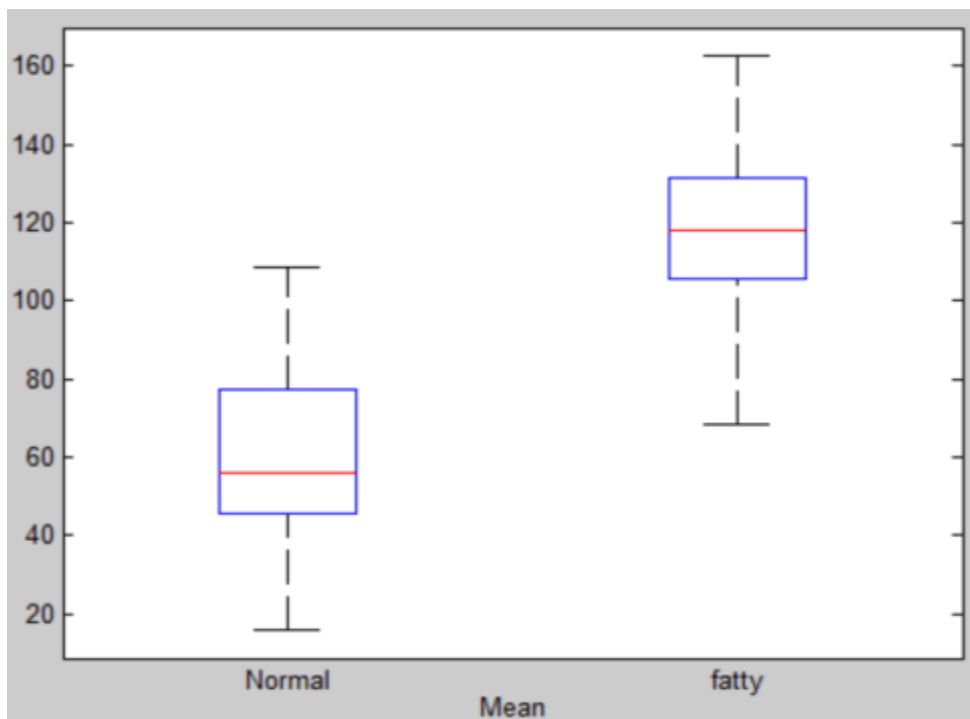


(C) Box plot of Sum Average

Figure 4.30: Box plot of highly discriminant features extracted from models SGLCM



(D) Box plot of Angular Sum



(E) Box plot of Mean

Figure 4.31: Box plot of highly discriminant features extracted from models FoS and FPS.

#### 4.5.2 Experiment 2 - Performance Evaluation of 10 Best Features Selected by MI Feature Selection Method.

The second experiment is carried out by using 10 best features out of 45 features. In this case, SMO and IBk classifiers perform almost equally but the sensitivity value of SMO is higher than that of IBk classifier. The 10 best selected features are: Sum Average, Sum variance, Sum of Square, Mean, Angular Sum, Roughness, Hurst Coefficient at Resolution 1, Correlation, Maximum Correlation Coefficient and Periodicity which are obtained from five models i.e. SGLCM, FOS, SFM, FPS and Fractal Feature. AdaBoost M1 classifier gives 93.33% accuracy and is good in identifying both normal liver as well as fatty ultrasound images. Moreover, for AdaBoost M1 classifier AUC value of 0.96, which is highest among all the cases as shown in Table 4.9.

**Table 4.9: Performance Evaluation of 10 Best Features**

Features Extracted	Classifiers	TP	TN	Sensitivity (%)	Specificity (%)	AUC	Miss Rate (%)	Accuracy (%)
		FP	FN					
<b>10 BEST FEATURES</b>	<b>SMO</b>	41	41	91.11	91.11	0.91	8.88	91.11
		4	4					
	<b>IBK</b>	42	41	93.33	91.11	0.95	6.66	92.22
		4	3					
	<b>ADABOOST M1</b>	42	42	93.33	93.33	<b>0.96</b>	<b>6.66</b>	<b>93.33</b>
		3	3					
	<b>BF-TREE</b>	40	38	88.88	84.44	0.92	11.11	86.66
		7	5					

#### 4.5.3 Experiment 3 - Performance Evaluation of 15 Best Features Selected by MI Feature Selection Method.

The third experiment includes 15 best features out of 45 features in which SMO classifiers gives 93.33% accuracy rate with 95.55% sensitivity and IBk classifiers gives 94.44% accuracy rate with 93.33% sensitivity. It has been observed from Table 4.10, AUC is higher in case of IBk classifier as compared to SMO classifier. The 15 best selected features are: Sum Average, Sum variance, Sum of Square, Mean, Angular Sum, Roughness, Hurst Coefficient at Resolution 1, Correlation, Maximum Correlation Coefficient, Periodicity, Skewness, Information Measure of Correlation 1, Spot\_Spot,

Edge\_Level, Wave\_Level which are obtained from five models i.e. SGLCM, FOS, SFM, FPS, TEM and Fractal Feature. In this experiment, AdaBoost M1 classifier gives 93.33% which provides better performance as compared to other classifiers with the highest AUC i.e. 0.96. In AdaBoost M1 classifiers the decision stump is used as a base classifier with 10 number of iterations. Whereas, in BF-tree classifiers the post pruning strategy is used with 5 number of folds in internal cross- validation.

**Table 4.10: Performance Evaluation of 15 Best Features**

Features Extracted	Classifiers	TP	TN	Sensitivity (%)	Specificity (%)	AUC	Miss Rate (%)	Accuracy (%)
		FP	FN					
<b>15 BEST FEATURES</b>	<b>SMO</b>	43	41	95.55	91.11	0.93	<b>4.44</b>	93.33
		4	2					
	<b>IBK</b>	42	43	93.33	95.55	0.94	6.66	<b>94.44</b>
		2	3					
	<b>ADABOOST M1</b>	42	42	93.33	93.33	<b>0.96</b>	6.66	93.33
		3	3					
	<b>BF-TREE</b>	40	39	88.88	86.66	0.92	11.11	87.77
		6	5					

#### 4.5.4 Experiment 4 - Performance Evaluation of 20 Best Features Selected by MI Feature Selection Method.

**Table 4.11: Performance Evaluation of 20 Best Features**

Features Extracted	Classifiers	TP	TN	Sensitivity (%)	Specificity (%)	AUC	Miss Rate (%)	Accuracy (%)
		FP	FN					
<b>20 BEST FEATURES</b>	<b>SMO</b>	44	42	97.77	93.33	0.95	<b>2.22</b>	<b>95.55</b>
		3	1					
	<b>IBK</b>	40	43	88.88	95.55	<b>0.98</b>	11.11	92.22
		2	5					
	<b>ADABOOST M1</b>	41	42	91.11	93.33	0.96	8.88	92.22
		3	4					
	<b>BF-TREE</b>	40	39	88.88	86.66	0.85	11.11	87.77
		6	5					

The experiment four is performed by using 20 best features out of 45 features. SMO classifier gives 95.55% accuracy with 97.77% sensitivity in case of best 20 features as shown in Table 4.11. The 20 best selected features are: Sum Average, Sum variance, Sum of Square, Mean, Angular Sum, Roughness, Hurst Coefficient at Resolution 1, Correlation, Maximum Correlation Coefficient, Periodicity, Skewness, Information Measure of Correlation 1, Spot\_Spot, Edge\_Level, Wave\_Level, Homogeneity, Information Measure of Correlation 2, Radial Sum, Spot\_Level, mean which is obtained from all Seven models. IBk and AdaBoost M1 classifier have same recognition rate in classifying fatty and normal liver but the sensitivity of IBk is less as compared to the sensitivity of AdaBoost M1 classifier. For IBk classifiers, the choice of value of k is made by changing the odd values of k from 1 to 7. It has been observed that the value of k=5 outperforms the other value and Moreover, it provides high value of AUC i.e. 0.98.

#### 4.5.5 Experiment 5 - Classification Performance of All Features

**Table 4.12: Performance Evaluation of All Features**

Features Extracted	Classifiers	TP	TN	Sensitivity (%)	Specificity (%)	AUC	Miss Rate (%)	Accuracy (%)
		FP	FN					
ALL FEATURES	SMO	44	42	97.77	93.33	0.95	2.22	95.55
		3	1					
	IBK	41	40	91.11	88.88	0.95	8.88	90.00
		5	4					
	ADABOOST M1	40	41	88.88	91.11	0.95	11.11	90.00
		4	5					
	BF-TREE	39	38	86.66	84.44	0.82	13.33	85.55
		7	6					

The experiment five considers the classification performance of all features. Overall, 45 features have been extracted after using 7 texture models. With the help of various classifiers like SMO, IBk, AdaBoostM1 and BF-Tree, the performance of these features is evaluated. The performance of classification using all 45 features is shown in Table 4.12. SMO classifier delivers better performance i.e. 95.55 % accuracy as compared to the other three classifiers. The IBk and AdaBoost M1 classifiers give equal accuracy i.e. 90% but the sensitivity of IBk classifier is more as compared to AdaBoost M1

classifier. In this experiment, the overall AUC 0.95 is obtained by SMO. From the experimental results it has been found that a set of 20 optimal features selected by the MI feature selection technique resulted in same accuracy as in the case of 45 features with SMO classifier.

#### 4.5.6 Comparative Analysis of Different Kernel Functions of SMO Classifier

**Table 4.13 Performance analysis of SMO classifier by using different kernel functions**

<b>SMO Classifier</b>	<b>Kernels Used</b>	<b>Sensitivity Rate (%)</b>	<b>Specificity Rate (%)</b>	<b>AUC</b>	<b>Miss Rate</b>	<b>Accuracy Rate (%)</b>
<b>5 Best Features</b>	RBF	91.11	88.88	0.90	8.88	90.00
	Polykernel	91.11	88.88	0.90	8.88	90.00
	PUK	88.88	93.33	<b>0.91</b>	11.11	<b>91.11</b>
	Normalised Polykernel	100	75.60	0.87	<b>0</b>	87.77
<b>10 Best Features</b>	RBF	88.88	84.44	0.86	11.11	86.66
	Polykernel	91.11	91.11	0.91	8.88	91.11
	PUK	93.33	91.11	<b>0.92</b>	6.66	<b>92.22</b>
	Normalised Polykernel	93.33	91.11	<b>0.92</b>	6.66	<b>92.22</b>
<b>15 Best Features</b>	RBF	91.11	91.11	0.91	8.88	91.11
	Polykernel	95.55	91.11	<b>0.93</b>	4.44	<b>93.33</b>
	PUK	95.55	91.11	<b>0.93</b>	4.44	<b>93.33</b>
	Normalised Polykernel	95.55	91.11	<b>0.93</b>	4.44	<b>93.33</b>
<b>20 Best Features</b>	RBF	91.11	91.11	0.91	8.88	91.11
	Polykernel	97.77	93.33	<b>0.95</b>	<b>2.22</b>	<b>95.55</b>
	PUK	93.33	93.33	0.93	6.66	93.33
	Normalised Polykernel	95.55	91.11	0.93	4.44	93.33
<b>45 Features</b>	RBF	93.33	93.33	0.93	6.66	93.33
	Polykernel	97.77	93.33	<b>0.95</b>	<b>2.22</b>	<b>95.55</b>
	PUK	95.55	88.88	0.92	4.44	92.22
	Normalised Polykernel	95.55	93.33	0.94	4.44	94.44



The SMO classifier utilizes feedback features from two classes to calculate maximum edge hyper-plane that distinguishes the two classes and provide optimal solutions [29]. If the features are not directly distinguishable, special kernel functions can be applied to change the data to a higher perspective feature space. This section carries out the comparison between some normally used kernel functions i.e. normalised polykernel [31], polykernel [31], Pearson VII Universal Kernel (PUK) [30] and Radial Basis Function (RBF) [32]. From the experimental results, it has been analysed that in case of 5 best and 10 best features, PUK kernel gives good results with accuracy more than 90 percent. This kernel is excellent in case of flexibility and can easily replace the set of commonly used kernel functions. whereas, in case of 15 best, 20 best and all 45 features together polynomial kernel provide better results as compare to other kernel functions with accuracy of 93.33% and 95.55%. The normalised polynomial gives zero miss rate in case of 5 best features but this kernel sometimes gives inappropriate result which is not good enough in terms of accuracy. In summary, polynomial kernel consumes very less time to test the performance of the classifier in contrast to other kernels and provide better accuracy as shown Table 4.13. Further, it has been analysed that performance of 20 best features selected by MI feature selection technique is same as that of all 45 features in the case of polynomial kernel. Therefore, instead of using 45 features, 20 best features selected by the MI feature selection technique can be used for the classification of liver ultrasound images.

#### 4.5.7 Comparison with previous work

**Table 4.14: Comparison of Present Work with the Previous Related Researches**

<b>Papers</b>	<b>Number of features extracted</b>	<b>Number of images used</b>	<b>Overall Accuracy (%)</b>
Singh. et al. [128]	27	30	92.0
Singh. et al. [21]	35	180	95.0
Proposed Method I	10	90	93.3
Proposed Method II	45	90	96.7
Proposed Method III	45	90	98.9
Proposed Method IV	20	90	95.5

Clearly, Table 4.14 demonstrates that when compared with the previous researches [128, 21], the present CAD system is better in terms of overall accuracy. But in the present work, an accuracy of 95.55% has been achieved with 20 best features selected by the MI feature selection technique. Very low Miss rate has been achieved which is the limelight of this thesis work and is not even previously targeted by the researchers.

## **4.6 Discussion**

Fatty Liver Disease (FLD) is one of the most critical diseases that should be detected and cured at the earlier stage in order to decrease the mortality rate. To identify the FLD, ultrasound images have been widely used by the radiologists. However, due to poor quality of ultrasound images, they found difficulties in recognizing FLD. To address this issue, computer-aided diagnostic methods are proposed in this thesis, and the efficiency of the proposed methods is assessed using different performance metrics.

In the Proposed Method I, extracted features are fed to the Decision Tree Classifier and parameter setting has been done to obtain the maximum accuracy. The experimental results showed that an accuracy of 88.9% has been obtained with Decision Tree Classifier. In the proposed work, PCA has been used for projecting original data into a new coordinate space. From the experimental results it has been found that when PCA is used for dimensionality reduction and the transformed features are passed to Decision Tree Classifier an accuracy of 93.3% has been achieved. After analysing the experimental results, it has been concluded that Decision Tree with PCA method enhances the prediction accuracy of the decisions tree classifier as well as simplifies the decision tree model.

In the Proposed Method II, the extracted forty-five features are passed to K-Nearest Neighbour (K-NN) Classifier for classification purpose. After extensive experiments it has been found that K-NN classifier gave best results with city block distance metric and value of k as 7. The overall accuracy obtained with these parameter settings is 96.7% with area under ROC curve as 0.99.

In the Proposed Method III, a two-layer feed forward neural network for the classification of liver ultrasound images has been proposed in this thesis work. After the extensive experiments it has been found that an overall accuracy of 96.8% with 100% sensitivity and 92.9% specificity has been achieved with this network.

The process is further carried out by Mutual Information (MI) feature selection method and classification algorithms in Proposed Method IV. The performance of 4 classifiers i.e. SMO, IBk, AdaBoostM1 and BF-Tree is evaluated for 5 different experiments based on different number of selected best features. Summarizing the result of all the experiments, SMO is outperforming with accuracy rate of 95.55%, miss rate of 2.22% and sensitivity rate of 97.77% on the present dataset with 20 best features selected by the MI feature selection technique. Also, it has been analysed that the performance of all 45 features in combination is same as that of 20 features when SMO classifier is used with polynomial kernel. Therefore, instead of using 45 features, the selected combination of 20 features can be used, which further reduces the computational cost in classifying the images. Therefore, combination of these 20 optimal features can be used for liver ultrasound image classification. Furthermore, for the extensive experiments of SMO classifier, results have been obtained with 4 different kernels i.e. RBF, Polykernel, Normalised kernel and PUK kernel, where the overall best results are given by Polykernel.

In conclusion, experiments demonstrated that the proposed techniques gave better results for the classification of liver ultrasound images into two categories. Therefore, the proposed methods can be used for the classification of fatty and normal liver ultrasound images with higher accuracy.



## **Chapter - 5**

### **Summary and Conclusions**

#### **5.1 Summary**

In the medical field, images, and especially digital images, are produced in enormous quantities and are used for diagnostics and therapy. Out of all the imaging modalities, Ultrasound is one of the popular imaging modalities due to its low cost, portable, real time imaging and non-ionizing nature. Ultrasound imaging has been widely used for the diagnosis of prostate, visualization of fetus development and to see various abnormalities in the organs that includes gallbladder, kidneys and liver. In medical field, liver plays a vital role in human body, as it maintains quality of blood as well as performs very important functions like storage of carbohydrates, excretion, fats and fatty acids etc.

Fatty liver is a disease where the fat content of the "hepatocytes" increases, which results in variation of the liver surface texture. To describe it, we can research and analyse the granular structure of the tissue or an area. The unique grainy pattern of fatty liver and normal liver can be represented as texture. Therefore, texture analysis can provide vital information that cannot be obtained via visual interpretation of ultrasound images for tissue characterization. Considering this concept as inspiration, several texture models were studied and evaluated so that the best features could be used to develop a better classification system.

*From the literature survey it has been found that the subjective evaluation of liver ultrasound images is less accurate and highly dependent on the experience of radiologist.* Therefore, in this thesis work in order to assist radiologists, Computer Aided Diagnostic methods are proposed for the classification of liver ultrasound images in two classes i.e. Fatty liver and Normal liver.

From a clinical point of view, Computer Aided Diagnosis (CAD) systems based on liver tissue can guide radiologists in its classification. In automated liver tissue classification, it is important to determine which features give the best distinction

between categories. In addition to structural and spectral descriptors, the texture of this area can help to differentiate between different tissues and can be represented by statistical descriptors derived from the image intensity histogram or the matrix of co-occurrence.

## 5.2 Conclusion

A review of related work in processing and analysis of ultrasound images has been done. From the literature survey it has been found that in recent years many approaches have been proposed for the analysis of ultrasound images and major work has been done in the area of Computer Aided Diagnosis of fatty liver (*Steatosis*). A major current focus is on use of machine learning techniques to classify the liver ultrasound images and use of feature selection techniques to identify an optimal set of features that not only captures the image texture but also improves the semantic interpretability.

With the ultimate goal of processing and analysis of Ultrasound images this thesis makes some contributions that are closely related to the classification of liver ultrasound images for disease diagnosis. The *first contribution* is extensive literature survey done in the area of ultrasound imaging in which various existing approaches and methods have been studied and analysed in detail. The *second contribution* is related to extraction of texture features from the region of interest using wide variety of texture models available in the literature as texture-based analysis is very useful in ultrasound tissue characterization. The *third contribution* has focussed on feature selection i.e. to identify and extract discriminating features that not only captures the texture of image but at the same time also improves correlation to the human visual similarity. The *fourth contribution* is based on use of different classifiers available in literature for the classification task with extensive parameter setting which is a unique kind of study in itself. For carrying out the proposed work, 90 ultrasound liver images have been collected from Delta Diagnostic Centre Patiala, India. The performance is evaluated using commonly used medical statistics: Sensitivity, Specificity, Accuracy and Area under ROC Curve. *Following are the major conclusions of the work carried out in this thesis:*

From the literature survey, it is clear that many researchers have done work on the classification of fatty and normal liver ultrasound images and to the best of author's knowledge, very less work is done on feature selection techniques in this domain. Furthermore, the researchers have focused more upon the accuracy rate instead of Miss Rate. But it is well known that classifying fatty liver as normal is more harmful than classifying normal liver as fatty. The performance of existing CAD systems is not good in terms of sensitivity while classifying the FLD.

In this thesis work, Computer Aided Diagnostic methods are proposed for the classification of liver ultrasound images in two classes i.e. Fatty liver and Normal liver. For this purpose, texture features are extracted by using seven different texture models i.e. SGLCM, FPS, GLDS, FoS, SFM, TEM and FF to represent the texture of Region of Interest (ROI) of size  $30 \times 30$  pixels extracted from the ultrasound liver image. *It is worth mentioning here that very few researchers in earlier studies have used all these models in conjunction for performance evaluation.*

Further, these extracted features are fed to the Decision Tree Classifier and parameter setting has been done to obtain the maximum accuracy. The experimental results showed that an accuracy of 88.9% has been obtained with Decision Tree Classifier. The use of Principal Component Analysis (PCA) has been widely studied in the literature for the dimensionality reduction process. Therefore, in the proposed work, PCA has been used for projecting original data into a new coordinate space. From the experimental results it has been found that when PCA is used for dimensionality reduction and the transformed features are passed to Decision Tree Classifier an accuracy of 93.3% has been achieved. The experimental results showed that there is increase of almost 4.4% accuracy when PCA has been used that clearly shows that PCA gives better representation of the data. Further it has been found that Area Under ROC with Decision Tree Classifier is 0.90 where as there is significant increase in Area under Curve when PCA is used with Decision Tree Classifier i.e. found to be 0.95. Comparing with the traditional decision tree algorithm, the experimental results show that Decision Tree with PCA method can not only simplify the decision tree model, but also can improve prediction accuracy of the decision tree.

From the experimental results it has been found that Decision Tree with PCA outperforms as compared to Decision Tree.

In the next work, the extracted forty-five features are passed to K-Nearest Neighbour (K-NN) Classifier for classification purpose. The selection of value of k in K-NN plays a significant role. In the proposed work, the KNN algorithm has been tested with different values of K (i.e. 1, 3, 5, 7, 9, 11 and 13) and that value of k has been selected for further experimentation in which the model is able to make good number of predictions with data that the model has not seen before. Further, in this work, 10 different distance metrics have been evaluated to obtain the maximum accuracy. After extensive experiments it has been found that K-NN classifier gave best results with city block distance metric and value of K as 7. The overall accuracy obtained with these parameter settings is 96.7% with area under ROC curve as 0.99.

Furthermore, in this thesis work a two-layer feedforward neural network has been modelled in the Proposed Method III. Sigmoid transfer function was used in the hidden layer of the neural network, and a SoftMax transfer function was used in the output layer as a standard network for the classification of hepatic ultrasound. The value of the hidden neurons is set as 10 for conducting the experiments. As the number of categories into which classification has to be done are two so the value of output neurons is set as 2. After extensive experiments it was found that with this network an overall accuracy of 98.9 percent with 100 percent sensitivity and 97.8 percent specificity was achieved.

In order to reduce the Miss Rate to a great extent. The process is further carried out by Mutual Information (MI) feature selection method and classification algorithms. The performance of 4 classifiers i.e. SMO, IBk, AdaBoostM1 and BF-Tree is evaluated for 5 different experiments based on different number of selected best features. Summarizing the result of all the experiments, SMO is outperforming with accuracy rate of 95.55%, miss rate of 2.22% and sensitivity rate of 97.77% on the present dataset with 20 best features selected by the MI feature selection technique. Also, it has been analysed that the performance of all 45 features in combination is same as that of 20 features when SMO classifier is used with polynomial kernel. Therefore, instead of using 45 features, the selected combination



of 20 features can be used, which further reduces the computational cost in classifying the images. Therefore, combination of these 20 optimal features can be used for liver ultrasound image classification. Furthermore, for the extensive experiments of SMO classifier, results have been obtained with 4 different kernels i.e. RBF, Polykernel, Normalised kernel and PUK kernel, where the overall best results are given by Polykernel.

In conclusion, experiments demonstrated that the proposed techniques gave better results for the classification of liver ultrasound images into two categories. The present work is likely to contribute significantly to the area of liver ultrasound imaging. The methods developed will in particular be useful for the processing and analysis of liver ultrasound images.

### **5.3 Scope for Future Work**

Suggested below are a few directions and challenges in which further work in the area of processing and analysis of ultrasound images can be taken up.

- (i) More focus is provided in the present work on classifying two classes i.e. fatty liver and normal liver. The study can be expanded in future to classify the liver ultrasound images into more categories.
- (ii) The work can be further extended by making use of other texture feature models that exists in literature for the classification purpose.
- (iii) Presently, the ROI selection is manual, which requires significant experience and domain knowledge. In future, a system can be proposed to automatically select the ROI from an ultrasound image.



## REFERENCES

1. Festi, D., Schiumerini, R., Marzi, L., Di Biase, A. R., Mandolesi, D., Montrone, L., & Colecchia, A. (2013). the diagnosis of non-alcoholic fatty liver disease—availability and accuracy of non-invasive methods. *Alimentary pharmacology & therapeutics*, 37(4), 392-400.
2. Stern, C., & Castera, L. (2017). Non-invasive diagnosis of hepatic steatosis. *Hepatology international*, 11(1), 70-78.
3. Sanches, J. M., Laine, A. F., & Suri, J. S. (2012). *Ultrasound imaging*. Berlin, Germany: Springer.
4. Li, C., Li, R., & Zhang, W. (2018). Progress in non-invasive detection of liver fibrosis. *Cancer biology & medicine*, 15(2), 124.
5. Sierra Aisa, C., Lucía Cuesta, J. F., Rubio Martínez, A., Fernández Mosteirín, N., Iborra Muñoz, A., Abío Calvete, M., & Rubio Félix, D. (2014). Comparison of ultrasound and magnetic resonance imaging for diagnosis and follow-up of joint lesions in patients with haemophilia. *Haemophilia*, 20(1), e51-e57.
6. Duseja, A., Najmy, S., Sachdev, S., Pal, A., Sharma, R. R., Marwah, N., & Chawla, Y. (2019). High prevalence of non-alcoholic fatty liver disease among healthy male blood donors of urban India. *JGH Open*, 3(2), 133-139.
7. Duseja, A., Singh, S. P., Saraswat, V. A., Acharya, S. K., Chawla, Y. K., Chowdhury, S., & Mishra, H. (2015). Non-alcoholic fatty liver disease and metabolic syndrome—position paper of the Indian National Association for the Study of the Liver, Endocrine Society of India, Indian College of Cardiology and Indian Society of Gastroenterology. *Journal of clinical and experimental hepatology*, 5(1), 51-68.
8. Seto, W. K., & Yuen, M. F. (2017). Nonalcoholic fatty liver disease in Asia: emerging perspectives. *Journal of gastroenterology*, 52(2), 164-174.
9. Chen, E-Liang & Chung, P & Chen, C & Tsai, H & Chang, Chein-I. (1998). An automatic diagnosis system for CT liver image classification. *IEEE transactions on bio-medical engineering*. 45. 783-94.

10. Mishra, A., & Younossi, Z. M. (2012). Epidemiology and natural history of non-alcoholic fatty liver disease. *Journal of clinical and experimental hepatology*, 2(2), 135-144.
11. Rangayyan, R. M. (2004). *Biomedical image analysis*. CRC press.
12. Azevedo-Marques, P. M. D., & Rangayyan, R. M. (2013). Content-based retrieval of medical images: landmarking, indexing, and relevance feedback. *Synthesis Lectures on Biomedical Engineering*, 8(1), 1-143.
13. Amaral, I. F. A. (2010). Content-based image retrieval for medical applications. *Faculty of Science, University of Porto*.
14. Bergman, L. A. (2002). *Image Databases: Search and Retrieval of Digital Imagery*. Wiley-Interscience.
15. CONSTANTINESCU, E. C., NICOLAU, C., & SĂFTOIU, A. (2018). Recent Developments in Tele-Ultrasonography. *Current Health Sciences Journal*, 44(2), 101.
16. Ali, M., Magee, D., & Dasgupta, U. (2008). Signal processing overview of ultrasound systems for medical imaging. *SPRAB12, Texas Instruments, Texas*.
17. Szabo, T. L. (2004). *Diagnostic ultrasound imaging: inside out*. Academic Press.
18. Lutz, H., & Buscarini, E. (Eds.). (2011). *Manual of diagnostic ultrasound* (Vol. 2). World Health Organization.
19. Sloss, A., & Kubler, P. (2009). Prescribing in liver disease. *Aust Prescr*, 32(2), 32-5.
20. Marchesini, G., Marzocchi, R., Agostini, F., & Bugianesi, E. (2005). Nonalcoholic fatty liver disease and the metabolic syndrome. *Current opinion in lipidology*, 16(4), 421-427.
21. Singh, M., Singh, S., & Gupta, S. (2014). An information fusion based method for liver classification using texture analysis of ultrasound images. *Information Fusion*, 19, 91-96.
22. Ludwig, J., Viggiano, T. R., McGill, D. B., & Oh, B. J. (1980, July). Nonalcoholic steatohepatitis: Mayo Clinic experiences with a hitherto unnamed disease. In *Mayo Clinic Proceedings* (Vol. 55, No. 7, pp. 434-438).
23. Musso, G., Gambino, R., Cassader, M., & Pagano, G. (2011). Meta-analysis: natural history of non-alcoholic fatty liver disease (NAFLD) and diagnostic

- accuracy of non-invasive tests for liver disease severity. *Annals of medicine*, 43(8), 617-649.
24. Ratziu, V., Charlotte, F., Heurtier, A., Gombert, S., Giral, P., Bruckert, E., ... & LIDO Study Group. (2005). Sampling variability of liver biopsy in nonalcoholic fatty liver disease. *Gastroenterology*, 128(7), 1898-1906.
  25. İçer, S., Coşkun, A., & İkizceli, T. (2012). Quantitative grading using grey relational analysis on ultrasonographic images of a fatty liver. *Journal of medical systems*, 36(4), 2521-2528.
  26. Li, G., Luo, Y., Deng, W., Xu, X., Liu, A., & Song, E. (2008, August). Computer aided diagnosis of fatty liver ultrasonic images based on support vector machine. In *2008 30th Annual International Conference of the IEEE Engineering in Medicine and Biology Society* (pp. 4768-4771). IEEE.
  27. Fan, J. G. (2013). Epidemiology of alcoholic and nonalcoholic fatty liver disease in china. *Journal of gastroenterology and hepatology*, 28, 11-17.
  28. Abenavoli, L., & Beaugrand, M. (2012). Transient elastography in non-alcoholic fatty liver disease. *Annals of hepatology*, 11(2), 172-178.
  29. Wlodzimirow, K. A., Eslami, S., Chamuleau, R. A., Nieuwoudt, M., & Abu-Hanna, A. (2012). Prediction of poor outcome in patients with acute liver failure— Systematic review of prediction models. *PloS one*, 7(12), e50952.
  30. Oh, M. K., Winn, J., & Poordad, F. (2008). diagnosis and treatment of non-alcoholic fatty liver disease. *Alimentary pharmacology & therapeutics*, 28(5), 503-522.
  31. Castera, L. (2008). Non-invasive diagnosis of steatosis and fibrosis. *Diabetes & metabolism*, 34(6), 674-679.
  32. Guha, I. N., Parkes, J., Roderick, P. R., Harris, S., & Rosenberg, W. M. (2006). Non-invasive markers associated with liver fibrosis in non-alcoholic fatty liver disease. *Gut*, 55(11), 1650-1660.
  33. Masuoka, H. C., & Chalasani, N. (2013). Nonalcoholic fatty liver disease: an emerging threat to obese and diabetic individuals. *Annals of the New York Academy of Sciences*, 1281(1), 106.

34. Ribeiro, R., & Sanches, J. (2009, June). Fatty liver characterization and classification by ultrasound. In *Iberian Conference on Pattern Recognition and Image Analysis* (pp. 354-361). Springer, Berlin, Heidelberg.
35. Sharma, V., & Juglan, K. C. (2020, May). Ultrasound-based Classification of Fatty Liver Disease: A Review. In *Journal of Physics: Conference Series* (Vol. 1531, No. 1, p. 012033). IOP Publishing.
36. Acharya, U. R., Faust, O., Molinari, F., Sree, S. V., Junnarkar, S. P., & Sudarshan, V. (2015). Ultrasound-based tissue characterization and classification of fatty liver disease: A screening and diagnostic paradigm. *Knowledge-Based Systems*, 75, 66-77.
37. Amin, M. N., Rushdi, M. A., Marzaban, R. N., Yosry, A., Kim, K., & Mahmoud, A. M. (2019). Wavelet-based computationally-efficient computer-aided characterization of liver steatosis using conventional B-mode ultrasound images. *Biomedical Signal Processing and Control*, 52, 84-96.
38. Rathore, S., Iftikhar, M. A., Hussain, M., & Jalil, A. (2011, December). Texture analysis for liver segmentation and classification: a survey. In *2011 Frontiers of Information Technology* (pp. 121-126). IEEE.
39. Sklansky, J. (1978). Image segmentation and feature extraction. *IEEE Transactions on Systems, Man, and Cybernetics*, 8(4), 237-247.
40. Rosenfeld, A. (1976). *Digital Picture Analysis*, Springer Verlag, Berlin 1976.
41. Haralick, R. M., Shanmugam, K., & Dinstein, I. H. (1973). Textural features for image classification. *IEEE Transactions on systems, man, and cybernetics*, (6), 610-621.
42. Lendaris, G. G., & Stanley, G. L. (1970). Diffraction-pattern sampling for automatic pattern recognition. *Proceedings of the IEEE*, 58(2), 198-216.
43. Weszka, J. S., Dyer, C. R., & Rosenfeld, A. (1976). A comparative study of texture measures for terrain classification. *IEEE transactions on Systems, Man, and Cybernetics*, (4), 269-285.
44. Badawi, A. M., Derbala, A. S., & Youssef, A. B. M. (1999). Fuzzy logic algorithm for quantitative tissue characterization of diffuse liver diseases from ultrasound images. *International Journal of Medical Informatics*, 55(2), 135-147.

45. Acharya, U. R., Fujita, H., Bhat, S., Raghavendra, U., Gudigar, A., Molinari, F., ... & Ng, K. H. (2016). Decision support system for fatty liver disease using GIST descriptors extracted from ultrasound images. *Information Fusion*, 29, 32-39.
46. Sharma, N., Ray, A. K., Sharma, S., Shukla, K. K., Pradhan, S., & Aggarwal, L. M. (2008). Segmentation and classification of medical images using texture-primitive features: Application of BAM-type artificial neural network. *Journal of medical physics/Association of Medical Physicists of India*, 33(3), 119.
47. Mittal, D., Kumar, V., Saxena, S. C., Khandelwal, N., & Kalra, N. (2011). Neural network based focal liver lesion diagnosis using ultrasound images. *computerized medical imaging and graphics*, 35(4), 315-323.
48. Kalyan, K., Jakhia, B., Lele, R. D., Joshi, M., & Chowdhary, A. (2014). Artificial neural network application in the diagnosis of disease conditions with liver ultrasound images. *Advances in bioinformatics*, 2014.
49. Byra, M., Styczynski, G., Szmigielski, C., Kalinowski, P., Michałowski, Ł., Paluszkiewicz, R., ... & Nowicki, A. (2018). Transfer learning with deep convolutional neural network for liver steatosis assessment in ultrasound images. *International journal of computer assisted radiology and surgery*, 13(12), 1895-1903.
50. Virmani, J., Kumar, V., Kalra, N., & Khandelwal, N. (2013). SVM-based characterization of liver ultrasound images using wavelet packet texture descriptors. *Journal of digital imaging*, 26(3), 530-543.
51. Rani, A., & Mittal, D. (2016). Detection and classification of focal liver lesions using support vector machine classifiers. *Journal of Biomedical Engineering and Medical Imaging*, 3(1), 21-21.
52. Subramanya, M. B., Kumar, V., Mukherjee, S., & Saini, M. (2015). A CAD system for B-mode fatty liver ultrasound images using texture features. *Journal of medical engineering & technology*, 39(2), 123-130.
53. Goodman, J. W. (1976). Some fundamental properties of speckle. *JOSA*, 66(11), 1145-1150.
54. Gupta, S., Chauhan, R. C., & Sexana, S. C. (2004). Wavelet-based statistical approach for speckle reduction in medical ultrasound images. *Medical and Biological Engineering and computing*, 42(2), 189-192.

55. Lee, J. S. (1981). Refined filtering of image noise using local statistics. *Computer graphics and image processing*, 15(4), 380-389.
56. Busse, L. J., Crimmins, T. R., & Fienup, J. R. (1995, November). A model based approach to improve the performance of the geometric filtering speckle reduction algorithm. In *1995 IEEE Ultrasonics Symposium. Proceedings. An International Symposium* (Vol. 2, pp. 1353-1356). IEEE.
57. Kuan, D. A. R. W. I. N. T., Sawchuk, A. L. E. X. A. N. D. E. R. A., Strand, T. I. M. O. T. H. Y. C., & Chavel, P. (1987). Adaptive restoration of images with speckle. *IEEE Transactions on Acoustics, Speech, and Signal Processing*, 35(3), 373-383.
58. Perona, P., & Malik, J. (1990). Scale-space and edge detection using anisotropic diffusion. *IEEE Transactions on pattern analysis and machine intelligence*, 12(7), 629-639.
59. Jin, J. S., Wang, Y., & Hiller, J. (2000). An adaptive nonlinear diffusion algorithm for filtering medical images. *IEEE Transactions on Information Technology in Biomedicine*, 4(4), 298-305.
60. Yu, Y., & Acton, S. T. (2002). Speckle reducing anisotropic diffusion. *IEEE Transactions on image processing*, 11(11), 1260-1270.
61. You, Y. L., & Kaveh, M. (2000). Fourth-order partial differential equations for noise removal. *IEEE Transactions on Image Processing*, 9(10), 1723-1730.
62. Mittal, D., Kumar, V., Saxena, S. C., Khandelwal, N., & Kalra, N. (2010). Enhancement of the ultrasound images by modified anisotropic diffusion method. *Medical & biological engineering & computing*, 48(12), 1281-1291.
63. Achim, A., Bezerianos, A., & Tsakalides, P. (2001). Novel Bayesian multiscale method for speckle removal in medical ultrasound images. *IEEE transactions on medical imaging*, 20(8), 772-783.
64. Michailovich, O., & Adam, D. (2003). Robust estimation of ultrasound pulses using outlier-resistant de-noising. *IEEE Transactions on Medical Imaging*, 22(3), 368-381.
65. Gupta, S., Chauhan, R. C., & Saxena, S. C. (2005). Homomorphic wavelet thresholding technique for denoising medical ultrasound images. *Journal of medical engineering & technology*, 29(5), 208-214.



66. Gupta, S., Kaur, L., Chauhan, R. C., & Saxena, S. C. (2007). A versatile technique for visual enhancement of medical ultrasound images. *Digital Signal Processing*, 17(3), 542-560.
67. Dantas, R. G., & Costa, E. T. (2007). Ultrasound speckle reduction using modified Gabor filters. *IEEE transactions on ultrasonics, ferroelectrics, and frequency control*, 54(3), 530-538.
68. Gungor, M. A., & Karagoz, I. (2015). The homogeneity map method for speckle reduction in diagnostic ultrasound images. *Measurement*, 68, 100-110.
69. Yang, J., Fan, J., Ai, D., Wang, X., Zheng, Y., Tang, S., & Wang, Y. (2016). Local statistics and non-local mean filter for speckle noise reduction in medical ultrasound image. *Neurocomputing*, 195, 88-95.
70. Zhang, J., Lin, G., Wu, L., & Cheng, Y. (2016). Speckle filtering of medical ultrasonic images using wavelet and guided filter. *Ultrasonics*, 65, 177-193.
71. Sagheer, S. V. M., & George, S. N. (2017). Ultrasound image despeckling using low rank matrix approximation approach. *Biomedical Signal Processing and Control*, 38, 236-249.
72. Khvostikov, A., Krylov, A., Kamalov, J., & Megroyan, A. (2017). Ultrasound despeckling by anisotropic diffusion and total variation methods for liver fibrosis diagnostics. *Signal Processing: Image Communication*, 59, 3-11.
73. Elyasi, I., & Pourmina, M. A. (2016). Reduction of speckle noise ultrasound images based on TV regularization and modified bayes shrink techniques. *Optik*, 127(24), 11732-11744.
74. Lee, J. S. (1981). Refined filtering of image noise using local statistics. *Computer graphics and image processing*, 15(4), 380-389.
75. Zhu, L., Fu, C. W., Brown, M. S., & Heng, P. A. (2017). A non-local low-rank framework for ultrasound speckle reduction. In *Proceedings of the IEEE Conference on Computer Vision and Pattern Recognition* (pp. 5650-5658).
76. Dass, R. (2018). Speckle noise reduction of ultrasound images using BFO cascaded with wiener filter and discrete wavelet transform in homomorphic region. *Procedia computer science*, 132, 1543-1551.

77. Jubairahmed, L., Satheeskumaran, S., & Venkatesan, C. (2019). Contourlet transform based adaptive nonlinear diffusion filtering for speckle noise removal in ultrasound images. *Cluster Computing*, 22(5), 11237-11246.
78. Rudin, L. I., Osher, S., & Fatemi, E. (1992). Nonlinear total variation based noise removal algorithms. *Physica D: nonlinear phenomena*, 60(1-4), 259-268.
79. Yu, J., Wang, Y., & Shen, Y. (2008). Noise reduction and edge detection via kernel anisotropic diffusion. *Pattern Recognition Letters*, 29(10), 1496-1503.
80. Pizurica, A., Philips, W., Lemahieu, I., & Acheroy, M. (2003). A versatile wavelet domain noise filtration technique for medical imaging. *IEEE transactions on medical imaging*, 22(3), 323-331.
81. Gupta, S., Chauhan, R. C., & Saxena, S. C. (2005). Robust multiscale non-homomorphic approach to speckle reduction of medical ultrasound images.
82. Singh, K., Ranade, S. K., & Singh, C. (2017). A hybrid algorithm for speckle noise reduction of ultrasound images. *Computer methods and programs in biomedicine*, 148, 55-69.
83. Roy, R., Ghosh, S., & Ghosh, A. (2018). Speckle de-noising of clinical ultrasound images based on fuzzy spel conformity in its adjacency. *Applied Soft Computing*, 73, 394-417.
84. Deka, B., & Bora, P. K. (2013). Removal of correlated speckle noise using sparse and overcomplete representations. *Biomedical Signal Processing and Control*, 8(6), 520-533.
85. Arnal, J., & Mayzel, I. (2020). Parallel techniques for speckle noise reduction in medical ultrasound images. *Advances in Engineering Software*, 148, 102867.
86. Yoon, C., Kim, G. D., Yoo, Y., Song, T. K., & Chang, J. H. (2013). Frequency equalized compounding for effective speckle reduction in medical ultrasound imaging. *Biomedical Signal Processing and Control*, 8(6), 876-887.
87. Zhu, L., Wang, W., Qin, J., Wong, K. H., Choi, K. S., & Heng, P. A. (2017). Fast feature-preserving speckle reduction for ultrasound images via phase congruency. *Signal Processing*, 134, 275-284.
88. Gupta, D., Anand, R. S., & Tyagi, B. (2014). Despeckling of ultrasound medical images using nonlinear adaptive anisotropic diffusion in nonsubsamped shearlet domain. *Biomedical Signal Processing and Control*, 14, 55-65.

89. Shao, D., Liu, P., & Liu, D. C. (2013). Characteristic matching-based adaptive fast bilateral filter for ultrasound speckle reduction. *Pattern Recognition Letters*, 34(5), 463-469.
90. Latifoğlu, F. (2013). A novel approach to speckle noise filtering based on artificial bee colony algorithm: an ultrasound image application. *Computer methods and programs in biomedicine*, 111(3), 561-569.
91. A. Rosenfeld and J. Weszka, "Picture Recognition" in Digital Pattern Recognition, K. Fu (Ed.), Springer-Verlag, Berlin, 1980.
92. J.C. Russ, The Image Processing Handbook, 3rd edition, CRC Press, USA, 1999.
93. M. Levine, "Vision in Man and Machine", McGraw-Hill, USA, 1985.
94. Bharati, M. H., Liu, J. J., & MacGregor, J. F. (2004). Image texture analysis: methods and comparisons. *Chemometrics and intelligent laboratory systems*, 72(1), 57-71.
95. Materka, A., & Strzelecki, M. (1998). Texture analysis methods—a review. *Technical university of lodz, institute of electronics, COST B11 report, Brussels*, 10(1.97), 4968.
96. Gonzalez, R. C., Woods, R. E., & Eddins, S. L. (2004). *Digital image processing using MATLAB*. Pearson Education India.
97. F. Tomita and S. Tsuji, "Computer Analysis of Visual Textures", Kluwer Academic Publishing, USA, 1990.
98. Haralick, R. M. (1979). Statistical and structural approaches to texture. *Proceedings of the IEEE*, 67(5), 786-804.
99. Cross, G. R., & Jain, A. K. (1983). Markov random field texture models. *IEEE Transactions on Pattern Analysis and Machine Intelligence*, (1), 25-39.
100. Pentland, A. P. (1984). Fractal-based description of natural scenes. *IEEE transactions on pattern analysis and machine intelligence*, (6), 661-674.
101. Chellappa, R., & Chatterjee, S. (1985). Classification of textures using Gaussian Markov random fields. *IEEE Transactions on Acoustics, Speech, and Signal Processing*, 33(4), 959-963.
102. Daugman, J. G. (1985). Uncertainty relation for resolution in space, spatial frequency, and orientation optimized by two-dimensional visual cortical filters. *JOSA A*, 2(7), 1160-1169.

103. Mallat, S. G. (1989). A theory for multiresolution signal decomposition: the wavelet representation. *IEEE transactions on pattern analysis and machine intelligence*, 11(7), 674-693.
104. Lu, Z. F., Zagzebski, J. A., & Lee, F. T. (1999). Ultrasound backscatter and attenuation in human liver with diffuse disease. *Ultrasound in medicine & biology*, 25(7), 1047-1054.
105. Bovik, A. C., Clark, M., & Geisler, W. S. (1990). Multichannel texture analysis using localized spatial filters. *IEEE transactions on pattern analysis and machine intelligence*, 12(1), 55-73.
106. Valckx, F. M., & Thijssen, J. M. (1997). Characterization of echographic image texture by cooccurrence matrix parameters. *Ultrasound in medicine & biology*, 23(4), 559-571.
107. Mountford, R. A., & Wells, P. N. T. (1972). Ultrasonic liver scanning: the A-scan in the normal and cirrhosis. *Physics in Medicine & Biology*, 17(2), 261.
108. Wells, P. N. (2006). Ultrasound imaging. *Physics in Medicine & Biology*, 51(13), R83.
109. Chivers, R. C., & Hill, C. R. (1975). Ultrasonic attenuation in human tissue. *Ultrasound in medicine & biology*, 2(1), 25-29.
110. Thijssen, J. M., Starke, A., Weijers, G., Haudum, A., Herzog, K., Wohlsein, P., ... & De Korte, C. L. (2008). Computer-aided B-mode ultrasound diagnosis of hepatic steatosis: a feasibility study. *IEEE transactions on ultrasonics, ferroelectrics, and frequency control*, 55(6), 1343-1354.
111. Lewis, J. R., & Mohanty, S. R. (2010). Nonalcoholic fatty liver disease: a review and update. *Digestive diseases and sciences*, 55(3), 560-578.
112. Fukushima, M., Ogawa, K., Kubota, T., & Hisa, N. (1997, November). Quantitative tissue characterization of diffuse liver diseases from ultrasound images by neural network. In *1997 IEEE Nuclear Science Symposium Conference Record* (Vol. 2, pp. 1233-1236). IEEE.
113. Gaitini, D., Baruch, Y., Ghersin, E., Veitsman, E., Kerner, H., Shalem, B., ... & Azhari, H. (2004). Feasibility study of ultrasonic fatty liver biopsy: texture vs. attenuation and backscatter. *Ultrasound in medicine & biology*, 30(10), 1321-1327.

114. Quan, J. R., Xie, X. Q., Lin, J. L., Chen, Y., Ling, W. W., Lu, Q., ... & Luo, Y. (2012). Ultrasound tissue characterization of hepatic fat in rats using radiofrequency signal analysis *Journal of Sichuan University. Medical science edition*, 43(1), 54-59.
115. Kadah, Y. M., Farag, A. A., Zurada, J. M., Badawi, A. M., & Youssef, A. B. (1996). Classification algorithms for quantitative tissue characterization of diffuse liver disease from ultrasound images. *IEEE transactions on Medical Imaging*, 15(4), 466-478.
116. Acharya, U. R., Sree, S. V., Ribeiro, R., Krishnamurthi, G., Marinho, R. T., Sanches, J., & Suri, J. S. (2012). Data mining framework for fatty liver disease classification in ultrasound: a hybrid feature extraction paradigm. *Medical physics*, 39(7Part1), 4255-4264.
117. İçer, S., Coşkun, A., & İkizceli, T. (2012). Quantitative grading using grey relational analysis on ultrasonographic images of a fatty liver. *Journal of medical systems*, 36(4), 2521-2528.
118. Sabih, D., & Hussain, M. (2012). Automated classification of liver disorders using ultrasound images. *Journal of medical systems*, 36(5), 3163-3172.
119. Donohue, K. D., Huang, L., Burks, T., Forsberg, F., & Piccoli, C. W. (2001). Tissue classification with generalized spectrum parameters. *Ultrasound in medicine & biology*, 27(11), 1505-1514.
120. Wu, C. M., Chen, Y. C., & Hsieh, K. S. (1992). Texture features for classification of ultrasonic liver images. *IEEE Transactions on medical imaging*, 11(2), 141-152.
121. Laws, K. I. (1979, November). Texture energy measures. In *Proc. Image understanding workshop* (pp. 47-51).
122. Wu, C. M., & Chen, Y. C. (1992). Statistical feature matrix for texture analysis. *CVGIP: Graphical Models and Image Processing*, 54(5), 407-419.
123. Yajima, Y., OHTA, K., NARUI, T., ABE, R., SUZUKI, H., & OHTSUKI, M. (1983). Ultrasonographical diagnosis of fatty liver: significance of the liver-kidney contrast. *The Tohoku journal of experimental medicine*, 139(1), 43-50.

124. Pavlopoulos, S., Kyriacou, E., Koutsouris, D., Blekas, K., Stafylopatis, A., & Zoumpoulis, P. (2000). Fuzzy neural network-based texture analysis of ultrasonic images. *IEEE Engineering in Medicine and Biology Magazine*, 19(1), 39-47.
125. Chen, E. L., Chung, P. C., Chen, C. L., Tsai, H. M., & Chang, C. I. (1998). An automatic diagnostic system for CT liver image classification. *IEEE transactions on biomedical engineering*, 45(6), 783-794.
126. Mukherjee, S., Chakravorty, A., Ghosh, K., Roy, M., Adhikari, A., & Mazumdar, S. (2007, December). Corroborating the subjective classification of ultrasound images of normal and fatty human livers by the radiologist through texture analysis and SOM. In *15th International Conference on Advanced Computing and Communications (ADCOM 2007)* (pp. 197-202). IEEE.
127. Sriraam, N., Roopa, J., Saranya, M., & Dhanalakshmi, M. (2009). Performance evaluation of computer aided diagnostic tool (CAD) for detection of ultrasonic based liver disease. *Journal of medical systems*, 33(4), 267-274.
128. Singh, M., Singh, S., & Gupta, S. (2012). A new quantitative metric for liver classification from ultrasound images. *International Journal of Computer and Electrical Engineering*, 4(4), 605.
129. Acharya, U. R., Fujita, H., Sudarshan, V. K., Mookiah, M. R. K., Koh, J. E., Tan, J. H., ... & Ng, K. H. (2016). An integrated index for identification of fatty liver disease using radon transform and discrete cosine transform features in ultrasound images. *Information Fusion*, 31, 43-53.
130. Saba, L., Dey, N., Ashour, A. S., Samanta, S., Nath, S. S., Chakraborty, S., ... & Suri, J. S. (2016). Automated stratification of liver disease in ultrasound: an online accurate feature classification paradigm. *Computer methods and programs in biomedicine*, 130, 118-134.
131. Krishnan, K. R., & Sudhakar, R. (2013). Automatic classification of liver diseases from ultrasound images using GLRLM texture features. In *Soft Computing Applications* (pp. 611-624). Springer, Berlin, Heidelberg.
132. Virmani, J., Kumar, V., Kalra, N., & Khandelwal, N. (2013). SVM-based characterization of liver ultrasound images using wavelet packet texture descriptors. *Journal of digital imaging*, 26(3), 530-543.

133. Jeon, J. H., Choi, J. Y., Lee, S., & Ro, Y. M. (2013). Multiple ROI selection based focal liver lesion classification in ultrasound images. *Expert Systems with Applications*, 40(2), 450-457.
134. Singh, M., Singh, S., & Gupta, S. (2014). An information fusion based method for liver classification using texture analysis of ultrasound images. *Information Fusion*, 19, 91-96.
135. Acharya, U. R., Raghavendra, U., Fujita, H., Hagiwara, Y., Koh, J. E., Hong, T. J., ... & Ng, K. H. (2016). Automated characterization of fatty liver disease and cirrhosis using curvelet transform and entropy features extracted from ultrasound images. *Computers in biology and medicine*, 79, 250-258.
136. Saba, L., Dey, N., Ashour, A. S., Samanta, S., Nath, S. S., Chakraborty, S., ... & Suri, J. S. (2016). Automated stratification of liver disease in ultrasound: an online accurate feature classification paradigm. *Computer methods and programs in biomedicine*, 130, 118-134.
137. Acharya, U. R., Fujita, H., Sudarshan, V. K., Mookiah, M. R. K., Koh, J. E., Tan, J. H., ... & Ng, K. H. (2016). An integrated index for identification of fatty liver disease using radon transform and discrete cosine transform features in ultrasound images. *Information Fusion*, 31, 43-53.
138. Xu, S. S. D., Chang, C. C., Su, C. T., & Phu, P. Q. (2019). Classification of liver diseases based on ultrasound image texture features. *Applied Sciences*, 9(2), 342.
139. Amin, M. N., Rushdi, M. A., Marzaban, R. N., Yosry, A., Kim, K., & Mahmoud, A. M. (2019). Wavelet-based computationally-efficient computer-aided characterization of liver steatosis using conventional B-mode ultrasound images. *Biomedical Signal Processing and Control*, 52, 84-96.
140. Krithiga, R. R., & Lakshmi, C. (2020). A novel automated classification technique for diagnosing liver disorders using wavelet and texture features on liver ultrasound images. *Multimedia Tools and Applications*, 79(5), 3761-3773.
141. De Azevedo-Marques, P. M., Mencattini, A., Salmeri, M., & Rangayyan, R. M. (Eds.). (2017). *Medical Image Analysis and Informatics: Computer-Aided Diagnosis and Therapy*. CRC Press.

142. Acharya, U. R., Koh, J. E. W., Hagiwara, Y., Tan, J. H., Gertych, A., Vijayanathan, A., ... & Yeong, C. H. (2018). Automated diagnosis of focal liver lesions using bidirectional empirical mode decomposition features. *Computers in biology and medicine*, 94, 11-18.
143. Meiburger, K. M., Acharya, U. R., & Molinari, F. (2018). Automated localization and segmentation techniques for B-mode ultrasound images: A review. *Computers in biology and medicine*, 92, 210-235.
144. Faust, O., Acharya, U. R., Meiburger, K. M., Molinari, F., Koh, J. E., Yeong, C. H., ... & Ng, K. H. (2018). Comparative assessment of texture features for the identification of cancer in ultrasound images: a review. *Biocybernetics and Biomedical Engineering*, 38(2), 275-296.
145. Acharya, U. R., Faust, O., Molinari, F., Sree, S. V., Junnarkar, S. P., & Sudarshan, V. (2015). Ultrasound-based tissue characterization and classification of fatty liver disease: A screening and diagnostic paradigm. *Knowledge-Based Systems*, 75, 66-77.
146. Owjimehr, M., Danyali, H., Helfroush, M. S., & Shakibafard, A. (2017). Staging of fatty liver diseases based on hierarchical classification and feature fusion for back-scan-converted ultrasound images. *Ultrasonic imaging*, 39(2), 79-95.
147. Bharath, R., Mishra, P. K., & Rajalakshmi, P. (2018). Automated quantification of ultrasonic fatty liver texture based on curvelet transform and SVD. *Biocybernetics and Biomedical Engineering*, 38(1), 145-157.
148. Sharma, V., & Juglan, K. C. (2018). Automated Classification of Fatty and Normal Liver Ultrasound Images Based on Mutual Information Feature Selection. *IRBM*, 39(5), 313-323.
149. Metz, C. E. (1978, October). Basic principles of ROC analysis. In *Seminars in nuclear medicine* (Vol. 8, No. 4, pp. 283-298). WB Saunders.
150. Park, S. H., Goo, J. M., & Jo, C. H. (2004). Receiver operating characteristic (ROC) curve: practical review for radiologists. *Korean journal of radiology*, 5(1), 11-18.
151. Singh, M., Singh, S., & Gupta, S. (2014). *Processing and analysis of ultrasound images for tissue characterization* (Doctoral dissertation).



152. Tuthill T A, Baggs R B, Parker K J. Liver glycogen and water storage: effect on ultrasound attenuation. *Ultrasound Med Biol.* 1989; 15(7): 621–627.
153. Haralick, R. M., Shanmugam, K., & Dinstein, I. H. (1973). Textural features for image classification. *IEEE Transactions on systems, man, and cybernetics*, (6), 610-621.
154. Ferdeghini, E. M., Pinamonti, B., Picano, E., Lattanzi, F., Bussani, R., Slavich, G., ... & L'Abbate, A. (1991). Quantitative texture analysis in echocardiography: application to the diagnosis of myocarditis. *Journal of clinical ultrasound*, 19(5), 263-270.
155. Lendaris, G. G., & Stanley, G. L. (1970). Diffraction-pattern sampling for automatic pattern recognition. *Proceedings of the IEEE*, 58(2), 198-216.
156. Wold, S., Esbensen, K., & Geladi, P. (1987). Principal component analysis. *Chemometrics and intelligent laboratory systems*, 2(1-3), 37-52.
157. Abdi, H., & Williams, L. J. (2010). Principal component analysis. *Wiley interdisciplinary reviews: computational statistics*, 2(4), 433-459.
158. Safavian, S. R., & Landgrebe, D. (1991). A survey of decision tree classifier methodology. *IEEE transactions on systems, man, and cybernetics*, 21(3), 660-674.
159. Hu, L. Y., Huang, M. W., Ke, S. W., & Tsai, C. F. (2016). The distance function effect on k-nearest neighbor classification for medical datasets. *Springer Plus*, 5(1), 1-9.
160. Kataria, A., & Singh, M. D. (2013). A review of data classification using k-nearest neighbour algorithm. *International Journal of Emerging Technology and Advanced Engineering*, 3(6), 354-360.
161. Chang, C. L. (1974). Finding prototypes for nearest neighbor classifiers. *IEEE Transactions on Computers*, 100(11), 1179-1184.
162. Abu Alfeilat, H. A., Hassanat, A. B., Lasassmeh, O., Tarawneh, A. S., Alhasanat, M. B., Eyal Salman, H. S., & Prasath, V. S. (2019). Effects of distance measure choice on K-Nearest neighbor classifier performance: A review. *Big data*, 7(4), 221-248.
163. Jain, A. K., Mao, J., & Mohiuddin, K. M. (1996). Artificial neural networks: A tutorial. *Computer*, 29(3), 31-44.

164. Van Gerven, M., & Bohte, S. (2017). Artificial neural networks as models of neural information processing. *Frontiers in Computational Neuroscience*, 11, 114.
165. Kalyan, K., Jakhia, B., Lele, R. D., Joshi, M., & Chowdhary, A. (2014). Artificial neural network application in the diagnosis of disease conditions with liver ultrasound images. *Advances in bioinformatics*, 2014.
166. Olaniyi, E. O., Oyedotun, O. K., & Adnan, K. (2015). Heart diseases diagnosis using neural networks arbitration. *International Journal of Intelligent Systems and Applications*, 7(12), 72.
167. Peng, H., Long, F., & Ding, C. (2005). Feature selection based on mutual information criteria of max-dependency, max-relevance, and min-redundancy. *IEEE Transactions on pattern analysis and machine intelligence*, 27(8), 1226-1238.
168. Liao, Y., & Vemuri, V. R. (2002). Use of k-nearest neighbor classifier for intrusion detection. *Computers & security*, 21(5), 439-448.
169. Witten, I. H., & Frank, E. (2002). Data mining: practical machine learning tools and techniques with Java implementations. *Acm Sigmod Record*, 31(1), 76-77.
170. Chimieski, B. F., & Fagundes, R. D. R. (2013). Association and classification data mining algorithms comparison over medical datasets. *Journal of health informatics*, 5(2).
171. Witten, I. H., Frank, E., Trigg, L. E., Hall, M. A., Holmes, G., & Cunningham, S. J. (1999). Weka: Practical machine learning tools and techniques with Java implementations.

## LIST OF PUBLICATIONS

### Research Paper Published in Journal:

1. Vishal Sharma and K.C. Juglan, “Automated Classification of Fatty and Normal Liver Ultrasound Images based on Mutual Information Feature Selection” *Innovation and Research in Bio Medical Engineering (Elsevier)* Vol. 39, Issue - 5, pp. 313-323, Nov 2018.
2. Vishal Sharma and K.C. Juglan, “Ultrasound based classification of Fatty Liver Disease: A Review”, in *Journal of Physics: Conference Series (IOP Publishing)*, Vol. 1531, Issue -1, pp. 012033, May 2020.

### Research Paper presented in Conference:

1. Vishal Sharma and K.C. Juglan, presented a paper titled “Computer Aided Diagnosis of Liver Ultrasound Images: A Review”, in 11th Chandigarh Science Congress (CHASCON-2017) held at Panjab University, Chandigarh (March 9-11, 2017).
2. Vishal Sharma and K.C. Juglan, “Ultrasound based classification of fatty liver disease: A Review, in RAFAS 2019 held at Lovely Professional University.

### Research Paper Submitted in Journal:

1. Vishal Sharma and K.C. Juglan, “PCA - Decision Tree based classification of Liver Ultrasound Images for Disease Diagnosis”, *Chaos, Solitons & Fractals: An interdisciplinary journal of nonlinear science (Elsevier)*.

